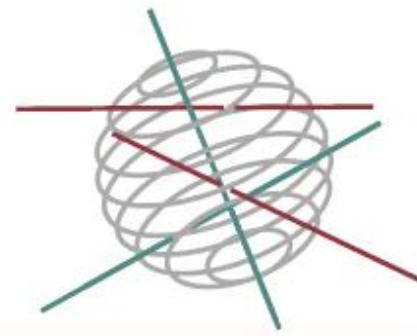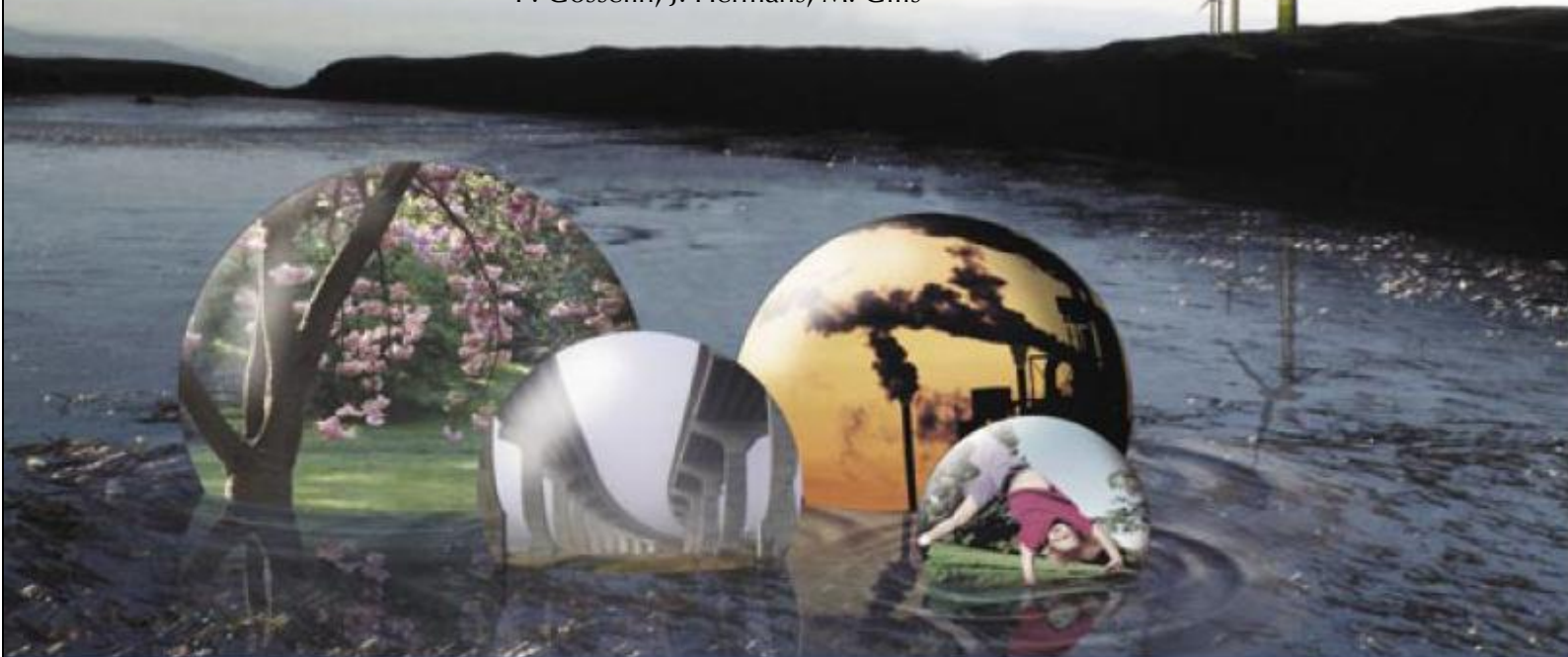# SSD

SCIENCE FOR A SUSTAINABLE DEVELOPMENT

CRITICAL EVALUATION OF MARINE CALCAREOUS SKELETONS AS RECORDERS OF GLOBAL CLIMATE CHANGE

"CALMARS II"

L. André, F. Planchon, F. Dehairs, M. Bauwens, V. Beelaerts, R.Mas,
R. Blust, H.Hansen, Ph. Dubois, C. Borremans, Ph. Willenz,
P. Gosselin, J. Hermans, M. Gilis

ENERGY
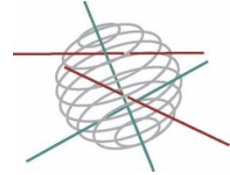
TRANSPORT AND MOBILITY

AGRO-FOOD

HEALTH AND ENVIRONMENT

CLIMATE

BIODIVERSITY

ATMOSPHERE AND TERRESTRIAL AND MARINE ECOSYSTEMS

TRANSVERSAL ACTIONS

.be

SCIENCE FOR A SUSTAINABLE DEVELOPMENT (SSD)

Climate

FINAL REPORT

CRITICAL EVALUATION OF MARINE CALCAREOUS SKELETONS AS RECORDERS OF GLOBAL CLIMATE CHANGE

"CALMARSII"

SD/CS/02

Promotors

Luc André
Royal Museum for Central Africa (RMCA)

Ronny Blust
Universiteit Antwerpen (UA)

Frank Dehairs
Vrije Universiteit Brussel (VUB)

Ph. Dubois
Université Libre de Bruxelles (ULB)

Ph. Willenz
Royal Belgian Institute of Natural Sciences (RBINSc)

Authors

Luc André, Frédéric Planchon
(RMCA/Section of Petrography-Mineralogy-Geochemistry)

Ronny Blust, Hanna Hansen
(UA/ Ecophysiology, Biochemistry and Toxicology Unit, Department of Biology)

Frank Dehairs, Maïté Bauwens, Veerle Beelaerts
(VUB/Department of Analytical Chemistry)

Remy Mas
(Laboratory of isotope geochemistry)

Ph. Dubois, Catherine Borremans
(ULB/ Laboratory of Marine Biology)

Philippe Willenz, Pol Gosselin
(RBINS/Department Invertebrates)

Julie Hermans, Melany Gilis
(RBINS/Department Invertebrates and ULB/ Laboratory of Marine Biology)

TABLE OF CONTENT

SUMMARY

A - Context

To understand the controlling mechanisms of the current climatic system, it is crucial to reconstruct the evolution of both present and past oceanic temperature and salinity, using robust and independent proxies. However, despite four decades of paleo-climate research, the community has not been able to come up with an independent proxy for paleo-salinity. Furthermore, most currently used proxies are biased by the so-called "vital effects", a term encompassing numerous biological controls on the biomineralization processes (Weiner and Dove, 2003). The calcareous skeletons of marine organisms studied in the previous "CALMARS I" project were demonstrated to hold several proxies of sea water temperature that are also influenced by salinity ($\delta^{18}O$, Mg/Ca) as well as potential salinity proxies (such as Ba/Ca) (Gillikin et al., 2006a; Rosenheim et al., 2005b; Rosenheim et al., 2004). As these organisms can live along salinity gradients, they offer an excellent opportunity to reconstruct temperature and salinity changes in the ocean using a multi-proxy approach and provide rare indicators of dynamic changes in river outflow. However, the interactions between these environmental factors and the biologically controlled processes of biomineralization have almost never been investigated despite their tremendous importance to determine the limits of applicability of proxies (Henderson, 2002). In addition to vital effects (also affecting $\delta^{18}O$), trace element concentrations in the marine environment also depend on varying input rates and source regions, related to the changes in the continental weathering processes. For instance, isotopic compositions of Ca and Mg have recently been proposed as proxies to better quantify origins of Ca and Mg fluxes to the ocean (De Villiers et al., 2005; Schmitt et al., 2003).

B - Objectives

The CALMARSII project aimed to improve the physical, chemical and biological understanding of the processes underlying proxy incorporation in skeletons, carry out a critical comparison and validation of different proxies and refine the use of calcareous marine skeletons for reconstruction of past salinity changes and continental weathering fluxes.

By bringing together a multidisciplinary network of biologists, chemists, geologists and engineers, our objectives were to (i) address the mechanisms of proxy incorporation to gain insight into the robustness of several proxies stored in biogenic carbonates; and (ii) reconstruct past environmental conditions. Based on species/proxy combinations, we have developed a multi-proxy approach using different types of marine carbonate skeletons and associated organic matrix. These proxies include both well-established ($\delta^{18}O$, $\delta^{13}C$, Ba/Ca, Mg/Ca, Sr/Ca) and newly developed ones (δD, $\delta^{26}Mg$).

The project has focused on bivalves, sclerosponges and echinoderms, since these taxa have some unique characteristics:

(i) All three groups offer species with large skeletons, which helps obtaining a mechanistic understanding of proxy incorporation;

(ii) Bivalves and echinoderms have a wide geographical and ecological distribution;

(iii) Bivalves and echinoderms have a high accretion rate, that enables detailed studies of inter-annual variations, such as annual minimum and maximum SST and SSS;

(iv) Skeletons of certain bivalve species consist of both aragonite and calcite. Analyzing the same proxy in both types of carbonate, which are known to record environmental conditions differentially, may allow us to deconvolve effects of multiple controls on the proxy (e.g. separate salinity from temperature effects);

One of the major drawbacks of bivalves and echinoderms are their relatively short life span that usually is on the order of decades or less. This makes such species less suited for continuous reconstructions on long time scales. On the other hand, annual minima and maxima are easily accessible, due to their rapid growth rates. In addition, by stringing together several specimens, longer chronologies can be still constructed (Schöne et al., 2005; Schöne et al., 2004; Wanamaker et al., 2008b);

(v) Sclerosponges are secreting their massive calcareous skeleton in carbon and oxygen isotopic equilibrium with surrounding seawater and have a very slow growth rate. Specimens of only 20 cm in diameter can potentially reach ages close to 1000 yr and therefore allow analyzing some climatic records over centuries.

C- Conclusions

During the CALMARSII project, important results were obtained on the three targeted taxa (sponges, echinoderms and bivalves) in order to validate their archival potential. In addition, the network has developed a modeling approach focused on the elimination of bias in temporal record, to non-linear multi-proxy and uptake kinetic modeling.

For Sponges, up to now, growth rate of massive basal skeletons of Calcispongiae was unknown. In situ calcein labeling experiments showed that the average skeletal growth rate of the calcisponge *Petrobiona massiliana* was 236 mm/year.

- SEM and epifluorescence microscopy observations highlighted some processes involved in the skeletal growth of *P. massiliana*. As previously described by Vacelet (1991), some calcareous spicules were entrapped within the calcitic mass during growth. These entrapped spicules (or their imprint) were also observed across the entire thickness of fractured skeletons, confirming that spicules do not dissolve in the mass of the skeleton (Vacelet, 1991). Intense calcein fluorescence was observed on the conical protuberances at the skeleton surface, indicating that they were actively growing at the time of incubation.

- Discontinuous calcein lines suggest that growth was spatially discontinuous. However, growth rates were similar at the apex of skeletal crests and in skeletal depressions or flat surfaces. Discontinuous growth results from an inhomogeneous spatial distribution of the basopinacocytes (i.e. the skeleton forming cells), or from differences in their activity.

- We observed a linear increase in Mg/Ca of 5% per °C in the skeleton of *P. massiliana*. This value is closer to that reported for inorganic calcite precipitation (3.1%; Oomori et al., 1987) than to that observed in foraminiferal calcite (10%; Lea et al., 1999). Our results, which agree with those reported for C. nicholsoni (Rosenheim et al., 2005a), highlight the importance of the thermodynamic control of magnesium incorporation in hypercalcified sponge skeleton. Even if skeleton deposition occurs in an organized chronological way, morphology or growth modalities can restrict the use of the skeleton of hypercalcified sponges as temperature recorder.

- Our study allows evaluating the potential use of the massive skeleton of *P. massiliana* as a reliable temperature recorder. In contrast with most hypercalcified sponges of the class Demospongiae, several factors such as ultidirectional growth axis, spatially discontinuous growth and a relatively short lifetime complicate the use of this species in high resolution temperature reconstructions.

- TEM and SEM observations allowed to confirm the role of basopinacocytes in the basal skeleton deposition, the extracellular localization of the mineralization sites, the formation of new skeleton layers by fusion of calcite cristals, the implication of an organic mineralization matrix rich in glycosaminoglycans, and finally a biomineralization discontinuous in time and space.

For echinoderms, the effects of temperature, salinity and growth rate on Mg/Ca and Sr/Ca ratios were studied in sea urchin and starfish calcite skeletons grown in experimental conditions. In both cases, Mg/Ca ratios were not related to growth rate and were positively related to temperature. An increase of the Mg/Ca ratio until a maximum value at higher considered temperatures was observed in the sea urchin skeleton. We suggest that this saturation is due to properties of the organic matrix of mineralization. Inverse relations between salinity and Mg/Ca or Sr/Ca were observed in the starfish skeleton and were attributed to metabolic effects.

The carbon and nitrogen isotopic compositions of the mussel shell organic matrix were studied along the salinity gradient of the Scheldt estuary. A clear evolution of the isotopic compositions follows the estuarine gradient; the $\delta^{15}N$ decrease with the salinity, the $\delta^{13}C$ has the opposite evolution. The incorporation of isotopes and trace element in the mussel shells was studied for the temperature, salinity and food availability controlled conditions. The isotopic results are only partially in agreement with the literature.

In an attempt to perform paleoclimatic reconstructions, we investigated chemical composition of bivalve shells coming from various archeological deposits. A series of specimens from coastal Belgium spanning more than 700 years has allowed us to obtain some information on past environmental conditions in the Scheldt estuary. Other bivalve specimens from the Arctic and Western Africa are currently under investigation. From the slow growing and long-lived sclerosponge sample, we obtained high resolution and continuous profiles of elements over a time period of 250 years.

The preliminary results indicate that the sclerosponge of Jamaica has recorded a large scale environmental contamination of arsenic that has started in the early 60's.

In terms of data treatment, averaging errors have always been neglected to date. Two methods were developed to eliminate these types of systematic errors from proxy records. The first method is a non-parametric method, which only corrects the averaging errors. The second method is a parametric method which simultaneously corrects for the averaging errors and constructs a time base, in assumption that the record is harmonic on a time grid. After the validation of the methods on mangrove data, the non-parametric method has been tested on δ18O from a *Chione cortezi* shell. The method showed no significant correction for the averaging effects. This result proves that the fading of the $\delta^{18}O$ signal is not due to averaging errors as stated in Goodwin et al. 2003, but due to physiological effects. Next the non-parametric method was tested on otolith data from the fish species *Paraconger papointi* this showed a significant correction for the averaging effects.

As a new potential proxy, we successfully set up the reliable determination of Mg isotope in biogenic carbonates with a precision of ~0.1‰. Such a low precision allowed us resolving part of the Mg isotopic fractionation patterns encountered in echinoderms and bivalves. The temperature sensitivity of $\delta^{26}Mg$ in sea urchin has been calibrated over an interval of ~10°C for two salinity regimes. T and S has a weak but visible influence on $\delta^{26}Mg$ and has to be taken into account for past $\delta^{26}Mg$ oceanic signature evaluation with sea urchin skeleton. For bivalve, Mg isotopes appear to significantly fractionate along their incorporation pathway from seawater to the shell. We show that the isotopic approach is a powerful tool to investigate biological interactions with Mg. Signatures of bivalve shell vary significantly with salinity stress and tends to support a more pronounced impact of metabolic activity.

Also as a new potential proxy, the deuterium isotopic composition from mussel shell lipid extract was measured for the first time. The measurements were done with mussels collected along the Scheldt estuary. The measured deuterium isotopic signal from mussel lipids and the expected signal for the deuterium composition of the Scheldt water show the same trends with salinity.

D - Contribution of the project in a context of scientific support to a sustainable development policy

The CALMARSII project has documented the archival potential of different calcifying species (sponges, echinoderms and bivalves) in order to infer climatic and environmental information. Fieldwork, experimental work, and modeling have provided new insights in the biology, chemistry and recording ability of these different organisms. Such information deserves future research in the field of biomineralization in a context of climate change and ocean acidification. For paleo-reconstruction using biogenic carbonates, we highlight the advantages and weaknesses of different calcifying species and also the difficulty to obtain true environmental signal from these archives.

We improved the reliability of already used paleorecorders by calibrating the effects of parameters that had not been taken into account. Deciphering between biological and environmental factors is still a challenge but we provide new perspectives using innovative modeling approaches.

E - Keywords

Biomineralization, trace element and isotope proxies, modeling, sea surface temperature, salinity, climate change, paleo-climate.

1. INTRODUCTION

The chemical and isotopic compositions of calcareous skeletons have long been recognized as records of past and present environmental conditions and thus allow reconstruction of the environmental history. Recent efforts have given a high priority in coral research to produce indicators of specific aspects of climate that can be integrated with other high resolution paleoclimatic data derived from tree rings, ice cores or sediments. Each type of archive provides a valuable record, with unique strengths but weaknesses. Because the composition of biogenic carbonates is also clearly influenced by biological factors, the correct interpretation of these chemical archives requires a precise understanding of the processes controlling the incorporation of elements. Furthermore, to make the reconstruction of past environmental conditions as reliable as possible at a global scale it implies that recorders from the widest taxonomic, geographical, and ecological ranges are used. Currently, such a large range is not available for the oceanic compartment.

Accordingly, the objective of the CALMARS research network is to extend series of environmental data from oceanic origin by using the skeleton of marine invertebrates belonging to different phyla, occurring from temperate regions to the tropics. Potential recorders have been selected among three taxa, viz. sclerosponges, bivalves, and echinoderms.

Echinoderms are abundant, widely distributed benthic invertebrates of which numerous recent and fossil specimens are available in museums. They have a well-developed endoskeleton made of high-magnesium calcite in which Sr is the main trace element (Dubois and Chen, 1989). The Mg/Ca ratio of the echinoderm skeleton is related to temperature (Chave, 1954; Clarke and Wheeler, 1922; Weber, 1969) and seawater Mg/Ca ratio (Ries, 2004). Another oceanographic parameter, salinity, could also affect significantly the Mg/Ca skeletal ratio. The importance of vital effects is still unclear: (Weber, 1969; Weber, 1973) suggested that the temperature effect was mainly driven by genetic factors and growth rate.

The objective of ULB research group was to determine the effects of temperature, salinity and growth rate on Mg and Sr incorporations in echinoderm skeletons, in order to estimate the potential of the echinoderm skeleton as a paleoenvironmental recorder and to better understand physiological processes involved in proxy incorporation. The oxygen isotopic composition of echinoderms has received little attention. The main works was done by (Weber and Raup, 1966; Weber, 1968). In our work, we measured the first paleotemperature equation for echinoderm (starfishes) from growing experiments under temperature and salinity controlled conditions.

For bivalves, we have focused on different species: *Mytilus edulis*, *Mytilus trossulus, Anadaria senilis* and *Ruditapes philippinarum*. For *Mytilus edulis*, the shell chemistry in relation to environmental variability has been well studied (Freitas et al., 2008; Gillikin et al., 2008; Wanamaker et al., 2008a). In the Scheldt estuary it has been demonstrated that oxygen and carbon isotope ratios and trace element compositions of the shell can serve as proxies for salinity and temperature (Gillikin et al., 2006a; Gillikin et al., 2006b; Wanamaker et al., 2008a; Wanamaker et al., 2007). The organic part of the shell was also investigated in order to developed new environmental proxy, as the $\delta^{15}N$ (O'donnell et al., 2003) of the organic matrix or the $\delta^{13}C$ of specific amino-acids (Serban et al., 1988).

Application of these proxies to shells from archaeological finds will yield information on past discharges of the Scheldt, estuarine dynamics and human influence in the river basin. In contrast to *M. edulis*, *Mytilus trossulus* has been much less studied. It appears, though, that this bivalve is also a faithful recorder of its environment (Klein et al., 1996a; Rainbow et al., 2000a). *M. trossulus* is the abundant Mytilus species in the arctic and enables us to study high-latitude environmental variability under the influence of ocean dynamics in relation with past climate changes. Although some authors have used Anadaria senilis in biomonitoring, studying heavy metal contents of the soft tissues (Joiris and Azokwu, 1999; Joiris et al., 1998; Otchere, 2003), so far no studies of its shell chemistry are known. Since these shells are abundant in ancient shell middens in Mauritania (Barusseau et al., 2007), chemistry of these shells probably opens a window to early-to-mid Holocene "green Sahara" climate and conditions of abandonment of human settlements (Zühlsdorff et al., 2007).

One of the focuses of the modeling group was the calibration of proxy records, by eliminating systematic averaging errors. Natural archives are always solid substrates. Hence, the proxies incorporated into a solid substrate are collected via sampling. Whether sampling means drilling a hole or counting a proxy per square meter, the sample always has a certain volume (the volume of the drill hole or the count space). As a consequence, a sample will give the mean value of the proxy over a corresponding volume. To our knowledge, the volume of the sample has always been neglected to date. However, this is only applicable when the width of the sample is small with respect to the variation that needs to be reconstructed. Researchers choose the smallest possible samples intuitively; however, working close to the detection limit will lower the signal-to-noise ratio, and thus the accuracy of the measurement. On the other hand, when the width of the sample covers a considerable part of the variation, the signal will be averaged and the variations will systematically be underestimated.

Because climate models are matched to proxies, proxies need to be as precise and as accurate as possible; otherwise the models, as well as the conclusions drawn, will be biased. Two methods have been developed to eliminate these averaging errors. The first method is a non-parametric method, the second method is a parametric method which simultaneously eliminates the averaging errors and creates a time axis for the proxy records.

In addition to conventional proxy approaches based on elements to calcium ratios or C and O stable isotopes, the project has set up the development of new descriptive parameter of the biomineralisation process. It includes the stable isotopic composition of Mg and the isotopic signature of H in the organic matrix of bivalve shell.

Owing to recent achievements in multiple-collector inductively-coupled-plasma mass-spectrometry (MC-ICP-MS) (Galy et al., 2001), Mg isotopic ratios (^{26}Mg/^{24}Mg and ^{25}Mg/^{24}Mg) are now accessible in most of environmental matrices including biogenic carbonates (Chang et al., 2003; Chang et al., 2004; De Villiers et al., 2005; Pogge Von Strandmann, 2008; Young and Galy, 2004). Resolving Mg isotope fractionation in biologically-precipitated shells and skeletons offers twofold interest. First, Mg isotope may fractionate according to calcification temperature and provide a new independent proxy similar to extensively studied δ^{18}O (Weber and Woodhead, 1972) or more recently δ^7Li (Marriott et al., 2004), δ^{44}Ca (Böhm et al., 2006) and δ^{88}Sr (Fietzke and Eisenhauer, 2006).

Second, Mg isotopic signature of biocarbonates can give new insights into the Mg cycling in calcifying organisms. Sensitive to different processes such as carbonate precipitation (Buhl et al., 2007; Galy et al., 2002) and biological uptake (Black et al., 2008; Black et al., 2006), this new isotopic systematics offers interesting perspectives to study the wide diversity of biomineralization processes. For instance, large fractionation factors reported for corals and foraminifera (Chang et al., 2004; Pogge Von Strandmann, 2008) suggest two distinct incorporation pathways. Corals appear to be close to the inorganic precipitation process of aragonite contrasting with lighter Mg isotopic signatures in foraminifera which support a strong biological influence associated to the intracellular process of chamber formation (Bentov and Erez, 2006).

The current paleoclimatology research shows a great interest for the salinity reconstruction. A proposed way to make progress is the development of the deuterium stable isotope from organic molecules extracted from sediments, microorganisms (Schouten et al., 2006; Van Der Meer et al., 2007; Van Der Meer et al., 2008) or macroorganisms. The deuterium was already measured for freshwater bivalves, using an exchange hydrogen technique (Carroll et al., 2006).

Following to the methods of (Wassenaar and Hobson, 2000; Wassenaar and Hobson, 2003) the percentage and the δD value of non exchangeable hydrogen were determined. Our group chooses another way to measure the deuterium content from bivalve shells. Our solution consists to analyze only the deuterium from the lipids. The advantage are multiple: the preparation is faster (1 day against 100 h), the fact to work with a same group of molecule rather the bulk organic reduce the biosynthetic pathway increasing the potential sensibility of the method (Sauer et al., 2001), the problem of the preservation and of exchangeable hydrogen is very reduce in the case of lipids allowing applications for paleoclimatology. The lipid content of the mollusk shells was mainly described by (Cobabe and Pratt, 1995; Cobabe and Ptak, 1999) and (Farre and Dauphin, 2009) but the mechanism of incorporation and the potential function in the biomineralisation of the lipids are still unknown.

2. METHODOLOGY

Study sites are located in the North Sea (Scheldt estuary, Belgium), in the North Atlantic (Disco Bay, Greenland and Svalbard, Norway) western Atlantic (Gulf of Morbihan, France and Banc d'Arguin, Mauritania) and in the Mediterranean Sea (Figure 1). For the tropic, sclerosponges samples (*Ceratoporella nicholsoni*) originate from the Caribbean Sea (Jamaica).
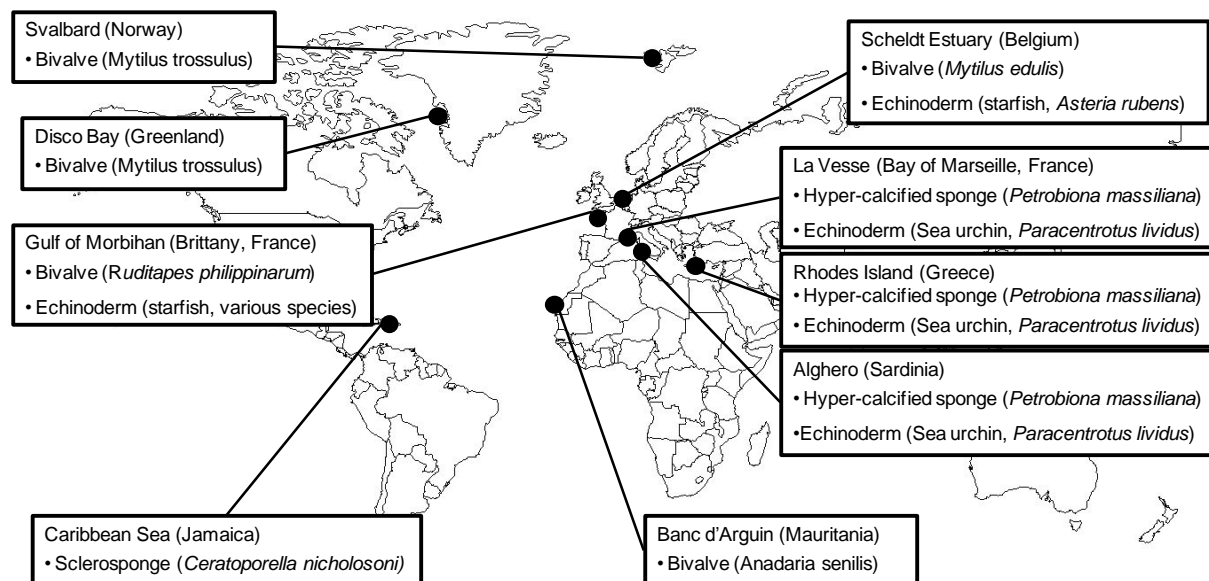
Figure 1. World map showing main sampling stations and marine organisms collected.

2.1 Sponges

Two species of sponges were considered in the project: the hypercalcified Mediterranean sponge *Petrobiona massiliana* and the calcified demosponge *Ceratoporella nicholsoni* (Lazareth et al., 2001; Rosenheim et al., 2005b; Rosenheim et al., 2004).

For *Petrobiona massiliana,* the study was performed during the first phase of the project focusing on the formation of basal skeleton as prerequisite to its use as a marine paleoclimate recorder. The aims were (1) to describe the sponge anatomy (viz. skeleton & soft tissues) and the mechanisms of the basal skeleton formation, (3) to estimate the annual skeletal growth rate (in situ experiments), (4) and to determined the chemical composition of the basal skeleton.

For *Ceratoporella nicholsoni,* we considered one specimen from Jamaica (Lazareth et al., 2001) in order to provide high resolution elemental profiles over a time interval between 1985 A.D. and 1771 A.D to infer paleoclimatic reconstruction.

2.1.1 Specimens of Petrobiona massiliana

Since seasonal morphological variations could influence the integration of the selected proxies into the skeleton, the description of the sponge anatomy implied to study specimens collected at different periods of their life cycle. Specimens of *Petrobiona massiliana* (Calcarea) were collected on a monthly basis in an underwater cave at La Vesse (Bay of Marseille, France); from June 2006 to July 2007 (14 samplings events). Samples were chemically fixed according to (Eisenman and Alfert, 1981); and processed for morphological analysis. Water temperature was recorded continuously by automatic probes located in the vicinity of the sponge population, and water samples were collected in the cave at each sponge sampling.

2.1.2 Scanning Electron Miscroscopy

The skeleton of *Petrobiona massiliana* was detailed in scanning electronic microscopy (SEM). Sponge specimens were air dried; their living tissues were later removed using protease or bleach and/or a micro water jet. In order to describe the different parts of the massive skeleton, whole individuals were studied, as well as slabbed or fractured ones. For scanning electron microscopy (SEM), specimens were dried by the critical point method (using CO_2 as transition fluid), mounted on aluminum stubs, coated with gold in a sputter coater and observed using a scanning electron microscope (Philips/FEI XL30 ESEM TMP and Jeol JSM-6100).

2.1.3 Preparation of the soft tissues

To study the soft tissues, specimens were fixed by immersion in 4% glutaraldehyde in cacodylate buffer (0.2M, pH 7.9) modified from (Eisenman and Alfert, 1981) and decalcified using EDTA solutions (from 1 to 3 months depending of the specimen size). They were rinsed in cacodylate buffer and post-fixed for 90 min in 1% osmium tetroxide in the same buffer. After a final buffer wash, they were dehydrated in graded ethanol series. For light microscopy, specimens were embedded in epoxy resin (Spurr, 1969).

Semi-thin sections (1 μm) were cut on a Leica Ultracut UCT. They were stained with a 1:1 mixture of 1% methylene blue in 1% natriumtetraborate and 1% Azur II. For SEM, specimens were prepared like previously described for the skeleton samples.

2.1.4 In vitro growth rate measurements

Living specimens of *Petrobiona massiliana* were collected in the underwater cave of La Vesse in June 2006 and brought back to the Marine Laboratory of the ULB. Specimens were transferred into aquaria to study their skeleton growth rates under various experimental conditions of temperature and salinity. Sponges were progressively acclimatized to those different environmental conditions (maximal slope of 0.5°C per day and of 1‰ every 3 days). However, all specimens progressively died within two weeks, leading to the conclusion that this part of the study had to be performed exclusively *in situ*.

2.1.5 In situ calcein labeling

The growth of *Petrobiona massiliana* was estimated *in situ* by repeated labeling with calcein. This long term experiment was initiated one year before this first phase of the project started. Sponges were incubated with calcein (100 mg/LSW for 24 to 72 hours) and left in their habitat for further growth After one year, eight specimens were collected and transversal ground sections of their skeleton were observed under an epifluorescence microscope.

2.1.6 In situ regeneration experiment

To examine newly formed skeleton, a regeneration experiment of *Petrobiona massiliana* was also initiated in situ in September 2006. About 1/4 of the body of each specimens was cut off. The duration of this experiment is determined by the capacities of regeneration of those specimens and is still under study. At the end of the experiment, concentrations of magnesium (Mg) and calcium (Ca) will be measured in the regenerated parts of the sponges by ICP-MS (MRAC) and the $\delta^{18}O$ by mass spectrometry.

2.1.7 Biomineralization of Mg at cellular level

A main concern in understanding the calcification processes of the basal skeleton of *Petrobiona massiliana* is the process of trapping elements

contained in sea water and their transfer through the sponge tissue from one cell type to another. One of the target proxies for which the different partners of CALMARS II share the same interest is magnesium (Mg). Since chemical fixatives would wash out the studied element from the sponge tissues, a protocol of cryofixation and cryosubstitution was developed in order to follow the cellular processes allowing the incorporation of Mg from the living tissue into the basal skeleton.

2.1.7.1 Specimen sampling for cryofixation

Living specimens of *Petrobiona massiliana* were collected in the underwater cave of La Vesse in September 2006 and March 2007. Sponges were cut into smaller sub-samples and frozen by rapid and calibrated immersion in liquid propane (-160°C) for 5 sec using a Cryoplunger LEICA EM CPC. Samples were stored and carried to Brussels at -196°C in liquid nitrogen. As the natural Mg concentration into the sponge tissue was unknown, a pre-treatment was applied to try to raise the concentration of this element into the soft tissues for easier detection in X-ray electron microscopy. Before cryofixation, specimens were incubated *in situ* in solutions enriched in Mg (*viz.* solutions 2 to 3 times more concentrated in Mg than the natural sea water). Bottomless vials glued on the substrate were used as small incubation chambers to perform these incubations without removing specimens from the wall of the cave.

2.1.7.2 Cryosubstitution protocol

To bring frozen specimen to ambient temperature, they were prefixed at -85°C in 0.1% tannic acid in acetone for 72h and fixed in 2% osmium tetroxide in acetone for 18h using a Freeze Substitution Device LEICA EM AFS2. Samples were transferred in a fresh bath of 2% osmium tetroxide in acetone and brought from -85°C to -30°C in 27.5h (slope of 2°C/h). Samples were transferred in 4 successive baths of pure acetone: (1) at -30°C for 22h, (2) from -30°C to 4°C in 17h (slope of 2°C/h), (3) at 4°C for 8h and (4) from 4°C to 22°C in 9h (slope of 2°C/h). Samples were then embedded in Spurr's epoxy resin and thin sectioned to be studied with an ESEM coupled with a X-ray microprobe.

2.1.8 Specimen of Ceratoporella nicholsoni

A specimen of *Ceratoporella nicholsoni*, already described by (Lazareth et al., 2001), was collected in a reef crevice at a depth of 30 m on the fore-reef

slope of Jamaica Bay (southern tip of Acklins Island), Bahamas, in August 1985. A diamond saw was used to cut a 5-mm-thick slab perpendicular to the surface of the specimen. Mean annual growth rate of 230 ± 45 mm/yr was obtained from in situ calcein labeling of 10 specimens over a 10 yr interval in Jamaica (Willenz and Hartman, 1999).

Absolute dating of the sample was performed using U/Th disequilibrium method. Measurements were carried out with MIC-ICP-MS AXIOM, a double focusing sector field instrument equipped with 10 Faraday cups and 3 ion counters, at IFM-GEOMAR, Kiel Germany. Four samples of approximately 450 mg each, of carbonate powder were taken near to the rim, the youngest part, of the sponge toward the oldest part, the baseline. The sample size has a mean average of 4.0±0.2mm (n=5, σ=0.5mm, SEM =0.2mm) so that the sampling hole covering an age interval of about 17±3 years given a growth rate of 0.233±0.033 mm/yr. U/Th dating results indicate that the skeleton of this specimen of *Ceratoporella nicholsoni* represents a time interval between 1985 A.D. and 1771 A.D. The minimum and the maximum growth rate vary between 0.129±0.012mm/a and 0.395±0.033mm/a. The years in A.D. were determined by interpolating between the U/Th aged samples. This chronology is in good agreement with observed trends in $\delta^{13}C$ and Pb (Lazareth et al., 2001).

2.2 Echinoderms

Long term growth processes (5 months) of sea urchin (juvenile stage, *Paracentrotus lividus*) and sea star (juvenile stage, *Asterias rubens*) were studied in closed aquarium systems. Variation of skeletal Mg/Ca and Sr/Ca ratios were studied along temperature and salinity field gradients and in different skeletal plate types of field collected specimen.

2.2.1 Growth of juveniles echinoderms in controlled conditions

2.2.1.1 Aquarium systems

16 temperature and salinity controlled aquarium systems containing each 100 liters of seawater were used. Salinity was measured daily in each aquarium and temperature was continuously logged. Salinity was adjusted by addition of Milli-Q water to compensate for evaporation. Every two weeks, water samples were taken in triplicates from the different systems and stored at -20°C until analysis.

2.2.1.2 Experiments with sea urchin.

Juveniles *Paracentrotus lividus* collected in the field in Marseille (France) were grown in 8 aquariums (15 individuals/aquarium) in different controlled conditions of temperature (13°C, 18.5°C, 20.5°C, 24°C) and salinity (36 and 39 psu). The initial size distributions were identical in all aquariums. Sea urchins were labelled with calcein at the beginning of the experiment in order to distinguish the skeleton formed prior to and during the experiment. Sea urchins were fed in excess with the brown alga *Laminaria saccharina* during the whole experiment. After five months, sea urchins were dissected. Newly formed interambulacral coronal plates were recognized by the lack of calcein labelling under an epifluorescence microscope. They were separated and weighted, providing an individual growth rate.

2.2.1.3 Experiments with starfish

Asterias rubens juveniles were collected in November 2006 on breakwaters in Knokke. They were grown under controlled conditions of temperature (11 and 18°C) and salinity (25, 28, 32, 35 psu) in 8 aquariums (30 specimens/aquarium). The initial size distributions were identical in all aquariums. The starfish arm length was measured monthly and food was provided ad Libitum using mussels from Knokke. The newly formed parts of juvenile arms were determined using the monthly size measurements and the results from a separate calcein labelling experiment (data not shown).

2.2.2 Magnesium partition in the different body compartments of *Asterias rubens*

Starfishes (*Asterias rubens*) were collected on a breakwater in Knokke in January 2007 and were dissected immediately. Coelomic fluid, gonads, pyloric caeca and integument were isolated. An entire arm of the starfish was kept to analyze the total skeleton. The different plates were isolated from the remaining cleaned skeleton.

2.2.3 Field samples

Sea urchins (*Paracentrotus lividus*) and water samples were collected in spring 2007 in Marseille (France), Alghero (Sardinia), and Rhodes (Greece). Starfishes (*Asterias rubens*) were collected in April and May 2006 along a field gradient of salinity in the Scheldt estuary.

Also, Sympatric starfishes (Asterias rubens, Marthasterias glacialis, Echinaster sepositus, Henricia sanguinolenta, Asterina gibbosa, Anseropoda placenta) were collected in Finistère (Brittany, France) in March and April 2006.

2.2.3.1 Sample preparation and analyses

Skeletal samples were cleaned of the associated soft tissues using analytical grade 2M NaOH. Cleaned samples were then mineralized by H_2O_2 and HNO_3. Mg, Sr, Ca concentrations of the solutions were analyzed with an Iris Advantage (Thermo Jarrel Ash) Inductively Coupled Plasma Atomic Emission Spectrometer (ICP-AES). The calibration was achieved using artificial multi-elemental solutions made from certified mono-elemental solutions (Merck) and using certified reference materials for quality check: HPS CRM Seawater (High Purity Standard) for the seawater samples and JCp-1 (coral) and JCt-1 (giant clam) (Standard Geological Survey of Japan) for the skeleton samples. Results for the certified reference materials were always within ± 10% of the certified values.

2.3 Bivalves

Different species of bivalves were considered in the project: in a large extent the blue mussel *Mytilus Edulis* and also, the Manila clam *Ruditapes philippinarum*, *Mytilus trossulus* and *Anadaria senilis*.

2.3.1 Uptake and accumulation of major and minor elements in the blue mussel *Mytilus edulis*

The incorporation of alkaline earth metals such as calcium, magnesium, strontium or transition metals such as manganese, copper or zinc in shells of bivalves depends on the environmental conditions, developmental stage and physiological status of the organism. Salinity and temperature are the two main environmental factors influencing the uptake by the soft tissues and incorporation of the various elements during shell formation. The concentration of the major alkali and alkaline earth metals in the circulatory fluid of bivalves is close to this of seawater with no or little physiological regulation. For transition metals this is not the case and the concentrations of some of the essential elements are regulated. Also, the intracellular concentrations of alkaline earth metals such as calcium and magnesium and some essential transition metals are under homeostatic control.

This means that with changing salinity the ion and osmo-regulatory system adjusts to the new situation to keep intracellular levels of these elements more or less independent of the external salinity. The capacity to regulate the different elements is however not the same for the different elements and salinity ranges (Neufeld and Wright, 1996).

The uptake of elements occurs via water and dietary exposure. Brackish and seawater environments are characterized by very high concentrations of the essential alkali and alkaline earth metals why the concentrations of most other elements, being essential or not, are orders of magnitude lower. Therefore it can be expected that for the major alkali and alkaline earth metals uptake via water is the dominant route of uptake as is also reflected in the fact that the composition of the exposure water and hemolymph is almost the same for these elements. For the most other elements the situation is entirely different and the relative contribution of water and diet as sources of elements will depend on the situation. Bivalves are efficient filter feeders which almost continuously pump water across the gills and direct particles, within a certain size range, to the digestive system. The diet consists of microalgae and other particles coated with organic material with minor element concentrations generally considerably higher than those of seawater. Thus, the ingestion and digestion of particles provides an important source of minor elements including the essential ones such as manganese, copper or zinc, but also non-essential ones such as barium, cadmium or lead. The relative contribution of water and diet as sources of elements can be determined if the rates of uptake from water and diet are known. In case of water exposure this rate depends on the concentration and forms in which the elements occur in solution (free ions versus complexes) and the kinetic characteristics (affinity and transfer rate) of the transporters involved in the uptake process. In case of dietary exposure the same principles hold but exposure is expressed in terms of element particle concentrations and ingestion rates. The transfer of the elements across the digestive system is expressed as the assimilation efficiency. Clearly, the concentration of microalgae and other particles varies strongly across the year depending on temperature cycles and primary productivity. This will also strongly influence the importance of the dietary route as a source of minor elements and ultimately be reflected in the accumulation of elements in the soft tissues and shells.

In addition the metabolic rate of poikilotherm organisms such as bivalves is directly dependent on temperature and also the rate of shell formation is highly temperature dependent. The similarities in elemental composition between seawater and extra-pallial fluid reflect the high degree of equilibration that exists between seawater and the hemolymph for these elements. Depending on metabolic activity the contribution of intracellular transport processes on the composition of the extrapallial fluid will change. Thus, differences in the intercellular – intracellular transport ratio within the mantle gives rise to variation in the elemental composition of the shell matrix. Intercellular transport supplies the extrapallial fluid with a solution of seawater like composition whereas intracellular transport produces a solution which is generally higher in calcium and metabolic carbon dioxide and carbonates and this will alter for instance the Sr/Ca and 13C/12C ratios (Carré et al., 2006; Gillikin et al., 2005; Klein et al., 1996a).

Within the framework of the Calmars II project the incorporation of a number of major and minor elements in the soft tissues and shells of mussels is studied under different exposure conditions (temperature, salinity, and sources). The focus is on the kinetics of uptake and elimination by the soft tissues and transfer to the shells. Mussels are exposed to different concentrations of the elements in water or food and the accumulation of the elements is followed by measuring the uptake and elimination of the elements on the basis of changes in total element tissue concentrations or that of a radio or stable isotope tracer. Mussel shell development and growth is studied over a range of temperatures and salinities and combinations of these. The effect of changes in whole animal and mantle tissue metabolic activity on the incorporation of the elements in the shells will be determined. The incorporation of seawater and dietary derived sources of elements in the tissues is studied and effects on elemental ratios evaluated. The results are used to construct a kinetic model that relates the incorporation of elements in soft tissues and shells to differences in temperature and salinity and aims to explain results in terms of the dynamics of the environment and the physiology of the organisms.

2.3.1.1 Mussel collection and maintenance

Mussels are collected from the East and Western Scheldt estuary or the Belgian or Dutch coastal zone. For experimental purposes mussels were generally collected from the relatively clean waters in the Eastern Scheldt

(Wemeldinge, The Netherlands). After collection animals were transported on ice to the laboratory where they were kept in a recirculating artificial seawater system at 15 $\pm$ 0.5 °C at salinity of 35 $^0/_{00}$ (or other experimental temperatures and salinities) for at least 3 weeks prior to experimentation. They were fed 3 times a week with an equivalent of 2 % of their dry soft tissue weight with enriched yeast cells (Lansy PZ (INVE Technologies, Belgium). The condition of the mussels was monitored on a regular basis by determining their Scope for Growth which includes measurements of filtration rate, respiration rate and energy budget (carbohydrates, proteins and lipids).

2.3.1.2 Metal uptake kinetic studies

To study metal uptake by whole mussels and individual tissues exposure was performed at different metal concentrations and conditions (Mubiana and Blust, 2009). Also experiments were performed with isolated gills to characterize accumulation in these important uptake compartments separately form the other parts. Metal uptake and accumulation was followed using three different approaches depending on the metal and availability of specific tracers (i.e. spiking with an inorganic metal salt, spiking with a radioactive gamma or beta tracer; spiking with a specific stable isotope of a given element. Recently, we have explored the use of stable isotopes as an alternative for the radiotracer experiments. This approach avoids the use of radioactive materials and allows to follow uptake, accumulation and compartmentalization processes over longer periods (weeks, months). The ICP-MS based analysis provides information on all the different isotopes of a given element so that both information on changes in total element concentrations and as well as the spiked isotopes is obtained which is usually not the case when working with radioactive tracers. In addition, radioactive tracers are not available for all metals of interest or have a very short half-live to be of practical application. A specific limitation of the use of stable isotopes in salt waters is the high concentrations of some of the key elements such as calcium or magnesium so that a high spike is required to obtain sufficient uptake for accurate quantification. So far we have only worked with standard resolution quadrupole ICP-MS which did not provide enough resolution and sensitivity in case of these elements. However, we have recently installed a high resolution ICP-MS instrument through Hercules funding which should allow these type of experiments and measurements with better precision.

2.3.1.3 Radioactive versus stable isotopes as tracers:

To study the uptake and accumulation of different elements by the mussels it was intended to use radio and stable isotopes. The use of stable isotopes is a new application in this area of research and has two advantages. Firstly, the safety and waste disposal issues related to the use of radioisotopes is avoided and secondly, ICP-MS allows the analysis of the different naturally abundant and spiked isotopes in one single run. However, in the current study most experiments were performed using radiotracer methods using gamma and/or beta emitters of the elements in combination with gamma or beta scintillation counting. We have also developed and applied a methodology for the use of stable isotopes for the mussel studies but the results obtained so far with a quadrupole ICP-MS system were of limited success given the fact that seawater contains very high concentrations of calcium, magnesium and chloride and high enrichment of the exposure solution with stable isotopes is required to obtain a good isotope signal resolution in the mussel tissues. This problem can be overcome by using high spike levels but would make the experiments very expensive. We have however, successfully applied the same technique to a series of other studies with freshwater organisms where the same problems do not occur due to the dilute nature of these environments (Komjarova and Blust, 2008). Based upon the expertise gained we have successfully applied for a magnetic sector ICP-MS which provides much higher resolution and sensitivity compared to a quadrupole ICP-MS instrument and overcome these analytical limitations.

2.3.1.4 Relative importance of water and particles (food) as sources of elements

The accumulation of elements by mussels is the results of the contributions of two main exposure routes and uptake pathways. To determine the relative importance of these pathways experiments were conducted to measure uptake from both sources in which the elements were spiked to either the water or the food. Experiments combining both exposure routes have not been completed and are difficult because of the rapid exchange kinetics between both sources for some of the elements of interest. A kinetic modeling approach is used to determine the relative importance of the exposure routes under different exposure scenarios (Hanssen et al., 2008).

2.3.2 Seasonal evolution of trace element translocation in soft tissues of Mytilus edulis

We conducted 22 surveys at the Knokke site with the following sampling frequency: in spring a weekly field survey), in summer and fall a 2-weekly survey) and in winter a monthly survey. Water temperature, conductivity, dissolved O_2, and seawater pH were monitored simultaneously. Mussel soft tissues were dissected to separate foot, gills, labia, mantle, gut, skirt, visceral mass, abductor muscle, hemolymph, and rest material. Trace, minor and major elements were measured by HR-ICP-MS and ICP-AES after acid digestion.

2.3.3 Mytilus Edulis along the Scheldt estuary salinity gradient

2.3.3.1 Sampling

We sampled *Mytilus edulis* along the salinity gradient of the Scheldt estuary in order to verify isotopic gradients ($\delta^{13}C$, $\delta^{15}N$ and δD) in bivalve shells sampled along the estuarine salinity gradient (Figure 2). Specimens of *M. edulis* were collected in March 2007 and June 2009 at 4 sites along the Westerscheldt spanning a salinity range between about 30 and 15 (low tide condition) (Figure 3). Below a salinity of 15 the blue mussel becomes scarce. At each sampling, between 50 à 100 specimens were collected from the intertidal zone, at low tide. A temporal evolution of salinity over the seasons (every 2 to 3 weeks measured at the river bank) was obtained earlier at these same sites over a full year 2002 (Gillikin et al., 2006b). Salinity data are also available from continuous buoy measurements at 3 different locations in the estuary (Figure 22).
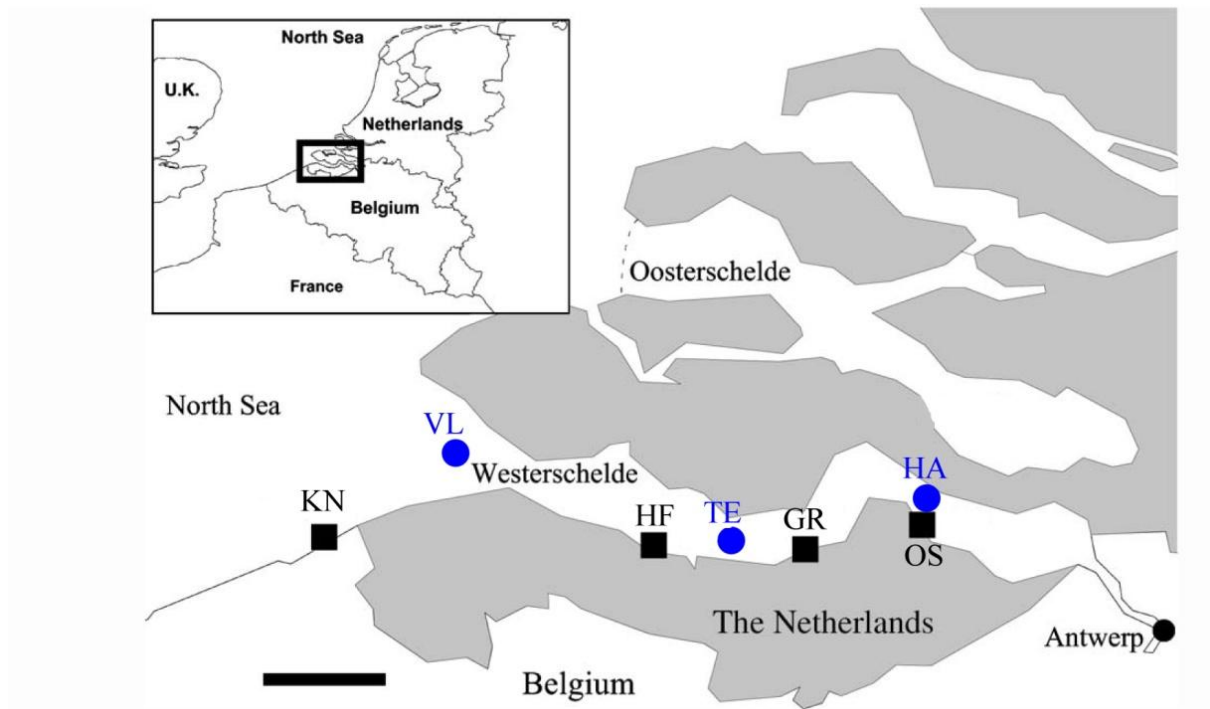
Figure 2. Sampling sites (black squares) along the Scheldt estuary (KN= Knokke; HF= Hooftplaat; GR= Griete; OS= Ossenisse) and position of the 3 Rijkswaterstaat measuring buoys (blue circles).
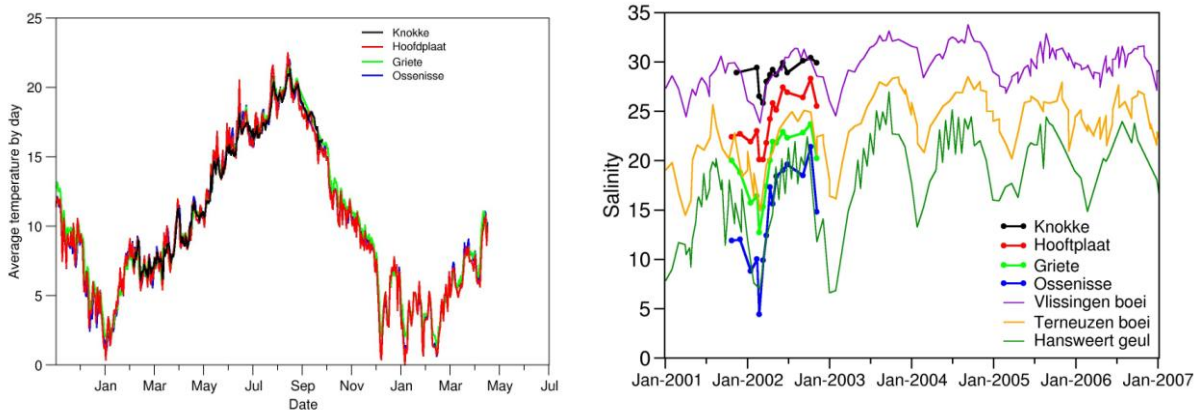
Figure 3. Temperature and salinity values for the 4 different sites along the Scheldt estuary from (Gillikin et al., 2006a).

2.3.3.2 Sample treatment

The valves are first cleaned (by brushing – Dremel®) and treated with sodium hypochlorite to remove any external contamination (including epibionts). The insoluble shell organic matrix is then recovered by dissolving shell carbonate in hydrochloric acid (1M). Whole organisms as well as well as dissected tissue separated into muscle, mantle and rest, were frozen and lyophilized.

For total lipids extracted from crushed shells, the samples are extracted 3 times. Each extraction uses successively MeOH; MeOH/DCM (1/1) and DCM under ultra-sound treatment. Lipid classes are subsequently separated on silica column. The neutral fraction is eluted with ether; the acidic lipids with a mix of hexane: ether: acetic acid (70:30:1) and finally polar lipids with methanol. The dry weight of the total organic matrix for M. edulis shells is on average 1% of the shell weight (n= 3, sd = 0.13%).

2.3.4 In-vitro growth of Mytilus edulis under controlled conditions

The effects of salinity, temperature, growth and metabolism on the isotopic composition of the *Mytilus* shells were experimentally determined by (Wanamaker et al., 2008a; Wanamaker et al., 2007). We conducted a similar experiment to evaluate the effects of temperature and salinity on O, C isotopes and trace metal profiles in bivalve shell carbonate.

Mytilus edulis specimens (around 80) of similar size (<20mm) and originating from Knokke were translocated (early Feb. 2007) and kept (till end of April 2007) under controlled laboratory conditions (in collaboration with ULB partner). The influence of temperature (8° and 16°C), salinity (28 and 18‰) and food availability (8 and 16 mg DW of the alga Tetraselmis suecica per week per mussel) on the incorporation of stable O and C isotopes in the shell was studied. These in vitro experiments (using 6 aquaria) allowed perturbing a single environmental condition, while other conditions were kept constant (Figure 4).
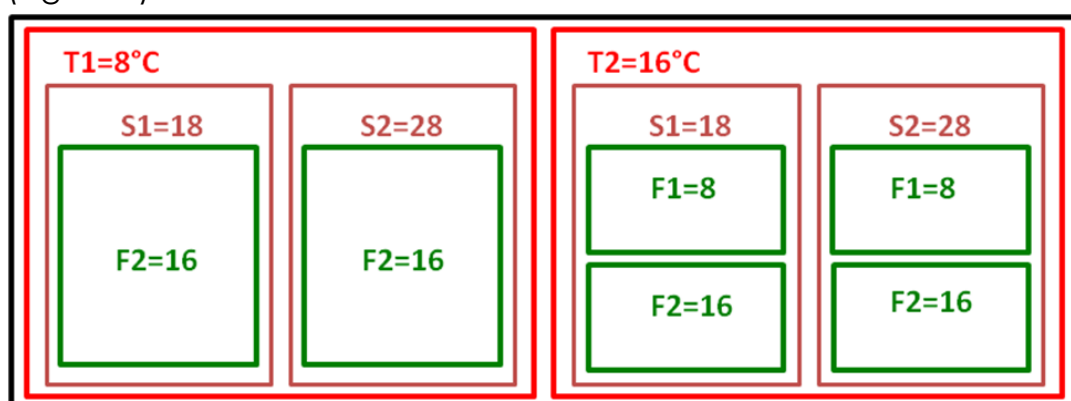
Figure 4. Set-up of the experiment showing the 6 aquaria with the different conditions of temperature (8° and 16°C), salinity (18 and 28) and food availability (= F, in mg DW /week/ individual).

2.3.5 Mg isotope in bivalve biomineralisation matrices

Our aim in this study was to provide the first Mg isotopic characterization of compartments involved in the bivalve shell formation (seawater, extrapallial fluid, hemolymph, soft tissues and shell). It represents a process-oriented study and addresses key questions about the origin and fate of Mg during biomineralisation and explores the use of Mg isotopes in bivalve shells as a new potential proxy.

2.3.5.1 Specimens of Ruditapes philippinarum

Live specimens of adult manila clams *Ruditapes philippinarum* were collected in April 2007 from subtidal zone sediments at two sampling sites in the gulf of Morbihan (Brittany, France) showing strong salinity contrast (Figure 5). At the first site, Locmariaquer (Loc), close to the mouth of the gulf and of the coastal ocean, one specimen was collected. At the second site, Le Bono (Bo), located upstream along the Auray River and subjected to estuarine-like salinity changes, seven specimens were retrieved. Internal fluids of every living specimen were carefully sampled immediately after their collection using syringes equipped with sterile needles. About 100-200 μl of extrapallial fluid (EPF) and hemolymph (H) were gathered in pre-cleaned 2 ml vials and stored at 4°C. At each site, 30 ml duplicate seawater samples were also collected in acid-cleaned High-Density Polyethylene (HDPE) bottles, filtered at 0.45 μm onboard, acidified at 1% with double-distilled HNO_3 and stored at 4°C.
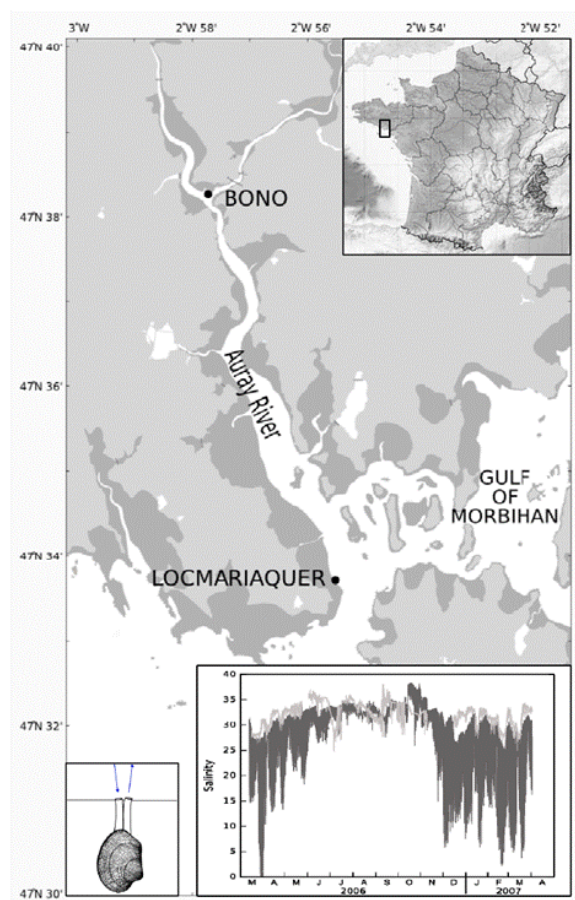
Figure 5. Schematic map showing the two sampling sites along the Auray river (Le Bono and Locmariaquer) in the gulf of Morbihan (France) with the measured salinities for the estuarine site (Le Bono, dark grey) and the oceanic site (Locmariaquer, light grey). Also, it presents a schematic view of the living position of the manila clam in the sediment.

2.3.5.2 Sample treatment

At the laboratory, soft tissues of all specimens were removed from the shells and further dissected in milliQ water to separate different organs including the muscle, the mantle and the remaining part. Three distinct fractions of soft tissues were then rinsed with de-ionized water, lyophilized, powdered and homogenized separately, before acid digestion. Mix acid and oxidative attack was performed with ~50 mg of sample placed in PFA Savillex with 2 ml of double-distilled HNO_3 and 2 ml of H_2O_2 at 70°C. Once a total dissolution was observed (1 day), solutions were evaporated to dryness, dissolved with 25 ml of 5% double-distilled HNO_3 solution and stored in 30 ml acid-cleaned HDPE bottles at 4°C. Low-volume samples from extrapallial fluids and the hemolymph were centrifuged and the supernatant were recovered in 2 ml pre-cleaned vials and stored at 4°C.

Once cleaned from their soft tissues, valves were extensively rinsed with de-ionized water and leaves under ultrasounds to remove sediments particles before a final drying at room temperature. The sampling of the two aragonitic components of the shell (prismatic and nacreous layers) was carried out after the removal of the periostracum surrounding shelf using an acid cleaned scalpel, by scraping, less than one millimeter off, from the edge toward the umbo on the maximum-growth axis. Recovered carbonate powders (5 to 20 mg) were dried, weighted and dissolved in acid-cleaned PFA beakers with 2 ml of 5% double-distilled HNO_3 and 2% ultra pure H_2O_2 solution at 80°C for 6 hours. Dissolved samples were then transferred in acid-cleaned HDPE storage bottles and stored at 4°C.

2.3.5.3 Certified reference materials

In addition to field samples, a series of representative certified reference materials were chosen to reproduce the diversity of matrices considered. It includes a seawater reference standard (CASS-4, National Research Council, Canada), an oyster tissue (SRM 1566) and also two marine biogenic aragonites, a coral *Porites sp.* (JCp-1, Geological Survey of Japan) and a giant clam *Tridacna gigas* (JCt-1). These different standards were processed in parallel with the samples, following the same procedures as described above, and with comparable sample amounts; 100-200 μl for certified seawater CASS-4, ~50 mg of oyster tissue SRM 1566 and ~20 mg of calcium carbonates JCp-1 (coral) and JCt-1 (giant clam).

2.3.6 δD in the organic matrix of biocarbonates

The general principle of δD analysis consists in assessing the deuterium signature of lipid compounds of the shell organic matrix. We analyzed mussel shells collected along the salinity gradient of the Scheldt estuary. In addition to shell sampling, sediments were collected from the same locations as the bivalves. The extraction procedure for the sediments is the same as for the shells (described before).

2.3.7 Modern and archeological bivalve shells as indicators of past climate

2.3.7.1 Mytilus edulis from Belgian archeological deposits

The shell chemistry of *Mytilus edulis* in relation to environmental variability has been well studied (Freitas et al., 2008; Gillikin et al., 2008; Wanamaker et al., 2008a). In the Scheldt estuary it has been demonstrated that oxygen ($\delta^{18}O$) and carbon isotope ratios ($\delta^{13}C$) and trace element compositions of the shell can serve as proxies for salinity and temperature (Gillikin et al., 2006a; Gillikin et al., 2006b; Wanamaker et al., 2007). Application of these proxies to shells from archaeological finds will yield information on past discharges of the Scheldt, estuarine dynamics and human influence in the river basin. Archaeological samples of *M. edulis* were collected from Middelburg (Roman age), Veere (Roman age and 5th century), Brugge and Oostkerke (13th, 14th, 15th, 17th, 18th and 19th century). We analyzed $\delta^{18}O$, $\delta^{13}C$ of the shells and $\delta^{15}N$ of the shell organic matrix (EA-IRMS).

2.3.7.2 Mytilus trossulus from the Arctic region

The Greenland ice cap (GrIC) is the world second largest ice mass. Current global warming causes accelerated melting, resulting in increased runoff since the early 1990's. Complete loss of the GrIC will result in a global sea level rise of ~7 m. Therefore it is crucial to gain insight in the dynamics of the GrIC through time. Instrumental data for Greenland cover the last few decades. Modeling studies investigate the natural variability in ice cap mass balance before that time, and under the influence of future global warming. Proxy data are crucial for the validation of these models. Since glacial meltwater has very low oxygen isotope ($\delta^{18}O$) values of -30 to -20 ‰, we expect variations in meltwater runoff to be distinguishable in $\delta^{18}O$ values of coastal water.

Blue mussels of the genus *Mytilus* have been demonstrated to be faithful recorders of environmental variability (e.g. temperature, salinity) in the chemical composition of their shell. Although most work has been done on *Mytilus edulis*, this is also true for *M. trossulus*, (Klein et al., 1996b; Rainbow et al., 2000b). Other bivalves have been demonstrated to be indicators of meltwater input. *M. trossulus* is the abundant *Mytilus* species in the Arctic and enables us to study high-latitude environmental variability under the influence

of current and past climate changes. *M. trossulus* reaches an age of >20 years and as such can record possible decadal scale runoff variability.

We aimed to evaluate *M. trossulus* shell chemistry as a proxy for past Greenland meltwater runoff. Research questions were:

- Do the apparently annual ridges on the shell correspond to yearly growth cycles?
- Can we distinguish between years of low and high meltwater runoff based on $\delta^{18}O$ records of the shells?
- Can we distinguish between shells of low runoff and high runoff time intervals?
- What can $\delta^{13}C$ and trace element records from these shells tell us about past environmental variability?

To answer these questions, different specimens of *M. Trossulus* were obtained:

- From Disko Bay (West Greenland) sampled in 2008;
- From Angmaksalik (East Greenland) sampled in 1933;
- From Spitsbergen sampled in 2007.

The different shells were analyzed $\delta^{18}O$, $\delta^{13}C$ and trace elements by LA-ICP-MS.

2.3.7.3 Anadaria senilis from Western Africa

The West African blood cockle (*Anadaria senilis*) is the most abundant bivalve in both numbers and biomass on the tidal flats of Banc d'Arguin (Mauritania). Due to its heavy shell it has few natural predators. It has however been used for human consumption for a long time. Land inwards of Banc d'Arguin hundreds of Neolithic shell middens, containing *A. senilis*, are present, usually associated with palaeo-coastlines (Barusseau et al., 1995). Human occupation of the area lasted from about 5000 BP to 2700-2600 BP. Abandonment of the settlements is associated with a climate shift towards the modern desert regime (Barusseau et al., 2007). Although some authors have used *A. senilis* in biomonitoring, studying heavy metal contents of the soft tissues (Joiris and Azokwu, 1999; Joiris et al., 1998; Otchere, 2003), so far no studies of its shell chemistry are known. It has been demonstrated that translucent growth lines in *A. senilis* occur yearly (Van der Geest, pers. comm). Combined with the life span of up to 30 years, this species offers great potential for palaeoclimatic reconstructions.

Chemistry of archaeological shells probably opens a window to early-to-mid Holocene "green Sahara" climate and conditions of abandonment of human settlements (Zühlsdorff et al., 2007).

From *A. senilis* shell chemistry, different questions can be addressed:

- Do $\delta^{18}O$ values show a seasonal pattern? What causes such a pattern, since both temperature and salinity are relatively constant in this environment?
- Do $\delta^{13}C$ values show a seasonal pattern? Can we link $\delta^{13}C$ values to environmental variability like primary productivity?
- What can trace element records tell about the environment the shell lived in?

For this purpose, modern and archaeological samples from the Banc d'Arguin (Mauritania) were analysed for $\delta^{18}O$ and $\delta^{13}C$ and trace elements with LA-ICPMS.

2.4 Analytical procedures

2.4.1 Elemental analysis

Elemental analyses were performed using Inductively Coupled Plasma Optical Emission Spectrometer (ICP-OES) and High Resolution Inductively Coupled Plasma Mass Spectrometer (HR-ICP-MS). ICP-OES was used to determine concentrations of Na, Mg, K, Ca, S and Sr in the different matrices concerned by the project (seawater, carbonates, soft tissues and biological fluids). With detection limits in the range of ng/g, ICP-OES was used for most of samples showing concentrations in the range of µg/g or down to sub µg/g. For more diluted samples and also to determine trace elements (Li, B, Cr, Mn, Fe, Cu, Zn, As, Mo, Cd, Sn, Ba, Pb occurring at low concentration levels, the HR-ICP-MS with consistently lower detection limits (pg/g to fg/g) was used.

Sample solutions were introduced in the plasma in 1 to 2% HNO_3 with In as an internal standard. Calibration was performed using external calibration curve with standards prepared from a mixture of mono-elemental and multi-elemental standard solutions and diluted to match the concentrations of the samples. Precision and accuracy of the methods were evaluated using matrix-matched Reference Standard Materials: Seawater (CASS-4), riverine water (SLRS-4), biogenic carbonates (JCt-1, Giant Clams and JCp-1, Corals) and organic tissues (NIST1566, Oyster tissue).

The general precisions measured during the project varied from one element to another but were on average between 2 to 5% for major elements (Na, Mg, Ca, Sr), 5 to 10% for minor and trace elements.

2.4.2 LA-ICP-MS

Installed in September 2008, the new Laser Ablation ICP-MS (LA-ICP-MS) system consists of a fast-eXcimer laser (UP193FX, New Wave Research) coupled to a Quadrupole ICP-MS (Thermo, X Series). The short pulse laser allows different sampling strategies; discrete analyses using single ablation spot and continuous analyses with an ablation line over a distance interval. The Laser is online with a quadrupole ICP-MS. The fast scanning capability, enhanced ion transmission and low oxide formation of the ICP-QMS have drastically increased the number of elements to be determined with Li, B, Mn, Fe, Cu, Zn, As, Mo, Cd and La now accessible, and also the reliability of well-studied elements (Mg, Sr, Ba, Pb and U). Example of LA-ICPMS performances is given in Figure 6 for the MACS-1 carbonate reference material developed by S. Wilson of the USGS. The data were acquired using Ca as an internal standard to account for sensitivity variations associated to ablation, ionization and ion transfer into the mass spectrometer.

MACS-1 Ref Standard
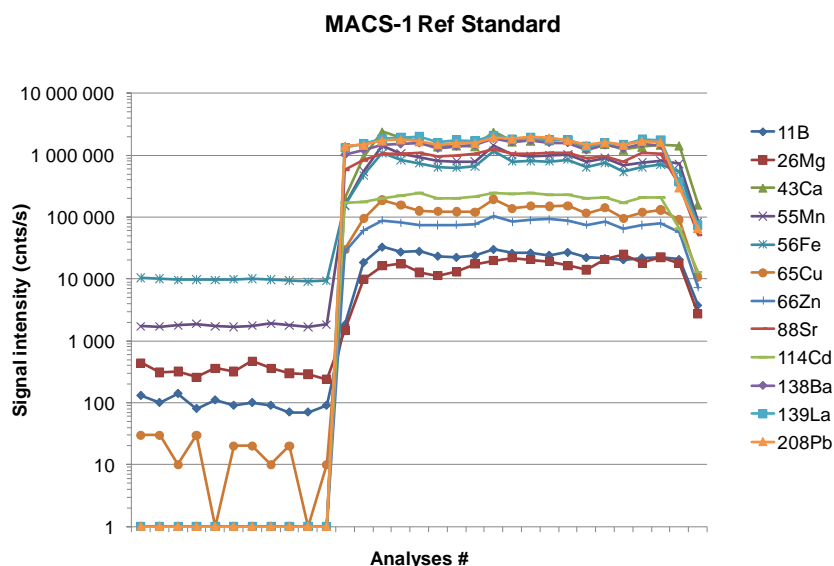
Figure 6. Measured signal intensities by LA-ICP-MS for B, Mg, Ca, Mn, Fe, Cu, Zn, Sr, Cd, Ba, La and Pb in MACS-1 pressed powder carbonate standard. The first part of the graph shows gas blanks performed online with the ablation cell and then once the ablation start signal intensities were monitored along 200 µm continuous path. Each data point represents an integration (dwell) time fixed to 100 ms and the sampling resolution is 11.7 µm per analysis.

Calibration of the system after daily optimization of signal beam intensities were done using NIST 612 and NIST 614 glasses (Table I), allowing a two points' calibration curve. The MACS-1 carbonate was used as an unknown for accuracy check for available certified elements (Table II).

	Concentrations (µg/g)		
	NIST 614	NIST 612	MACS-1
Li	1.7	42	-
B	1.3	35	25.3
Mg	35	77	10
Ca	83643	85214	393000
Mn	1.4	38	118
Fe	13.3	56	162
Cu	1.4	37	124
Zn	2.2	38	123
As	0.7	37	-
Sr	45	76	219
Mo	0.8	38	-
Cd	0.6	28	117
Ba	3.2	38	114
La	0.8	36	126
Pb	2.3	39	121
U	0.8	37	-

Table I. Certified concentrations of elements (ppm) in the reference standards used for LA-ICP-MS; NIST 612 and 614 are glasses and MACS-1 is a carbonate powder.

Precision of the measurements were estimated with optimized operating conditions (Table II) and ranged from 5% for (Mg/Ca, Sr/Ca, Ba/Ca, Pb/Ca and U/Ca) to 10% for low abundance elements like Zn/Ca, Mo/Ca or La/Ca.

LA-ICPMS Operating conditions:

Thermo Scientific X-Series 2 ICP-MS

Forward Power :	1400 W
Cool Ar flow rate :	13.0 l/min
Auxiliary Ar flow rate :	0.80 l/min
Nebuliser Ar flow rate :	0.70 l/min
Carrier gas He flow rate :	0.650 l/min
Pole Bias :	-1
Hexapole Bias :	-4
Oxide production (ThO/Th) :	0.1-0.2 %
Dwell time :	100 ms
Acquisition mode :	TRA (Time Resolved Analysis)
Detector mode :	Dual (pulse and analogue counting)

ESI New Wave UP-193FX Fast Excimer ArF

Wavelength :	193 nm
Pulse length :	4 ns
Irradiance :	2 GW/cm^2
Fluence :	10 J/cm^2
Output energy :	60 % (Energy : 8 mJ)
Repetition rate :	40 Hz
Spot size :	50 µm (preablation : 100 µm)
Scan speed :	15 µm/s (preablation : 30 µm/s)
Ablation mode :	continuous, line

Table II. Operating conditions of the LA-ICPMS for carbonate sample determination

2.4.3 Isotopic analysis

2.4.3.1 $\delta^{13}C$-$\delta^{18}O$ of carbonates

The Kiel III is an automated carbonate preparation device that works using the method originally outlined by McCrea in 1950. Briefly, carbonates are reacted with 100 % phosphoric acid at 70 °C for six minutes, and are then cryogenically purified using liquid nitrogen. The reaction of phosphoric acid with CaCO3 produces solid calcium hydrogen phosphate, water, and carbon dioxide through the following chemical reaction:

CaCO3 + H3PO4 → CaHPO4 + H2O + CO2

The standards used for correction in our laboratory are MAR1 then MAR2, produced by the University of Ghent, Belgium. The NBS-19 standard was run to check for accuracy (Table III).

	NBS 19		MAR 1		MAR 2	
	$\delta^{13}C$	$\delta^{18}O$	$\delta^{13}C$	$\delta^{18}O$	$\delta^{13}C$	$\delta^{18}O$
Referenced value	1,95	-2,20	-	-	-	-
Measured	2,03	-2,20	1,96	-2,81	3,47	-0,05
Std Dev	0,12	0,08	0,09	0,09	0,06	0,13
N	28	28	9	9	29	29

Table III. Average values and standard deviations for reference materials used during the period 21/08/08 and 15/09/08.

2.4.3.2 $\delta^{13}C$ and $\delta^{15}N$ of organic material

Dry tissues were homogenized using an agate mortar and pestle. Briefly, one mg of homogenized tissue was subsampled and placed in a silver cup (5 x 12 mm). The sample was then decalcified by adding a few drops of dilute HCl in situ, after which the sample was dried for 24 hours at 60 °C and folded closed. Samples were analyzed for $\delta^{13}C$ with an Element Analyzer (Flash 1112 Series EA ThermoFinnigan) coupled via a CONFLO III to an IRMS (Delta^{plus}XL, ThermoFinnigan). Sucrose was used as a standard (IAEA-CH-6, $\delta^{13}C$ = -10.4 ± 0.1 ‰). Results are reported using the conventional δ notation relative to the VPDB standard. The analytical precision of the method is on the order of 0.1 ‰. Using this same instrument and method, previous studies report a long term analytical precision of 0.08 ‰ on 214 analyses of the IAEA-CH-6 standard (1σ).

2.4.3.3 Water $\delta^{18}O$

Water samples for $\delta^{18}O$ ($\delta^{18}O_W$) analysis were taken by filling 100 ml polyethylene containers and adding 60 µl of supersaturated $HgCl_2$ solution (7 g per 100 ml). Containers were capped tightly and wrapped with Parafilm to avoid evaporation and were stored at room temperature. All water $\delta^{18}O$ was measured using the CO_2 equilibration technique (Epstein and Mayeda, 1953). The procedure for measuring $\delta^{18}O_W$ is modified from (Prosser et al., 1991), where equilibration and gas extraction is done directly in a headspace vial. Ten ml headspace vials were first flushed with He gas and are capped with a rubber septum and aluminium seal. Approximately 500 µl of sample water was injected into the vial, then 200 µl of pure CO_2 from a tank was injected using a gas tight syringe. The samples were then placed in a shaker for 2 hours and left to equilibrate for about 24 hours for freshwater and more than 48 hours for seawater at ambient laboratory temperature (± 23 °C). In addition to samples, two in-house well-calibrated (against VSMOW, GISP and SLAP)

secondary standard water samples were similarly processed (a seawater (SW1) and tap water (TAP0409) standard; see (Gillikin et al., 2006b). After equilibration, 1000 µl of CO_2 from the headspace is drawn into a gas tight syringe and is injected into the carrier gas stream after the combustion columns of a ThermoFinnigan Delta[plus]XL continuous flow IRMS. Precision was better than 0.15 ‰ (1σ), determined by repeated analysis of the seawater standard and replicate sample analyses.

2.4.3.4 $\delta^{13}C$ of dissolved inorganic carbon

Water samples for determination of $\delta^{13}C$ of dissolved inorganic carbon (DIC) were sampled by gently over-filling headspace vials (25, 20, 10 or 6 ml) with seawater (Gillikin and Bouillon, 2007). Sixty µl of supersaturated $HgCl_2$ solution was added and the vials were capped and stored at room temperature until analysis. A method slightly modified from (Salata et al., 2000) was used for $\delta^{13}C_{DIC}$ analysis. A headspace was created by inserting an empty, fully depressed, syringe and needle through the septum, then inserting a needle attached to a He bottle, until the required volume of water has been replaced. After the He syringe is removed, the pressure is equalized in the other syringe. Once the headspace is created, 99 % phosphoric acid was added. Samples were shaken, and placed on their side or turned upside down so that there is no contact between headspace and septum to reduce the possibility of exchange with atmospheric CO_2. Samples were allowed to equilibrate for one day in a sample shaker.

To correct for the partitioning of CO_2 between headspace and the water phase and to calculate the $\delta^{13}C$ of the total DIC, the equation of (Miyajima et al., 1995) was used:

$$\delta^{13}C_{DIC} = \frac{V_{headspace} * \delta^{13}C_{measured} + \left(V_{bottle} - V_{headspace}\right) * \beta * (\delta^{13}C_{measured} + \varepsilon_g^a)}{V_{headspace} + \left(V_{bottle} - V_{headspace}\right) * \beta}$$

where β = 0.872 at 23° C (ostwald solubility coefficient) and ε_g^a is calculated from e = -373/T + 0.19 thus ε = -1.07 at 23° CV_{bottle} and $V_{headspace}$ = internal volume of sampling vial and headspace volume, respectively. These data were further corrected using calibrated CO_2 gas (from a tank), which is injected periodically throughout the analysis period. Typically, the standard deviation of this gas was less than 0.2 ‰ for the day.

2.4.3.5 GC-c-IRMS

$\delta^{13}C$ specific compounds were measured on an Agilent 6890A GC with GC Combustion III interface. A DB5 30m column was used. The oven was held for 2 min at 50°C then heated at 4°C/min to 300°C where the final temperature was held for 15 min. The $\delta^{13}C$ value of the compounds is obtained using a well calibrated CO_2 reference gaz. A mix of 4 pure compounds (alkane C15, C20, C25 and C30) previously calibrated via Elemental Analyser-IRMS (using IAEA-CH6 as a reference) shows that the offset on the $\delta^{13}C$ is < 0,3‰ (see Table IV).

	GC-c-IRMS	EA-IRMS	Δ
C15	-28,31	-28,21	0,10
C20	-29,605	-29,36	0,25
C25	-29,998	-29,99	0,01
C30	-33,084	-32,82	0,26

Table IV. $\delta^{13}C$ composition of 4 alkanes as determined by GC-c-IRMS and EA-IRMS

2.4.3.6 EA-TC-IRMS

The deuterium isotopic compositions were determined in the Marine Organic Biogeochemistry lab. at Royal NIOZ (The Netherlands), under the direction of S. Schouten and M. van der Meer. The EA-TC-IRMS (Thermo) allows the production of H2 from the organic molecules (or water) at 1440°C using glassy carbon as catalyst. The IRMS is a Thermo delta plus XL. The H3 factor is determined before each series of analyses in order to correct for the presence of H3+ ions. The samples were weighed in silver cups to obtain the appropriate quantity to yield about 1V of amplitude for m/z=2 (i.e., around 50 µg of pure material). Standards used were NBS 22 and IAEA-CH7 (Table V). Instrumental precision is ±5‰.

	NBS 22	IAEA-CH7
Reference value	-118,50	-100,30
Measured value	-112,74	-99,41
Average	5,57	2,42
Number	49	18

Table V. δD value for reference materials as obtained during week of Aug. 24, 2009

2.4.3.7 Mg isotopes

Sample purification

The reliable determination of Mg isotopic ratios using MC-ICP-MS requires the use of purified sample solutions to minimize instrumental mass bias created by Ar-plasma-interfering species (Galy et al., 2001). Adapted from (Chang et al., 2003), all chromatographic separations were performed with a cationic-exchange resin (AG50W-X12, 200-400 mesh, H^+ form, Bio-Rad) using a two-column procedure allowing a full Mg purification from matrix-derived elements Na, K, Ca and Sr together with a complete recovery (> 99.9%).

The resin is first cleaned by successive agitation and settling, 3 times with 6M HCl and water, followed by 3 times with water alone. At each step, fine particles are removed with the liquid and the resin is finally stored in water. Polyethylene columns are packed with 2 ml of pre-clean resin and washed with 10 ml of 6M double-distilled HCl, followed by 10 ml of 1M Suprapur HF, repeated three time. Each column was calibrated using synthetic standard solution containing Na, Mg, K, Ca and Sr and prepared from mono elemental solutions. As illustrated in Figure 7, a two-step procedure was developed to ensure a full Mg purification.
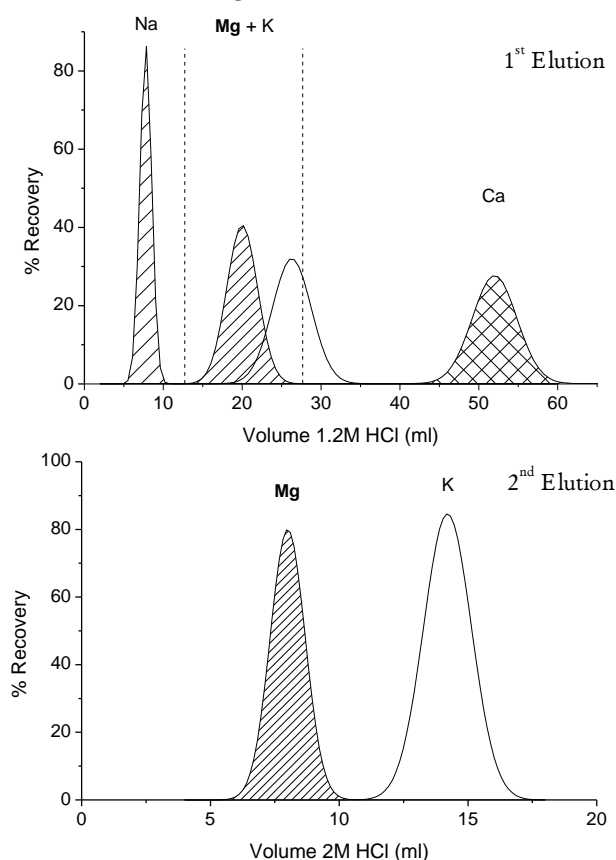

Figure 7. Calibration chromatogram of Mg solid-phase extraction using cationic-exchange resin AG50WX12. The 1st elution is performed with 1.2M HCl and allows the complete separation of Na, Ca and Sr (eluted after Ca, not shown) from the Mg+K fraction. For the 2nd elution, the Mg fraction is further cleaned from the remaining K using 2M HCl.

For the first elution, the resin is conditioned with 5 ml of 1.2M double-distilled HCl and the sample is loaded in 0.5 ml of 1.2M HCl. After 1 ml wash with 1.2M HCl, the Na fraction is eluted with 11 ml of 1.2M HCl, followed by the Mg+K fraction, obtained with 16 ml of 1.2M HCl. After this fraction, 1 ml is further eluted to systematically check the absence of Mg and to prevent from any changes in retention volume due to the ageing of the resin. Once collected, the Mg+K fraction is dried down and re-dissolved in 2M HCl for the second step. Before the second elution, columns are first rigorously cleaned with 10 ml of 10M HCl, followed by 10 ml of 6M HCl and 5 ml of water, and then conditioned with 5 ml of 2M HCl. The samples are loaded in 0.5 ml 2M HCl and wash with 2 ml before the collection of the Mg fraction with 9 ml. As for the 1st column, one final ml is eluted for quality control. All fractions obtained were dried down and re-dissolved in 2% HNO_3 for quantitative and isotopic analysis. The concentrations of Na, Mg, K, Ca and Sr were determined by ICP-OES and/or HR-ICP-MS, and allowed the full-Mg yield (> 99.9%) to be systematically checked for each sample. Total blank contributions for the whole procedure appear to be negligible, evaluated to 0.15 ng for Mg and < 0.5 ng for Na, Ca and Sr. They represent less than 0.1% of the minimum Mg mass processed for the low-size samples (~1 µg).

Mass spectrometry

Mg isotopic ratios were determined using a Nu Instruments plasma source mass spectrometer coupled to an ARIDUSII desolvation unit (Cetac™). Samples, transferred by a self-aspirating PTFE nebulizer (100 µL/min) into a heated spray chamber (110°C) followed by a hot desolvation membrane (165°C) were introduced in the plasma in the form of dry aerosol. Three Mg isotopes were simultaneously collected using 3 Faraday collectors (out of 12) with 10^{11} Ω resistors in Low-Resolution ($\Delta M/M > 300$) entrance slit settings. Dry plasma mode combined with a high-efficiency interface pump (Big 80) greatly enhanced the sensitivity of the MC-ICP-MS and allowed working with a low Mg concentration (50 to 100 ng/g) for a signal intensity of 8 V for ^{24}Mg. Data were acquired in static mode with 4 blocks of 10 ratios over 10 s integration time. Relative instrumental errors (2σ) associated to an isotopic ratio measurement average (N=200) at 0.004 ‰ (95% confidence interval) for both isotopic ratios.

For samples, measurements were carried out with a standard-sample bracketing method, in order to minimize mass discrimination effect and instrumental mass bias induced by the MC-ICP-MS (Galy et al., 2001). Just before the analysis, samples were adjusted to the same concentration as the standard (± 10%) and acidified at 1% with double-distilled HNO_3. Between standards and samples, the system was cleaned from memory effects using milliQ water for 30 s, then 5% HNO_3 for 30 s and finally 1% HNO_3 for 4 minutes. Cleaning efficiency was checked by monitoring the background intensity observed on the most abundant isotope (^{24}Mg) which was on average less than 10 mV. The results are reported in the conventional delta notation as $\delta^{26}Mg$ and $\delta^{25}Mg$, the permil deviation of the measured 26Mg/24Mg and 25Mg/24Mg ratios of samples against the reference standard DSM3 (Galy et al., 2003):

$$\delta^x Mg = \left(\frac{\left({}^xMg / {}^{24}Mg \right)_{sample}}{\left({}^xMg / {}^{24}Mg \right)_{DSM3}} - 1 \right) \times 1000 \text{ (with x = 26 or 25)}$$

Data precision

The precision of Mg isotopic ratios was estimated at 95% confidence interval by considering a combined expanded uncertainty U_c composed of three contributions: counting uncertainty U_{cnt}, uncertainty associated to the mass drift between bracketing standards U_{drift} and measurement reproducibility U_{rep} deduced from replicates analysis.

The uncertainty terms U_{cnt} and U_{drift} were available for each $\delta^{26}Mg$ and $\delta^{25}Mg$ value. U_{cnt} expressed as relative standard deviation (in permil) was estimated by error propagation law as follows:

$$U_{cnt}(\delta \, ^xMg) = k \times 1000 \times \sqrt{\left(\frac{\sigma_{R_{x,std1}}}{R_{x,std1}} \right)^2 + \left(\frac{\sigma_{R_{x,std2}}}{R_{x,std2}} \right)^2 + \left(\frac{\sigma_{R_{x,sple}}}{R_{x,sple}} \right)^2}$$

With x = 26 referring to $^{26}Mg/^{24}Mg$ and x = 25 to $^{25}Mg/^{24}Mg$.

The coverage factor k = 2 was used for 95% confidence interval estimate. $\sigma(R_{x,sple})$, $\sigma(R_{x,std1})$ and $\sigma(R_{x,std2})$ were the instrumental standard errors (n = 40 measured isotopic ratios) for the sample ($R_{x,sple}$) and the two standards ($R_{x,std1}$ and $R_{x,std2}$). $\sigma(R_{x,std})$ and $\sigma(R_{x,sple})$ ranged from $6.7 \cdot 10^{-7}$ to $4.3 \cdot 10^{-6}$ (average $1.6 \cdot 10^{-6}$, n = 295) for $^{26}Mg/^{24}Mg$ and from $6.3 \cdot 10^{-7}$ to $2.3 \cdot 10^{-6}$

(average 1.3 10^{-6}, n = 295) for $^{25}Mg/^{24}Mg$. The estimated counting uncertainty U_{cnt} varied from 0.02 to 0.08 ‰ (average = 0.03 ‰, n = 135 brackets) and from 0.02 to 0.06 ‰ (average = 0.03 ‰, n = 135 brackets) for $\delta^{26}Mg$ and $\delta^{25}Mg$, respectively.

The component U_{drift} which accounted for the error introduced by the mass bias between two bracketing standards was evaluated by non-statistical approach considering $R_{x,std1}$ and $R_{x,std2}$ the limits of the interval containing the extrapolated standard isotopic ratio $R_{x,std}$ at the time of sample determination. Assuming a uniform (rectangular) probability distribution of $R_{x,std}$ within this interval, U_{drift} expressed as relative standard deviation (in permil) was approximated at 95% confidence interval (k = 2) as follows:

$$U_{drift}(\delta\ ^{x}Mg) = k \times 1000 \times \frac{\left| R_{x,std2} \middle/ R_{x,std1} - 1 \right|}{2\sqrt{3}}$$

The observed ranges for U_{drift} were 0.001 to 0.16 ‰ (average 0.05 ‰, n = 320 brackets) and 0.001 to 0.09 ‰ (average 0.03 ‰, n = 125 brackets) for $\delta^{26}Mg$ and $\delta^{25}Mg$, respectively.

The reproducibility component U_{rep} was expressed as relative standard deviation (in permil at 95% confidence interval) of the mean $\delta^{26}Mg$ and $\delta^{25}Mg$ values obtained for n replicates (with n > 2). For non-purified in-house mono-elemental Mg standard (Alfa Aesar, Johson Matthey Company) U_{rep} was 0.09 and 0.05 ‰ (n = 40) for $\delta^{26}Mg$ and $\delta^{25}Mg$ and represented the long-term measurement repeatability over three years. For standards and samples processed through chemical purification, U_{rep} in $\delta^{26}Mg$ and $\delta^{25}Mg$ were 0.05 and 0.03 ‰ (n = 3) for purified DSM3, 0.05 and 0.02 ‰ (n = 11) for seawater CASS-4, 0.10 and 0.05 ‰ (n = 15) for aragonitic coral JCp-1, 0.09 and 0.06 ‰ (n = 3) for aragonitic clam JCt-1 and 0.04 and 0.03 ‰ (n = 3) for Oyster tissue SRM 1566. For the samples U_{rep} was evaluated only when n > 2 and ranged from 0.04 to 0.13 ‰ and from 0.02 to 0.09 ‰ in $\delta^{26}Mg$ and $\delta^{25}Mg$, respectively. The similar U_{rep} obtained for non-purified in-house standard, matrix-matched standard reference materials and samples suggested that the main error source was linked not to sample preparation protocol and/or sample heterogeneity but more to the variable instrumental mass bias of the MC-ICP-MS.

From Figure 8 which presents $U(\delta^{26}Mg)$ versus $U(\delta^{25}Mg)$ for the three uncertainty components considered (U_{cnt}, U_{drfift} and U_{rep}), pronounced correlations can be observed (R^2 of 0.70 to 0.79) together with mass-dependent-like relationship (slope of 0.499 to 0.554). The final estimate of the combined uncertainty U_c (in permil at 95% confidence interval) was performed following Root-Sum-Square (RSS) method with the three contributions evaluated above as follow:

$$U_c(\delta\ ^xMg) = \sqrt{\overline{U_{cnt}(\delta\ ^xMg)^2} + \overline{U_{drift}(\delta\ ^xMg)^2} + U_{rep}(\delta\ ^xMg)^2}$$ where x refers either to 26 or 25.

With $\overline{U_{cnt}(\delta\ ^xMg)}$ and $\overline{U_{drift}(\delta\ ^xMg)}$ the average counting and mass drift uncertainty of n values. For samples with n < 3, the maximum U_{rep} obtained for the standard reference material JCp-1 (0.050 and 0.024 ‰) was conservatively applied. Finally, the chromatographic separation was also positively tested by processing 10 µg of Mg of DSM3 standard. No significant isotopic shift was observed compared to the non-purified standard ($\delta^{26}Mg = 0.04\pm0.05$‰, $\delta^{25}Mg = 0.02\pm0.05$‰) confirming the integrity of overall procedure.
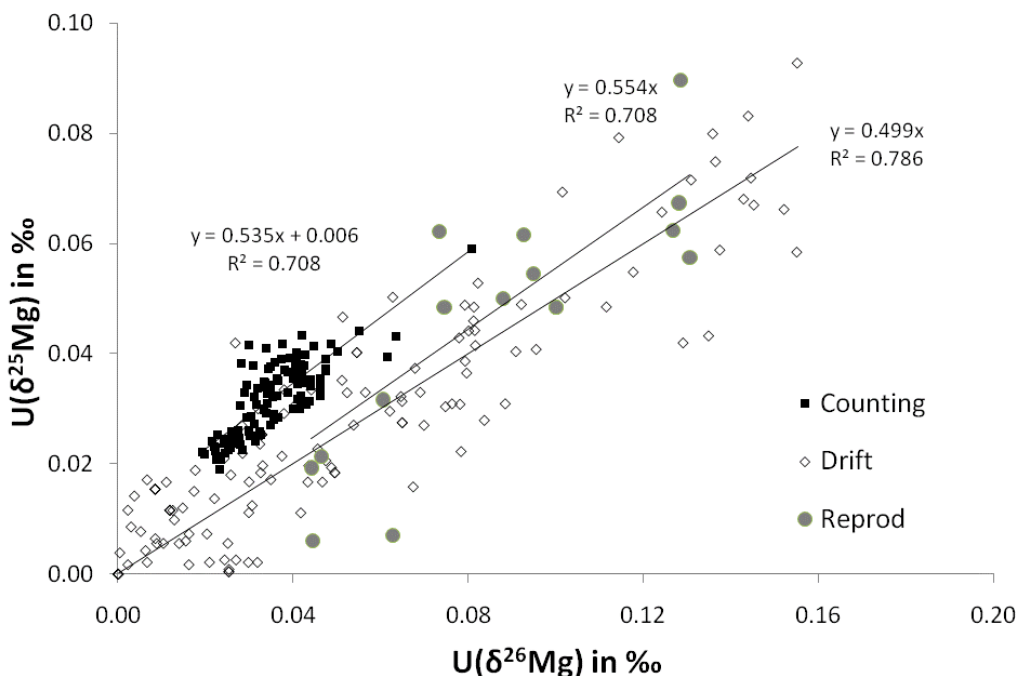

Figure 8. Comparative plot of the uncertainty components (Counting, mass drift and reproducibility) associated to Mg isotopic ratios determination.

2.4.3.8 δD in the organic matrix of biocarbonates

All results for deuterium were obtained with an EA-TC-IRMS at Royal NIOZ with the collaboration of S. Schouten and M. van der Meer (training in the framework of the ESF Paleosalt project).

2.4.4 Specific organic compounds

2.4.4.1 GC-MS

Specific compounds present in the total lipid extract were identified by GC-MS. We used a Trace GC Ultra with Trace MS Plus GC/MS combination. The GC column was a CPSil 8 30m (nonpolar). The temperature program consisted in increasing the temperature from 50°C (2min) to 300°C (15°C) with a gradient of 4°C/min. The lipids were identified based on retention times, comparison with pure compounds and the mass spectrum of the compounds using the NIST 2005 lipid library.

2.4.5 Ancillary measurements

For the echinoderm juvenile growth experiment, temperature, salinity and pH were measured using a WTW Multi 340i multi-meter equipped with a conductivity cell and a pH electrode. These measurements were performed daily for temperature and salinity and twice a week for the pH. Temperature was also logged at 6-hours intervals with Stow Away Tidbit temperature loggers (Onset) as a control. Nitrites and nitrates were measured using Tetra ready-to-use tests.

2.5 Modeling and data processing

2.5.1 Uptake and accumulation model in the blue mussel Mytilus edulis

The basic model depicts the organism as a two compartmental or three compartmental structures. More complex models can be developed but this is generally not needed for the current purposes. The organism is described as consisting of a central compartment through which exchanges with the environment from water or food take place (Van Campenhout et al., 2009). This compartment exchanges material with a peripheral compartment which represents the more slowly exchanging pools.

The shell compartment is represented by a (uni-directional) flux from the central to the shell compartment (Blust, 2001). In case that element uptake and elimination kinetics in the soft tissue can be described by a one compartmental model then the peripheral compartment may represent the shell tissue. The model is schematically represented in Figure 9.
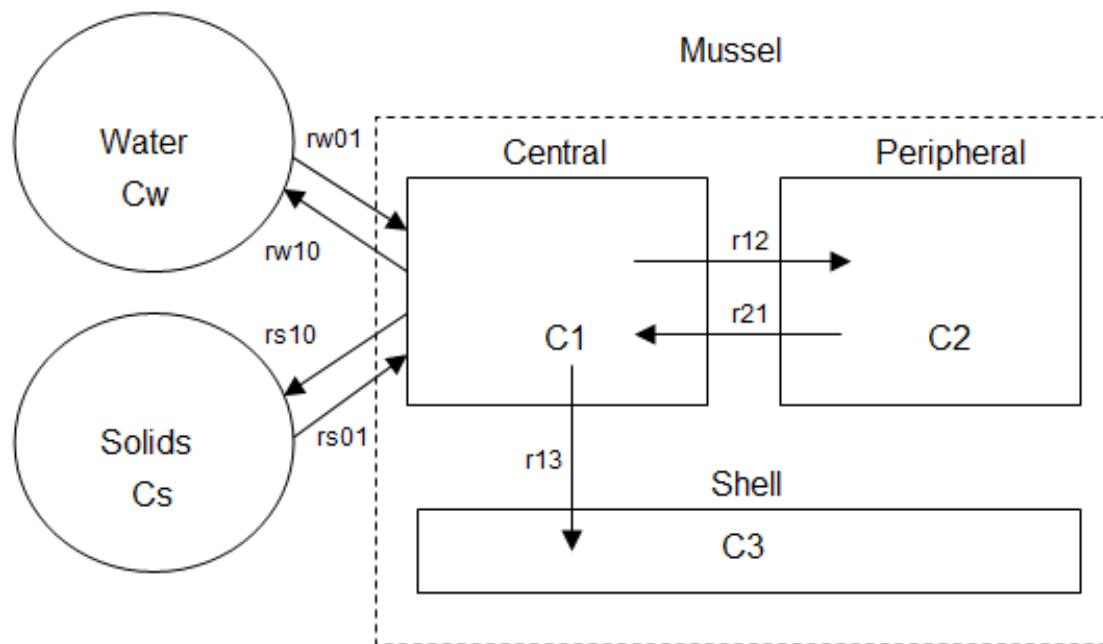

Figure 9. Two and three compartmental models for the uptake and accumulation of metals from water and solids (particles and food) in a bivalve.

The uptake of metals from water can be described by a linear or hyperbolic relationship between the concentration in the organism (C0) and uptake rate constant from solution (r01) multiplied by the water concentration (Cw).

$$C_0 = r_{01} \int C_w dt$$

The kinetic parameters describing internal exchanges and elimination from the central compartment can be by two exponential loss terms.

$$C_0 = C_1 e^{-k_1 \cdot t} + C_2 e^{-k_2 \cdot t}$$

In which C1 is the concentration in he central compartment and C2 in the peripheral compartment at the onset of the elimination period. It can be shown that the rate constants in figure X are related to k1 and k2 according to.

$$r_{21} = \frac{C_1 k_2 + C_2 k_1}{C_1 + C_2}$$

$$r_{12} = k_1 + k_2 - r_{21} - r_{10}$$

$$r_{10} = \frac{k_1 k_2}{r_{21}}$$

The bioconcentration factor for accumulation from solution is given by:

$$BCF = \frac{C_o}{C_w} = \frac{r_{01}}{k_1 k_2}(k_1 + k_2 - r_{10})$$

and the bioaccumulation factor for accumulation from solid material is given

$$BAF = \frac{C_o}{C_s} = \frac{AE \cdot IR}{k_{1,s} k_{2,s}}(k_{1,s} + k_{2,s} - r_{10,s})$$

Combination of these two terms allows determining the relative importance of the two sources in overall element accumulation by the mussels. In case of a one compartmental soft tissue model the peripheral compartment becomes equivalent to the shell tissue and the term r21 is set equal to zero. In case of a two compartmental soft tissue model an additional shell compartment has to be considered and an additional rate constant r13 included. It has to be noted that the rate constants are not true constants but parameters that may change in relation to environmental factors such as temperature influencing the rate of transport and other processes such as growth.

The uptake from water or food, the internal compartmentalisation and transfer to the shell and elimination from the soft tissue are described in terms of membrane transport processes (i.e. Michaelis-Menten kinetics). The model is kept as simple as possible without losing physiological realism (i.e. tissues are presented by a limited number of kinetic pools). The model is developed using SAAMII modeling software developed by the University of Washington at Seattle. After complete parameterisation of the model it is possible to

simulate, on the basis of mechanisms, the effects of changes in temperature, salinity and food availability on the uptake and accumulation of the minerals considered. The relative importance of water and food as sources of mineral accumulation in the soft tissues and transfer to the shells can be determined under variable conditions.

2.5.2 The elimination of a bias: averaging-errors in proxy records

Processing solid substrates to assess the incorporated proxies, involves the sampling of the accreting substrate (e.g. the carbonate of a shell, coral, or other) along its growth or accretion axis. Whether sampling means drilling a hole or counting a proxy per square meter, the sample always has a certain volume (the volume of the drill hole or the count space). As a consequence, a sample will give the mean value of the proxy over a corresponding volume. To our knowledge, the volume of the sample has always been neglected to date. However, this is only applicable when the width of the sample is small with respect to the variation that needs to be reconstructed. Researchers choose the smallest possible samples intuitively; however, working close to the detection limit will lower the signal-to-noise ratio, and thus the accuracy of the measurement. On the other hand, when the width of the sample covers a considerable part of the variation, the signal will be averaged and the variations will systematically be underestimated. This is exemplified in a simulation, shown in Figure 10.
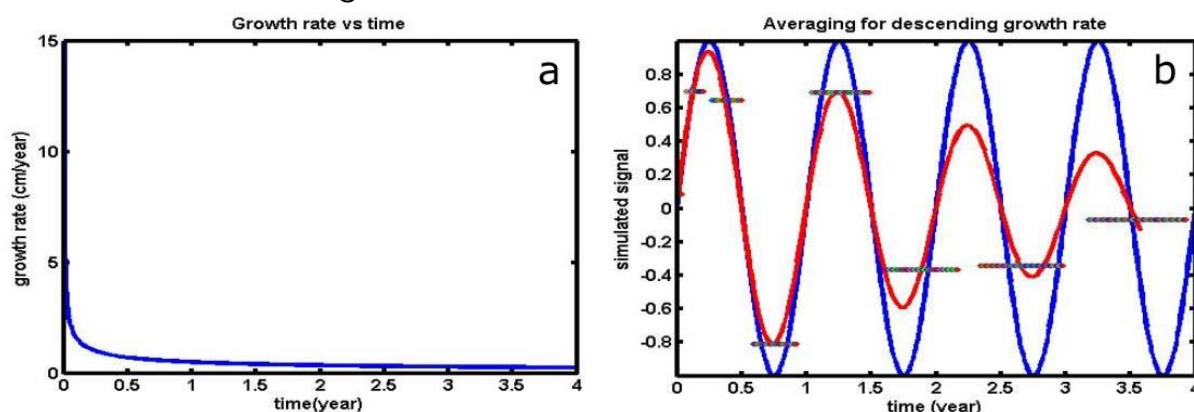

Figure 10. The effect of time averaging for a descending growth rate. (a) Growth rate. (b) Averaging, red line: measured signal, blue line: true signal, horizontal lines: samples.

As can be seen in this illustration, averaging effects can cause a severe bias in the measurement. Without a correction for such effects, the amplitude shows an apparent decline with time, while in reality this is not the case. It is

clear that the problem is an underestimation of the amplitude of the signal due to averaging. Because climate models are matched to proxies, proxies need to be as precise and as accurate as possible; otherwise the models, as well as the conclusions drawn, will be biased. A calibration method which reduces averaging errors in the measurements is thus needed.

2.5.2.1 1st Approach

In a first approach a non parametric model was established, enabling us to correct for this underestimation. For simplicity, averaging effects are assumed to be in one direction only, i.e. the direction of the axis on which the measurements were performed (this is also the direction of the growth axis), see Figure 11 with two negligible dimensions (height and depth) and one non-negligible dimension (width). Typical examples for this type of samples are the quadrants in dendrological research (Verheyden et al., 2005), sediment cores of ocean floors, and ice cores (Epica Community Members, 2007). However, the conclusions of this study also hold for a large extent of other shapes of samples. In principle this method can be applied to any proxy record, measured with a sample size that is large compared with the variation that needs to be reconstructed.
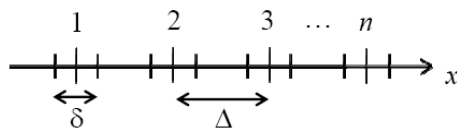

Figure 11. Convention: the arrow points in the direction of the growth axis. The samples have a certain volume over which is averaged. δ is the width of the sample, Δ is the distance between two samples, n is the sample position, which is related to the distance as follow: x = nΔ.

2.5.2.2 Linear growth rates

In Figure 12, the effects of averaging in the time domain can be seen. The width of the sample was 0.4 year and the simulated signal, $y(t)$, had the following form:

$$y(t) = \sin(t) + \tfrac{1}{2}\sin(2\pi t + 1)$$

(1)

where t denotes the time.

When the experimental conditions are such as in Figure 12a, the underlying ideal signal will be averaged over the width of the sample.

This means that the sample value will be an average of the true signal from one end of the sample to the other. In the frequency spectrum the consequences of averaging can be seen in terms of frequency components and amplitude Figure 12b. It is clear that averaging causes amplitude reduction. This small attenuation of the lower frequency components and large attenuation of the higher frequency components is typical for a low pass filter. It will show that the true signal has been filtered by a low pass filter. The goal in this first approach is to characterize the filter and, then recover the true signal by compensating for the filter effect on the measured signal.
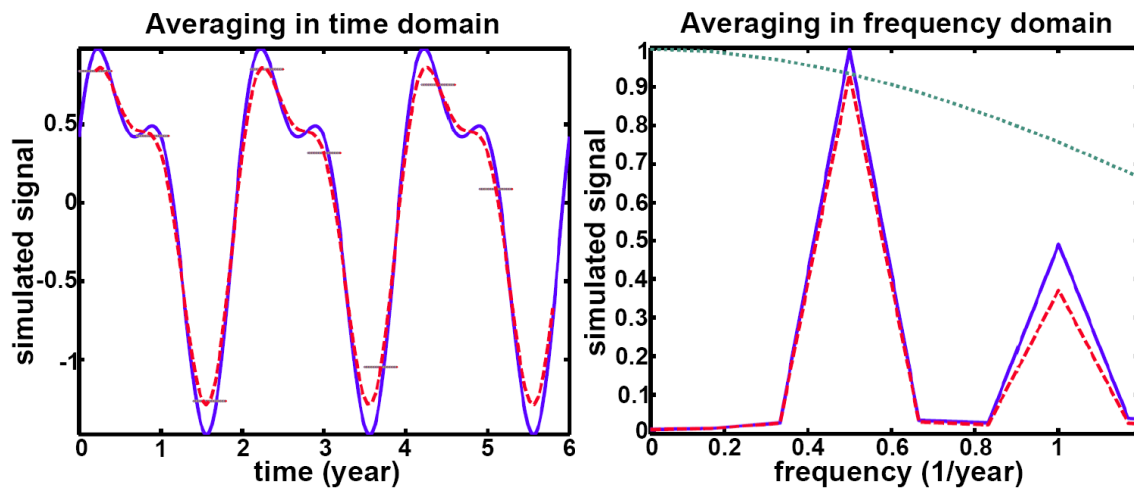

Figure 12. The effects of time averaging in time domain (a) and in the frequency domain (b). Dashed: measured signal, full: true signal, horizontal lines: samples, dotted: filter (sinc-function).

2.5.2.3 Mathematical approach

In Beelaerts et al, 2008, the relation between the true signal and the measured signal is established, and the filter is characterized. It is shown that averaging (the amplitude attenuation) is equivalent to multiplying the true frequency spectrum by a sinc-function $\left(\mathrm{sinc}(x) = \dfrac{\sin x}{x} \right)$. The sinc function is only dependent on the width of the sample:

$$\Im\left[\overline{y(x_k)}\right](\omega) = \mathrm{sinc}\left(\frac{\delta\omega}{2}\right)\Im\left[y(x_k)\right](\omega)$$

(2)

where $\overline{y(x_k)}$ is the discrete measured signal as a function of the sampling position x_k, ω is the angular frequency, $y(x_k)$ is the discrete ideal signal at position x_k, $\Im\left[y(x_k)\right](\omega)$ is the Fourier transform, and δ is the width of the sample and.

After characterizing the filter, a correction (compensation) is effected to obtain the signal in the frequency domain as follows: simply multiply the measured signal by the inverse of the sinc-function.To assess whether it is important to account for averaging errors, a comparison must be made between the size of the errors and the measurement uncertainties. In Figure 13 the errors due to averaging are shown as a function of the ratio of the sample width vs. the variation that needs to be reconstructed. The larger the sample widths in comparison with the variation, the larger the averaging-errors and the more sensitive and important the method will be. The limitations of this non-parametric approach are discussed in Beelaerts et al. 2008a.
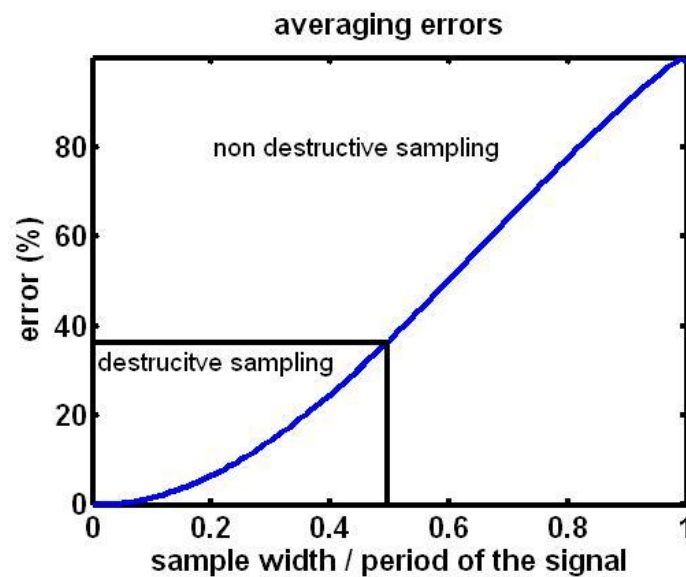

Figure 13. The errors due to averaging in percentage in function of the ratio of the sample width and the period of the signal of interest.

Results

In Figure 14 the results for the correction of the noiseless signal are shown in the frequency domain (a) and the time domain (b). It is clear from the frequency spectrum that both frequency components are completely reconstructed: the dotted line coincides with the full line. This signal is then transformed back to the time domain with an inverse Fourier transform, the result is shown in Figure 14b. The amplitude of the corrected signal is equal to one, which is the amplitude of the lowest frequency component. In conclusion, the correction for frequency components from DC to $f_s/2$ is optimal for non-overlapping sampling. When $f_s/2$ exceeds the first zero of the sinc-function, the correction for the high frequency components is limited.
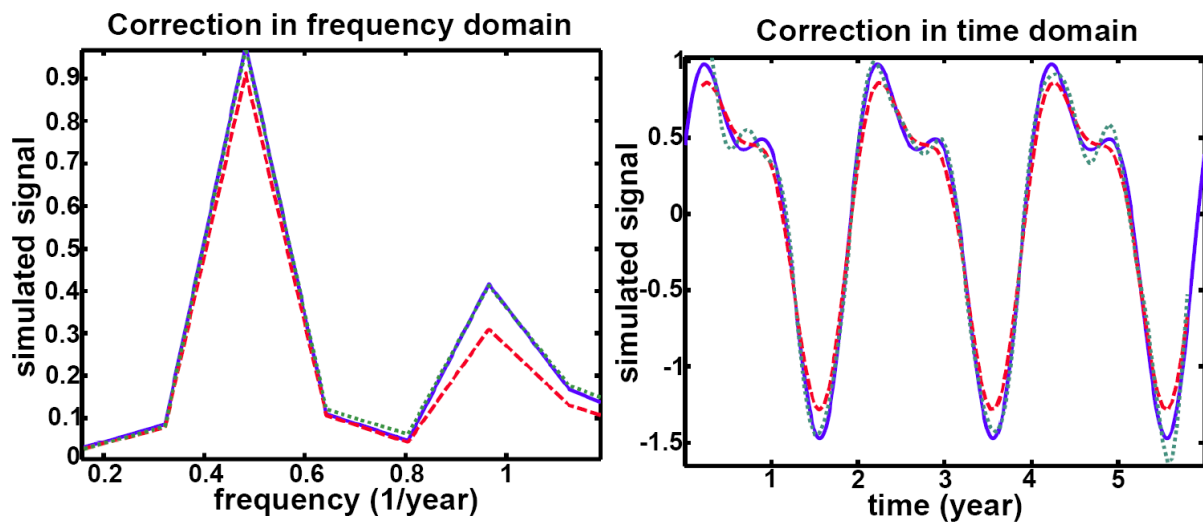
Figure 14. The corrected signal in frequency domain (a) and in time domain (b). Dashed: measured signal, full: ideal signal, dotted: corrected signal.

2.5.2.4 Non-linear growth rate

In reality growth rates or accretion rates are never constant. On the contrary, they depend on environmental parameters, which are in turn not constant. Here a simulation with a descending growth rate is presented. The signal on a distance scale looks like a compressed sine and during the transformation to the time base the signal is stretched to a normal sine; this is because of the decline of the growth rate. Not only is the signal stretched, but also are the samples. As a consequence, the averaging effect is larger near the end of the signal on both the time and distance scales. When the effects of averaging are not taken into account, it seems as if the measured signal is fading, due to some physiological or environmental factors, and thus may be misinterpreted Figure 15.
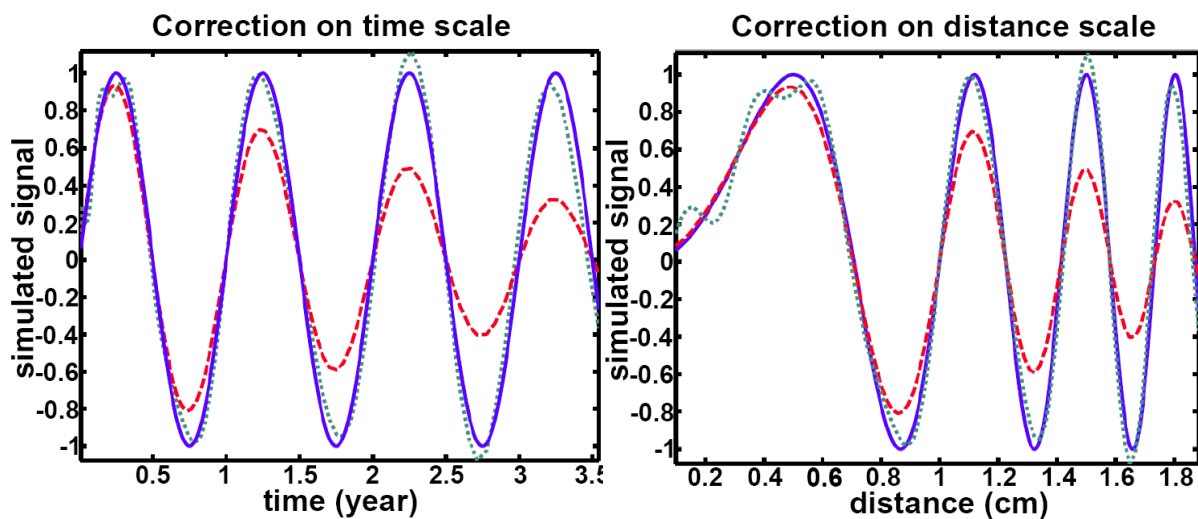
Figure 15. Correction for descending growth rate on a distance scale (a) and on a time scale (b). Dashed: measured signal, full: true signal and corrected signal.

2.5.2.5 Results

In practice, the data were transformed to the frequency domain via multiplication by the inverse of the sinc-function. The inverse Fourier transform provided the corrected data, shown in Figure 15. These results are very promising, because even for very low amplitudes the signal is reasonably well reconstructed.

2.5.2.6 Remark

The accretion rate of natural archives is dependent on environmental and physiological factors. Each data record therefore has its unique non-constant accretion rate and thus its own non-linear distance-time relationship. Natural archives are sampled at a distance grid along their accretion axis. Starting from these distance series, a time series needs to be constructed, as comparison of different data records is only meaningful on a time grid.

The non-parametric correction for averaging does not provide an estimation of the time base. The time base can be calculated via the procedure explained in (De Ridder et al., 2005). This nonlinear distance to the time transformation method (= time base) requires a parametric signal model; here a harmonic signal model was chosen.

In the second approach this parametric approach will be used to integrate the time base distortion and the correction for the averaging effect. The noise reductions, which are an additional advantage of a parametrical model, result in a maximum precision, while the model selection simultaneously maximizes the accuracy.

2.5.2.7 2nd Approach

In a second approach a parametric model was established, enabling us to correct for this averaging effect and simultaneously construct a time base. For simplicity, the averaging effect is again assumed to be in one direction only (Figure 11). To indentify the distance-time relationship and establish a signal model, some assumptions about the unknown signal need to be made. Here, the signal on a time scale y(t) is assumed to be harmonic. This is an obvious assumption, because proxy records often exhibit a seasonal cycle. As stated before the distance-time relationship is never constant, this means that the harmonic signal will be nonlinearly distorted on a distance scale. The aim in this approach is thus to create a parametric model which estimates a nonlinearly distorted harmonic signal, in the presence of additive noise and averaging effects. Parametric models which estimate a harmonic signal in the presence of additive noise and a non-linear distortion are intensively studied in literature (De Ridder et al., 2005; Schoukens et al., 1997; Vandersteen et al., 2001; Verspecht, 1994). The novelty here is that the parametric signal model includes the averaging effects.

2.5.2.8 The parametric signal model.

The true signal which is incorporated in the natural archives is the continuous signal to be measured. This true proxy signal is assumed to be harmonic, thus it can be modeled as a sum of sine waves:

$$y(x,\theta) = A_0 + \sum_{k=1}^{H} \left[A_k \cos(k\psi(x,L)) + A_{k+H} \sin(k\psi(x,L)) \right]$$

(3)

with x, the distance, $\theta = [A_0, A_1, ..., A_{2H}, L]$, A_0 the unknown offset, A_k to A_{k+H} the amplitudes of the kth harmonic $(k \in \{1,...,H\})$, H the number of signal harmonics; and $\psi(x,L)$ a nonlinear function of x modeled as a sum of a linear and a nonlinear contribution:

$$\psi(x,L) = 2\pi\lambda_0(x + \sum_{l=1}^{b} B_l \phi_l)$$

(4)

with λ_0 the spatial frequency expressed in m^{-1}, B_l the vector of unknown phase distortion parameters, ϕ_l a set of splines, $l = 1,2,...,b$ and $L = [\lambda_0, B]$.
The distance time relationship is non-linear and can be expressed as follows:

$$2\pi f_0 t = \psi(x)$$

(5)

When the true signal is sampled, each sample value is equal to the average of the continuous proxy signal over the width of the sample. This means that the model of the measured averaged signal $\overline{y}(x_n,\theta)$ is related to the model of the continuous signal $y(x,\theta)$ we want to identify as:

$$\overline{y}(x_n,\theta) = \frac{1}{\delta} \int_{x_n-\frac{\delta}{2}}^{x_n+\frac{\delta}{2}} y(x,\theta)dx \qquad (6)$$

with x_n the distance at sampling position n, δ the sample width (Fig. 29.) $y(x,\theta)$ the model for the continuous proxy signal, as described in Equation (3).

After estimating the parametric model Equation (6), the distance-time relationship Equation (5) is calibrated. This can be done by dating one observation if we know when this event occurred (absolute time), or dating two observations if we know how much time has passed between two observations (relative time):

$$\begin{cases} 2\pi f_0 t_1 = \psi(x_1) \\ 2\pi f_0 t_2 = \psi(x_2) \end{cases} \qquad (7)$$

with x_1 and x_2 the two observations with corresponding relative times t_1 and t_2. From Equation (7) it follows that:

$$f_0 = \frac{\psi(x_2) - \psi(x_1)}{2\pi(t_2 - t_1)} \qquad (8)$$

The time can now be calculated with Equation (5).

<u>The identification algorithm.</u> The parameters $\theta = \lfloor A_0, A_1, ..., A_{2H}, L \rfloor$ can be determined by minimizing the difference
between the measured data $\overline{y}(x_n)$ and the model of the model of the measured averaged signal $\overline{y}(x_n,\theta)$. For more details see Beelaerts et al 2008b.

2.5.3 Multiple regression analysis of proxy record

All currently paleo-temperature proxies proposed in literature ($\delta^{18}O$, Mg, Sr, Li, ...) are influenced by a second environmental parameter (mostly salinity). We believe that combining several proxies in a multi proxy model can partly solve this problem.

The use of multi proxy models is advised for the following two reasons: (i) the fact that a proxy signal is generally influenced by a number of environmental parameters can be mathematically expressed by a set of equations (1); solving these for the environmental condition involves a new set of equations in which every environmental parameters can be described by multi proxy equations. This means that every proxies add some information to the final paleo-temperature equation.

$$
\begin{cases}
Mg = a_1.Temp + b_1.Sal + d_1.chla + ... + C_1 \\
Sr = a_2.Temp + b_2.Sal + d_2.chla + ... + C_2 \\
Ba = a_3.Temp + b_3.Sal + d_3.chla + ... + C_3 \\
...
\end{cases}
\Leftrightarrow
\begin{cases}
Temp = \alpha_1.Mg + \beta_1.Sr + \varphi_1.Ba + ... + C_{1'} \\
Sal = \alpha_2.Mg + \beta_2.Sr + \varphi_2.Ba + ... + C_{2'} \\
chla = \alpha_3.Mg + \beta_3.Sr + \varphi_3.Ba + ... + C_{3'} \\
...
\end{cases}
\quad (1)
$$

(ii) intuitively we may accept that adding information to an initial guess will result in more accurate solutions, as is also proven by the law of large numbers in probability theory. This theorem states that the sample average converges almost surely to the 'true' value when the number of measurement is increasing. Since expanding the number of measurements is often time consuming and expensive using multiple proxies in one model can be an easy way to expand a dataset (Table VI). Despite these clear advantages applications of multi-proxy models they are scarce in literature.

Source	Species	Initial MAE	Multi-proxy MAE
Wanemaker et al. (2008)	*Mitilus edulis*	**Mg**: 2.8 **Sr**: 3.1	**Mg-Sr**:2.6
Klein et al. (1996)	*Mitilus trosullus*	**Mg**:1.5 **Sr**:3.2 **C:**1.9 **O**:0.6	**Mg-Sr-O-C**:0.5
Van der putten (2000)	*Mitilus edulis*	**Mg**:2.13	**Mg-Sr**: 1.90 **Mg-Sr-Ba-Pb**:1.78
E. Versteegh (pers. comm.)	*Unionidae* sp.	**O**: 2.29	**O-Mg**: 2.13 **O-C-Mg-Sr-Ba-Pb**: 2.11
C. Poulain (pers. comm.)	*Ruditapes philippinarum*	**Mg** : 2.13	Mg+Sr 1.90 **O-C-Mg-Sr-Ba**: 1.78

Table VI. Multiple regression analysis on several proxy datasets demonstrates the benefit of using multi-proxy models; the model performances are given in Mean Absolute Error (MAE).

2.5.4 Non-linear Multi-Proxy Approach

In case different individuals of a single species which thrived under the same environmental conditions exhibit similar patterns in shell trace element and stable isotope (TEI) chemistry, we can assume that their chemical signature is a result of the environment. Unfortunately relations between TEI's and environmental conditions, though usually non-linear, cannot be described via classical non-linear models (exponential, logarithmic, polynomial, etc.). Other models need to be considered. A spline-model (a model based on successive Gaussian-like functions) is ideal to describe the different non-linear events occurring in nature, such as plankton blooms, upwellings, etc. Using such a model it is possible to propose a transfer function that describes the variations in the proxy-records. The problem using this non-linear transfer function is that a unique proxy concentration does not correspond with a single unique environmental situation. Therefore we are forced to use a multi-proxy approach.

We commonly used 80% of TEI datasets (a dataset is the suit of TEI's measured in a single shell) to train our model while the remaining 20% was used to validate model outcome. A dataset thus should consists of TEI profiles for 5 or more single specimens of the same species that grew under the same environmental conditions: this means that at least 4 specimens are required for training the model and one for validating it. Minimizing the differences in the experimental group is necessary to minimize the non-environmental variations in the data. Differences in the periodic signals can be considered as an unexplained noise-component. Separate models can be constructed for different species and different study-sites. This will yield insight in effect of site- and species-specificity on the periodic TEI signals.

Intuitive approach.

Building or training a model for a specific data set involves compacting the information in the data set by rewriting it in the form of a transfer function with a limited number of parameters. We opted for the use of one transfer function describing the TEI variations over time. This function is then used to link the TEI signature to the environmental parameters, as shown in Figure 16. Once the model is build, every single measurement (consisting of different TEI's) can be linked to one point in the transfer function by looking at the shortest distance to the function. This shortest distance can be weighted with the variances of each proxy. System identification tools will offer the possibility to construct an additional weighting factor which gives an insight in the usefulness of every proxy. The ideal weighing factor is the one that leads to the best reconstruction of the environmental parameters.
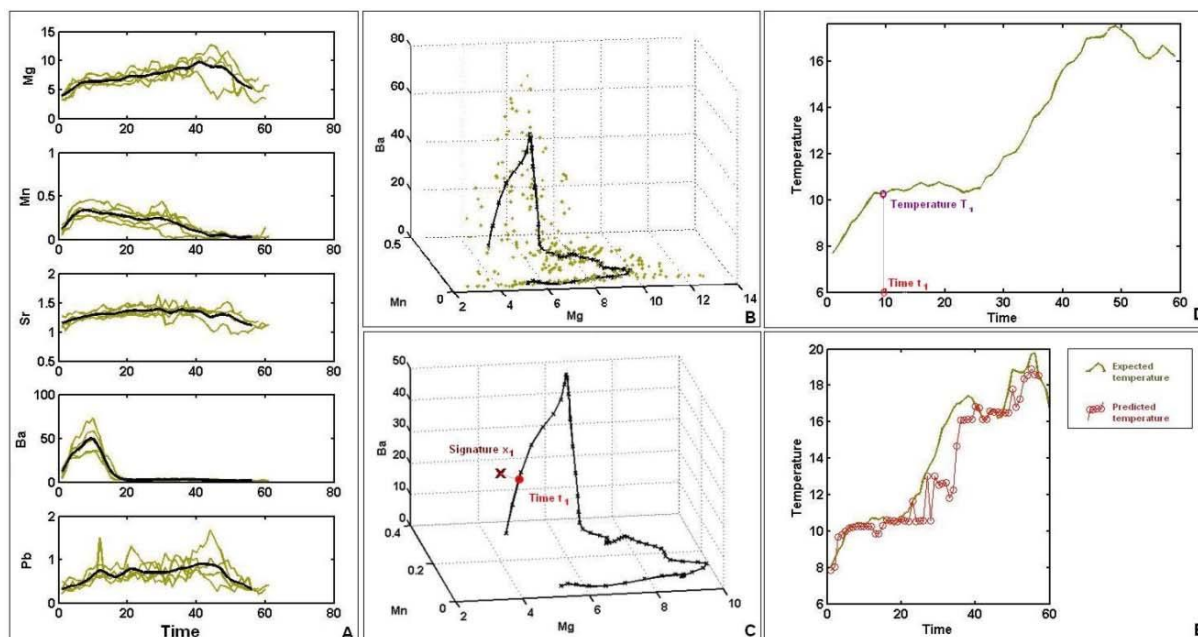
Figure 16. (A.): Construction of a non-linear transfer function for single proxies over time. (B.): rewriting the transfer functions in one n-dimensional function (there are as many dimensions as proxies). (C.): Linking of a measurement (chemical signature) to a unique time-position. (D.): Linking of the time-position to the corresponding environmental parameter(s). (E.): Validation of the method, comparing the measured environmental parameter(s) to the predicted environmental parameter(s).

3. RESULTS

3.1 Sponges

3.1.1 Anatomic survey of Petrobiona massiliana

3.1.1.1 Morphology

P. massiliana is in most case cone-shaped but it's not always the case. As the general shape of the body could also have an influence on the integration of the proxies, measurements were performed in order to eventually characterize specific morphotypes. Measurements included two perpendicular lengths of the basal area (to estimate the surface of the basal area using oval as model) and the height of the living tissues (to estimate the volume of the sponge using cone as model). Those measurements allow to clearly differentiating three morphotypes (Figure 17): "*Classical*" (cone-shaped sponge), "*Flat*" (Same average basal surface than the Classical but reduced average volume, Figure 18) and "*High*" (Same average volume than the Classical but reduced average basal area, Figure 18). The "Flat" morphotype has been described as a distinct species, *Petrobiona incrustans* (Sarà, 1963), but this was later refuted by (Vacelet, 1991) based on spicule criteria.
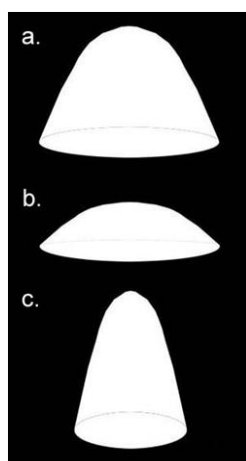

Figure 17. Schematic representation of the 3 morphotypes of P. massiliana: A. Classical, B. Flat, C. High (Not to scale).
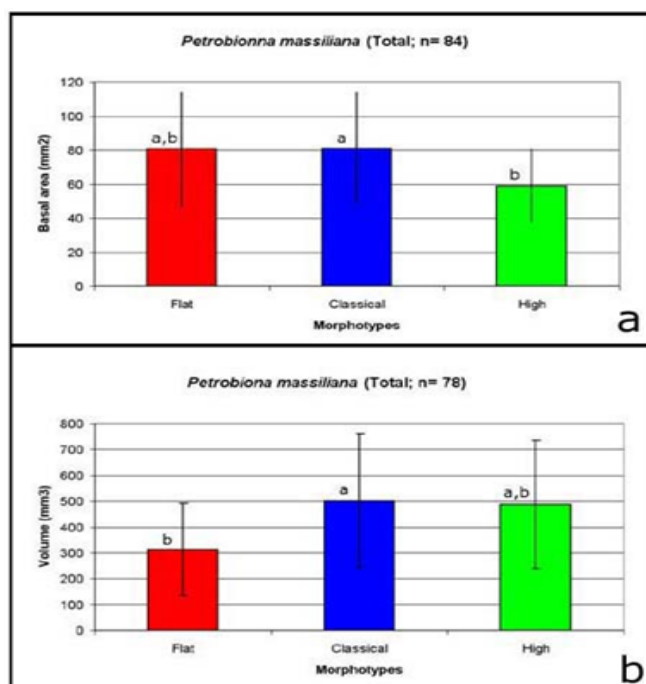
Figure 18. Morphotypes of *P. massiliana*: (a) Basal area (mm², m. ± s.d.) and (b) body volume (mm³, m. ± s.d.) of the sampled specimens. There is no significant difference between the series designed by the same letter (Tukey test, p.= 0.05).

3.1.1.2 Description of the skeleton

P. massiliana produces calcitic elements including a massive basal skeleton (secreted by basopinacocytes lining the lower margin of the living tissues) and spicules (secreted by sclerocytes located in the interstitial layer called mesohyl). The apical surface of the basal skeleton of *P. massiliana* is covered by large spiny crests made of massive calcite that support most of the living tissues (Figure 19). Numerous narrow canals open between the apical crests and are more abundant in the central region of the basal skeleton (Figure 19). These canals extend within the massive skeleton following an axis perpendicular to the basal plane of the sponge. Spicules are discrete independent skeletal elements supporting the sponge body. Four types of spicules were observed (Figure 19): microdiactines (composed of two rays or "actines"), triactines (composed of three rays), diapasons (composed of three rays with parallel paired rays) and tetractines (composed of four rays). Spicules are scattered in the entire sponge body but are particularly abundant in the most outer region called cortex (or ectosome).

Microdiactines are also specifically associated to the basal canals. If the basal skeleton of *P. massiliana* was previously described as "aspicular" (Vacelet 1964), we have confirmed the observations of Reinert (1989) who revealed that some spicules were progressively entrapped within the basal skeleton during its formation.
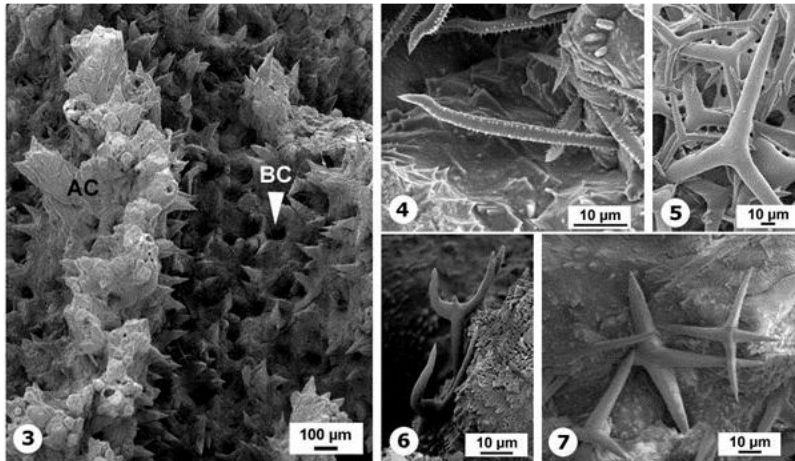

Figure 19. Skeletons elements of *P. massiliana* (3) Apical view of the central region of the basal skeleton covered by apical crest (AC) and by the aperture of narrow basal canals (BC); (4) Microdiactine; (5) Triactine; (6) Diapason and (7) Tetractine.

3.1.1.3 Seasonal morphological variations.

The main variation observed was the occurrence of oocytes and the gradual development of sponge larvae. (Vacelet, 1964) indicated that oogonies and oocytes appear in *Petrobiona massiliana* between April and May. We observed them later in the year, between June and September (Fig. 5). Larvae at different advanced stages of development (*viz.* somatoblastula and advanced amphiblastula) were found in July 2006 (Figure 20).
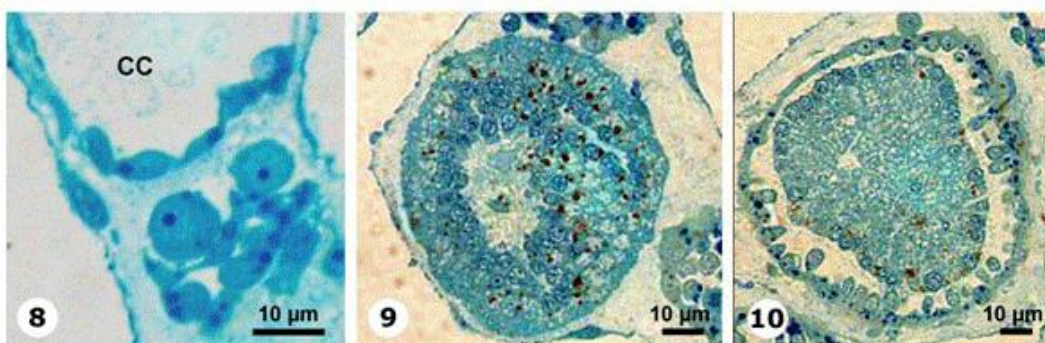

Figure 20. Oocytes and advanced larval forms in P. massiliana. (8) Oocytes located in the mesohyl at the basis of the wall of a choanocytes chamber (CC) (August 2006); (9) Somatoblastula (July 2006); (10) Advanced amphiblastula (July 2006).

The development of the larvae seems to have an impact on other components of the sponge tissues. Choanocytes are columnar cells supporting a long apical flagellum surrounded by a crown of microvilli (Figure 21). Choanocytes are organized in sphere-shaped choanocyte chambers (Figure 22). The presence of larvae is correlated to a transformation of the choanocytes from about 20 % of the chambers: the cell body elongates into an hourglass shape (Figure 22). In order to estimate the influence of larvae development on the physiology of the sponge (including the formation of the skeleton), some measurements were performed to quantify (1) the density of choanocytes per choanocyte chamber, (2) the surface ratio between mesohyl and cellular elements (choanoderm & pinacoderm) in the choanosome and, (3) the density of basopinacocytes along the interface between soft tissues and basal skeleton, giving an information on the skeletogenesis intensity. These analyses are still in progress.
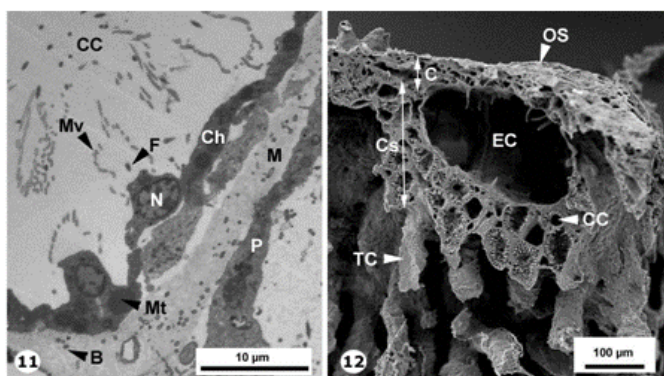

Figure 21. Soft tissues of *P. massiliana* with (11) Cross section of the wall of a choanocyte chamber (CC) showing mesohyl (M) sandwiched between a layer of choanocytes (Ch) and a layer of pinacocytes (P); (12) Cross section of the soft tissues of specimen showing the cortex (C), the choanosome (Cs) and the trabecular cord (TC). Abbreviations. B: symbiotic bacteria; EC: exhalant channel; F: flagellum; Mt: mitochondria; Mv: microvilli; N: nucleus; OS: outer surface of the sponge.
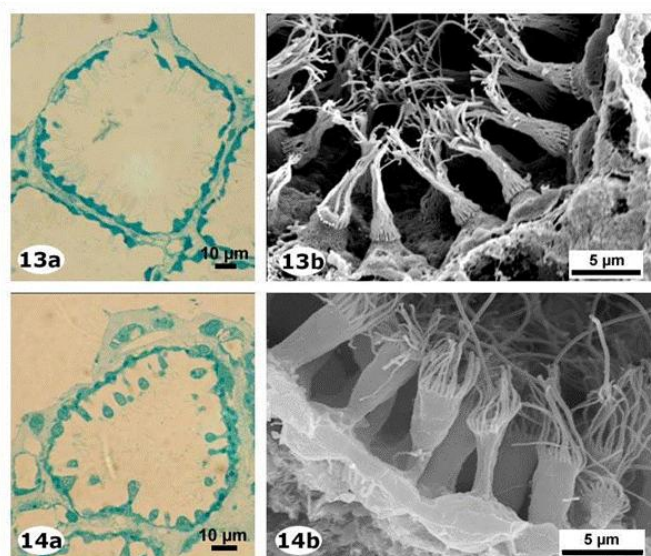
Figure 22. Choanocytes and hourglass choanocytes in P. massiliana with (13) Cross-section of a choanocytes chamber (light microscopy, 13a) and detail of choanocytes (SEM, 13b) in specimens deprived from larvae; (14) Cross-section of a choanocytes chamber (light microscopy, 14a) and detail of glass hour choanocytes (SEM, 14b) in specimens including larvae.

3.1.2 Skeleton growth rate measurements

The skeletal growth was estimated by measuring the distance along a growth axis between the calcein labelling and the external margin of the skeleton (Figure 23). The mean annual growth rate was estimated to 212 µm/y (individual minimum and maximum mean values of 153 and 271 µm/y, respectively; Figure 23). The growth rate did not differ significantly from one specimen to another (non parametric Kruskal Wallis analysis of variance on ranks, p= 0.482). The growth rate of *P. massiliana* is similar to data obtained under the same experimental conditions for the Caribbean coralline sponge *Ceratoporella nicholsoni* (233 µm/y) (Willenz and Hartman, 1989). In *C. nicholsoni*, calcein marks are continuous. On the contrary, the skeleton of *P. massiliana* seems to growth discontinuously in time with a higher rate at the top of the skeleton crests.
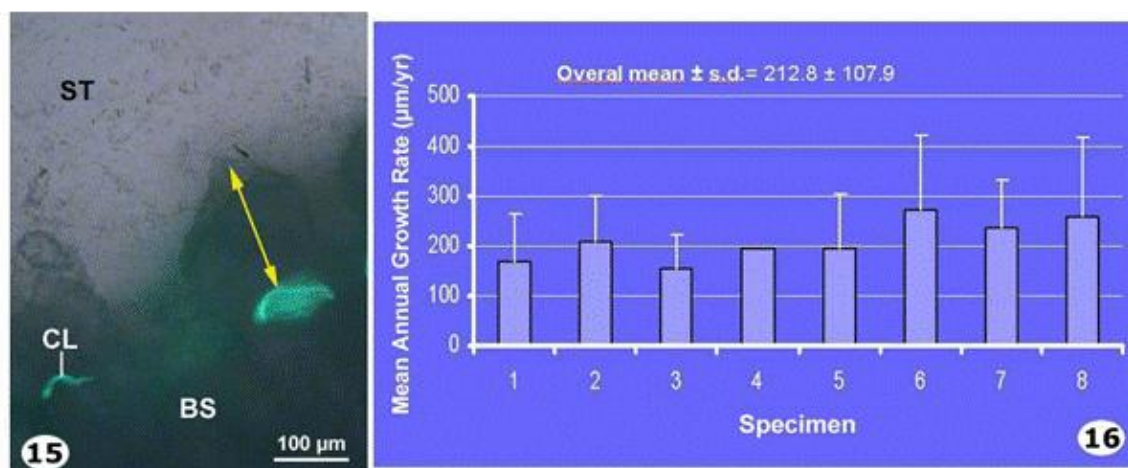
Figure 23. In situ estimation of P. massiliana growth by calcein labeling with (15) Ground section of P. massiliana one year after calcein staining showing the increment of the apical crest (yellow line) between the calcein labelling (CL) and the bottom of the soft tissues (ST) (epifluorescence microscopy); (16) Mean linear annual growth rate (+ s.d.) of 8 specimens. Abbreviations. BS: basal skeleton.

3.1.3 Biomineralization of Mg at cellular level

3.1.3.1 Observations in soft tissues

On these sections, it was possible to distinguish the different regions of the soft tissues (*viz.* cortex, choanosome and trabecular cord), the massive basal skeleton and the spicules (Figure 24). However, the Mg concentrations in the living issues appeared under the detection limit of the ESEM (less that 1% of the total matter). Moreover, no difference between the untreated specimens and the ones previously incubated in high Mg content solutions could be detected. The analysis of the water collected in the vials at the end of the experiment showed a concentration of Mg similar to the surrounding water indicating leaks in the incubation chambers during the experiments. Since the sponges do not survive when transferred to the laboratory, these experiments should have to be repeated again in situ during the next six months. This experiment had to been abandoned, due to the interruption of our contract
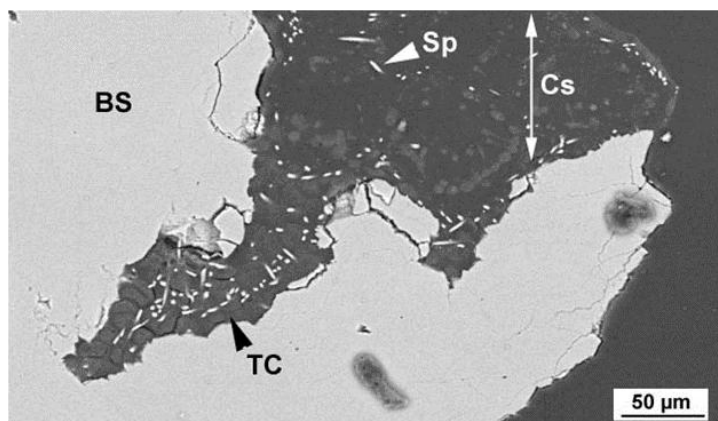
Figure 24. Ground section perpendicular to the surface of the sponge body showing the choanosome (Cs), the trabecular cord (TC), the basal skeleton (BS) and the spicules (Sp) (ESEM).

3.1.3.2 Observations in skeletal elements

Since the inclusion of spicules into the basal skeleton could induce an heterogeneity of the skeletal mass, ruining any future sequential analysis, a first mineralogical study of the different skeletal elements of *Petrobiona massiliana* was performed on the same samples. The Mg content was compared between the spicules and the basal skeleton. The analyses confirmed that all skeletal elements were made of highly magnesian calcite and indicated that there was no mineralogical difference between spicules and basal skeleton (Figure 25). The later was then an homogenous mass According to (Jones and Jenkins, 1970), Mg content of Calcarea skeletal elements vary from 1.25 to 3.15 %. Our observations on *P. massiliana* indicated a Mg content of 2.54 ± 0.27 % in the basal skeleton and 2.63 ± 0.38 % in the spicules. The calcite of *P. massiliana* is then relatively highly dosed in Mg for a Calcarea.
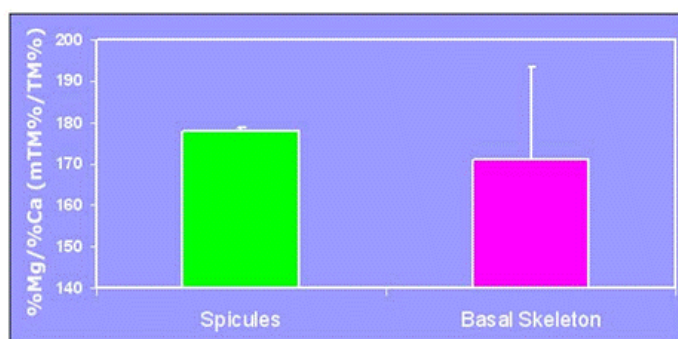

Figure 25. Mg/Ca ratios in spicules and basal skeleton expressed in percentages of total matter (%TM).

3.1.4 High Resolution elemental profiles in Ceratoporella nicholsoni

Profiles of Li, B, Mg, Mn, Fe, Cu, Zn, As, Sr, Mo, Cd, Ba, Pb, La, and U in the skeleton of *Ceratoporella* nicholsoni were acquired using the recently installed LA-ICPMS. Continuous ablation path along the specimen representing a time interval of ~250 yrs has allowed to obtained unprecedented high resolution elemental to calcium ratios profiles with a spatial resolution varying between 3 to 20 µm/analysis. As illustrated in Figure 26 for Mg/Ca and Ba/Ca ratios, large fluctuations can be observed over the ~250 yrs period for these two conventional proxies. Pronounced co-evolution of Mg and Ba in the sclerosponge can be observed. As already discussed by (Rosenheim et al., 2005a), Mg and Ba signals in sclerosponge do not refer to water temperature variations but highlight the presence of both vital effects (associated to growth rate variability) and other environmental controlling factors.

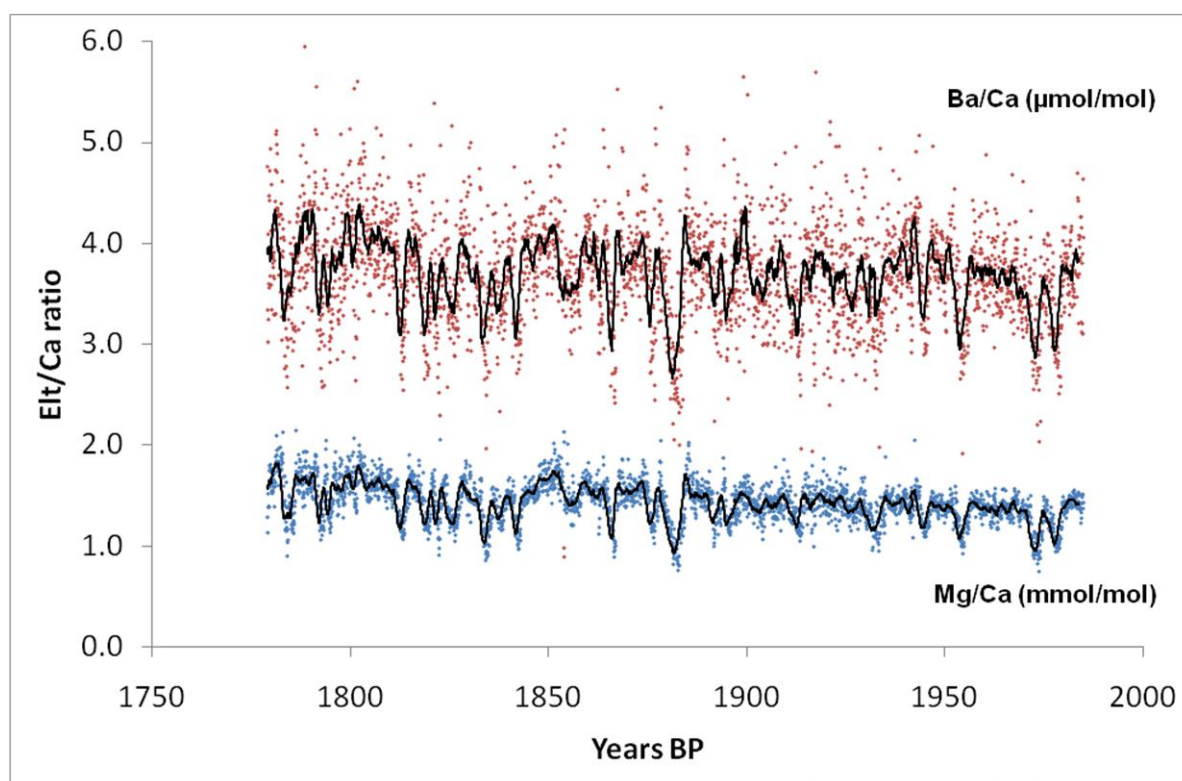**Figure 26. High resolution profile of Mg/Ca (mmol/mol) and Ba/Ca (µmol/mol) in sclerosponge *Ceratoporella nicholsoni obtained* by LA-ICPMS with successive continuous ablation path (spatial resolution: 11.3 µm/pt, n = 3996; black line represents 20 pts running mean).**

Figure 27 gives another example of high resolution profile obtained for Pb/Ca. Extensively studied in the sclerosponge (Lazareth et al., 2001; Rosenheim et al., 2005a) and other environmental archives, the Pb environmental contamination of the 20th century is now precisely documented. Pb/Ca profile obtained during the CALMARSII project appears to be in excellent agreement with earlier studies (Lazareth et al., 2001) both in term of magnitude and timing. This new high resolution data offer new perspective to study both long but also short time scale environmental contamination dynamics of the coastal ocean.
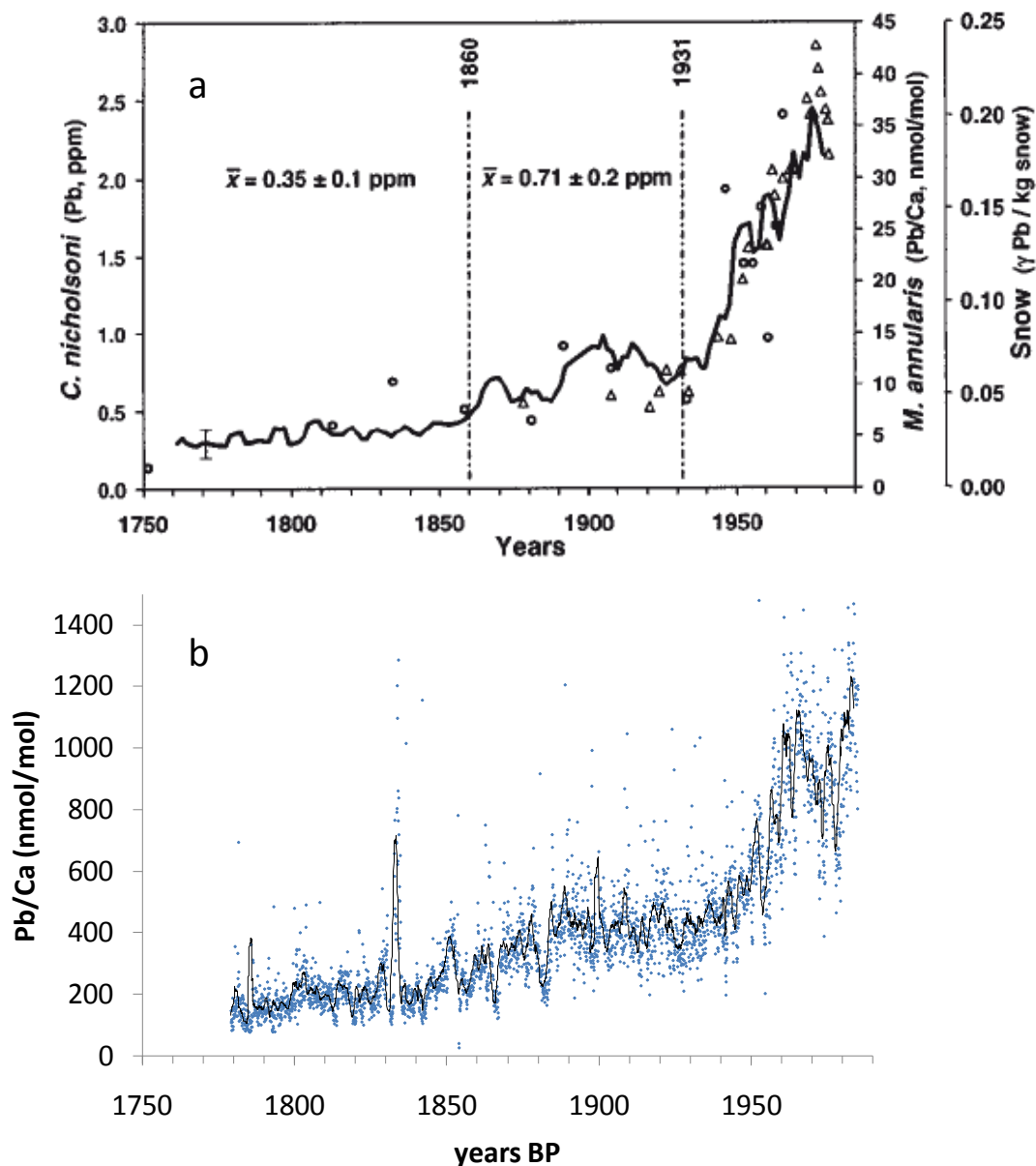
Figure 27. (b) High resolution profile of Pb/Ca (nmol/mol) in sclerosponge *Ceratoporella nicholsoni obtained* by LA-ICPMs with successive continuous ablation path (spatial resolution: 11.3 µm/pt, n = 3996; black line represents 20 pts running mean) and comparison with the published profile (a) for the same specimen and polar snow record (Lazareth et al., 2001).

In addition to the well-studied elements, we have optimized our methodology to expand the number of elements to be determined in biogenic carbonates. As an example, we were able to reliably determined the first high resolution profile of As/Ca ratio in the sclerosponge (Figure 28). As/Ca ratio remains fairly stable in the oldest part of the sponge from 1850-1950 showing only short time scale fluctuations. This situation change in the early 60's where a significant increase can be observed until the more recent period covered by the

sponge (1985). Maximum As/Ca ratios are observed in the 80's and are up as twice the preindustrial levels encountered in 1850's. This sclerosponge profile of As incorporation over time tends to support that as for Pb, a massive and large scale pollution of the environment has occurred for this element. Registered in shallow tropical waters of Jamaica, this temporal evolution is in good agreement with other archives for which As records are available, such as peat bogs and lake sediments. Interpretations and statistical treatments on these profiles are currently in progress.
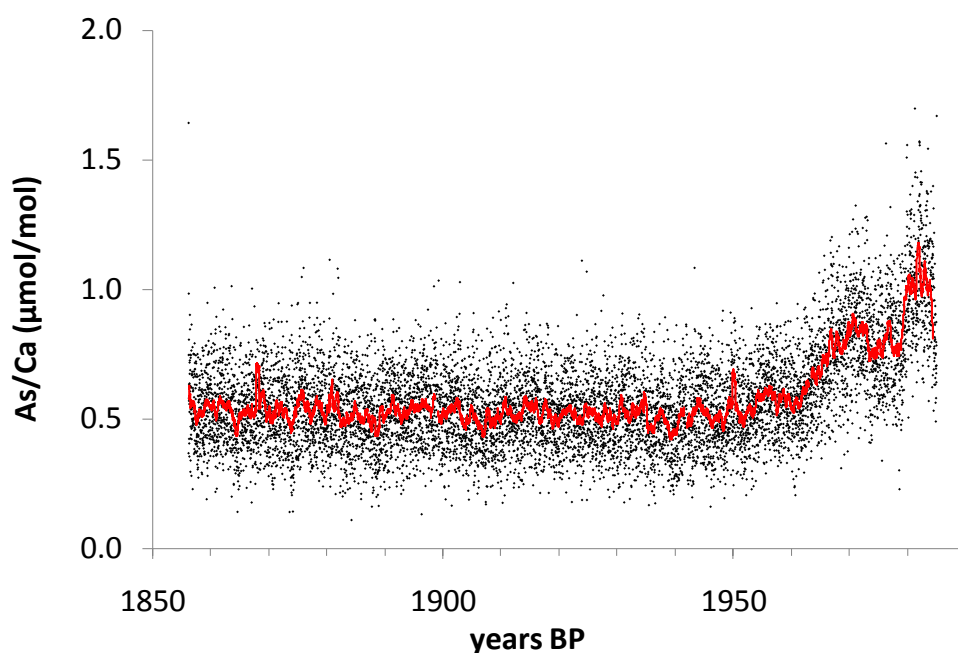
Figure 28. First high resolution As/Ca profile in sclerosponge *Ceratoporella nicholsoni* (spatial resolution 3.5 µm/pt; n = 9784 pts and red line corresponds to 40 pts running mean).

3.2 Echinoderms

3.2.1 Sea urchin growth in controlled conditions

3.2.1.1 Mg/Ca and Sr/Ca in cultured sea urchins

The Mg/Ca ratio in the skeleton was only dependent on temperature. Neither growth rate nor salinity was significantly related to this ratio in the considered ranges (Table VII). The Mg/Ca temperature relationship is better described by a non linear saturation model (Figure 29).

Figure 29. Mg/Ca ratio in the skeleton of *Paracentrotus lividus* grown in aquarium according to temperature and salinity (♦ 36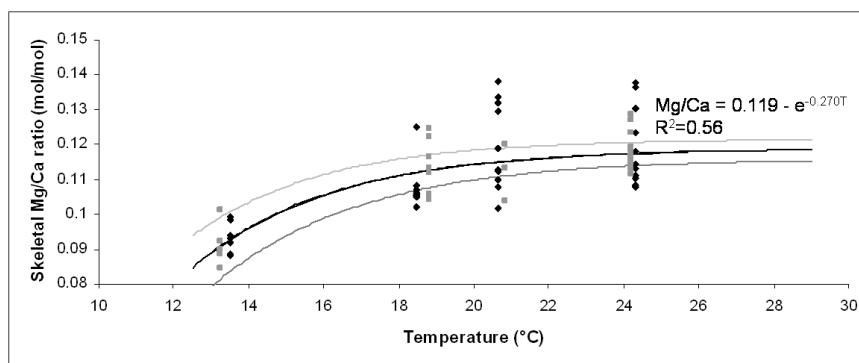 psu and ▪ 39 psu); equation of the non linear model and 95 % confidence interval (lower: Mg/Ca = 0.116 – e $^{-0.254T}$; upper: Mg/Ca = 0.122 - e $^{-0.287T}$).

The skeletal Sr/Ca ratio was dependent on all considered variables, except seawater Sr/Ca : temperature (according to a negative quadratic relation) (Figure 30), growth rate (positive linear relation) and salinity (negative linear relation) (Table VII). Temperature and growth rate explained each ca 20% of the variability and salinity a further 9%.

	1st variable	2nd variable	3rd variable	4th variable	5th variable	R^2	Sign. of additional variable
	T	-	-	-	-	0.520	$<10^{-8}$
Mg/Ca	T	T^2	-	-	-	0.563	$<10^{-6}$
	T	T^2	S	-	-	0.567	0.45
	T	T^2	S	GR	-	0.571	0.4
	T	-	-	-	-	0.001	0.71
	T	T^2	-	-	-	0.232	$<10^{-5}$
Sr/Ca	T	T^2	S	-	-	0.336	$<10^{-3}$
	T	T^2	S	GR	-	0.519	$<10^{-5}$
	T	T^2	S	GR	Sr/Ca $_{SW}$	0.531	0.175

Table VII. Statistical results of the stepwise multiple regressions between Mg/Ca and Sr/Ca ratios in the newly formed skeleton of *Paracentrotus lividus* and possible independent variables (T = temperature, T² = square temperature, GR = growth rate, S = salinity, Sr/Ca $_{SW}$ = seawater Sr/Ca ratio)
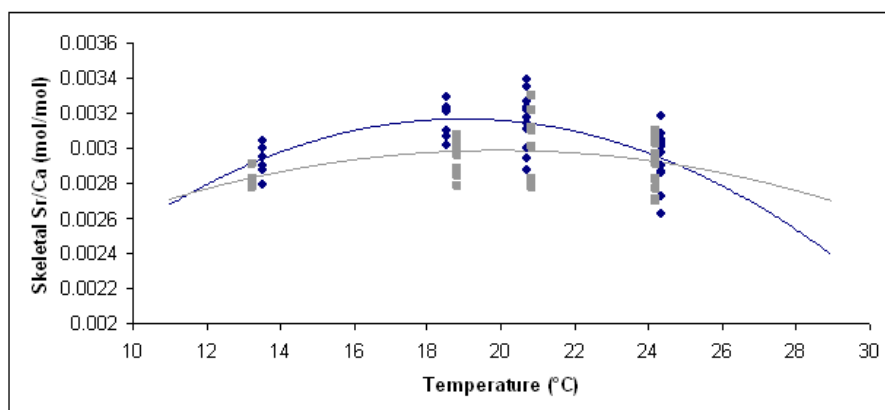
Figure 30. Sr/Ca ratio in the skeleton of *Paracentrotus lividus* grown in aquarium according to temperature and salinity (♦ 36 psu and ■ 39 psu); quadratic equations at each salinity (36‰: Sr/Ca=-7.78*10^{-6}T^2+2.94*10^{-4}*T+3.76*10^{-4} ; 39‰: Sr/Ca=3.53*10^{-6}T^2+1.41*10^{-4}*T+1.59*10^{-3})

3.2.1.2 Mg isotope in cultured sea urchin

Mg isotopic ratios determined in the specimens described above exhibit a weak but linear temperature dependency of their Mg isotopic composition (Figure 31). The observed variability (maximum 0.4‰ for 10°C temperature range) is only 4 times the measurements uncertainties (~0.1‰) and is as a paleothermometer limited in precision. However it is worth noticing that the deduced linear trends and slopes (mean: -0.015 ‰/AMU/°C) are comparable in magnitude with the T dependency observed in inorganic calcite precipitated at the equilibrium (-0.02 ‰/AMU/°C, Galy *et al.* 2002). This gives additional support for Mg fractionation occurring at/or close to equilibrium in the sea urchin with a lack of strong kinetic controls.
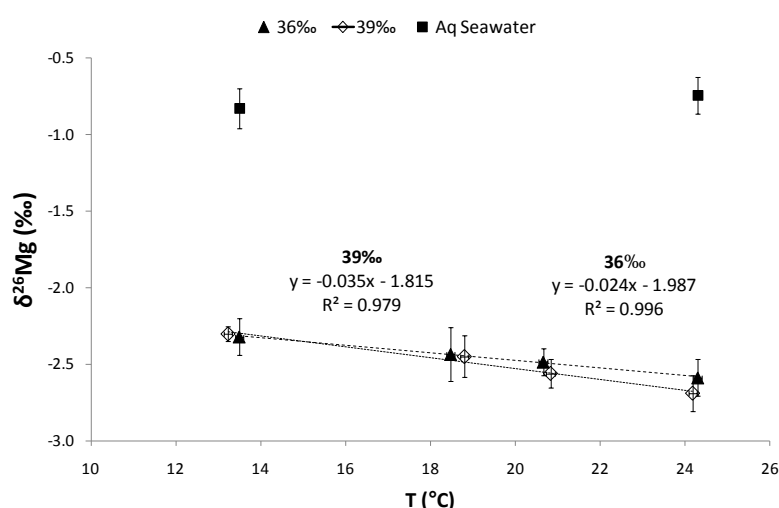
Figure 31. Mg isotopic signatures (δ²⁶Mg) measured in cultured sea urchin under salinity and temperature controlled conditions. Sea urchin values were obtained from juvenile interambulacral plates grown during the experiment and correspond to at least three specimens cultured in similar conditions. Also plotted, the isotopic signatures of the water sampled in two distinct aquariums. Uncertainties are at 95% confidence interval.

3.2.1.3 Mg isotope variability in sea urchin skeleton

We measured δ²⁶Mg in different components of skeletons from one specimen of sea urchin (*Paracentrotus lividus*) collected in La Vesse (Marseille, France). We have considered various interambulacral plates along a meridian axis of the test in order to follow any variations due the ageing of the organism, and also the spines and the mouth. The results (Figure 32) show significant variability in these different skeletal parts. The spines exhibit the highest δ²⁶Mg (-2.3±0.1‰), followed by the interambulacral plates (-2.67±0.12‰) and finally the mouth with the most depleted values (-2.82±0.12‰). The signature homogeneity observed in the interambulacral plates from a meridian axis of the test suggests that stable fractionation processes are registered in these skeletal parts and therefore might be representative of an average value of δ²⁶Mg observed during the life of the sea urchin.
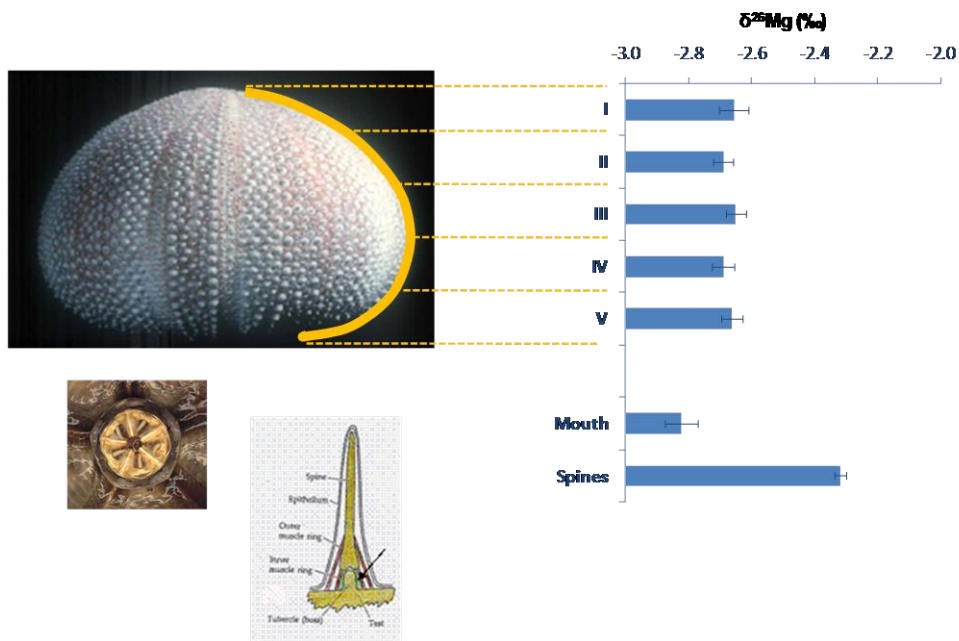
Figure 32. δ²⁶Mg (in per mil) in ambulacral plates collected along the meridian axis of the test of *Paracentrotus lividus* (I to V), in the spine and the mouth.

3.2.1.4 Isotopic constrains on echinoderm biocalcification

The measured skeletal δ²⁶Mg in sea urchin significantly differ from the fractionation produced by a pure inorganic precipitation (theoretically evaluated to -3.52 ± 0.2 ‰ with seawater signature of -0.82 ± 0.1 ‰). This difference (1 ‰) clearly suggests the presence of vital effects during sea urchin biomineralization. These biologically mediated effects tend to moderate the enrichment of the light fraction of Mg.

To further constrain the nature of these vital effects, we have measured the isotopic composition of other matrices involved in the sea urchin metabolism (soft tissues and coelemic fluids) for different specimens grown under temperature and salinity controlled conditions. Soft tissues (gonads) of three specimens display narrow range of δ²⁶Mg values (-1.4±0.1‰ to -1.91±0.1‰) and show significant enrichment in light Mg isotope compared to seawater (-0.8‰). For internal fluids, δ²⁶Mg values measured for seven specimens display variable signatures between -0.65 to -1.2‰ comparable with seawater or slightly enriched in heavy isotopes depending on the specimen considered. These results highlight that Mg incorporation pathway towards the intercellular and intracellular medium of the sea urchin is able to fractionate the isotopic signature of the parent seawater.

Considering that skeletal signatures are enriched in heavy isotope compared to the mere precipitation of low-Mg calcite, the opposite trend observed in the soft tissues suggests that skeletal Mg is not of biological origin and can be the result of an export process of Mg from the calcifying cells. This hypothesis is in agreement with the precipitation of HMC which requires consistently lower Mg concentration compared to present-day seawater. Alternative hypothesis may be linked with the potential involvement of an amorphous carbonate transient phase (Raz et al., 2003). If such a process is a general feature of echinoderm biomineralisation, it might change the fractionation process of Mg by regulating the solid-fluid equilibrium and therefore the Mg incorporation into the skeleton. In this case, amorphous calcium carbonate may act as a single path fractionation process, and differently to calcite inorganic precipitation tends to lower the proportion of light Mg isotopes into the biomineral.

3.2.2 Starfish growth in controlled conditions

3.2.2.1 Mg/Ca, Sr/Ca, in cultured star fish

	1st variable	2nd variable	3rd variable	R^2	Sign. of additional variable
Mg/Ca	Salinity			0.25	$< 10^{-5}$
	Salinity	Temperature		0.57	$< 10^{-5}$
	Salinity	Temperature	Growth rate	0.57	0.7
	Salinity	Temperature	Size	0.57	0.8
Sr/Ca	Salinity			0.70	$< 10^{-5}$
	Salinity	Temperature		0.86	$< 10^{-5}$
	Salinity	Temperature	Growth rate	0.86	0.7
	Salinity	Temperature	Size	0.86	0.9

Table VIII. Statistical results of the stepwise multiple regressions between Mg/Ca and Sr/Ca ratios in the newly formed skeleton and possible dependent variables.

Both temperature and salinity affected Mg/Ca and Sr/Ca ratios in the newly formed skeleton (Table VIII). On the contrary, neither growth rate nor final size was significantly related to these ratios in the encompassed ranges (Table VIII). Salinity effects accounted for 25% of the variation in Mg/Ca ratios and

temperature for a further 32%. Thus, individual variation was responsible for 43% of the variation with 95% confidence interval (CI 95) ranging between 83 - 116 mmol/mol, i.e. 8% of the mean to 22%, according to the considered conditions. It is noteworthy that the Mg/Ca vs salinity relationships differed according to temperature (Figure 33).

The Sr/Ca ratio was highly dependent on salinity, the latter explaining 70% of the variation, temperature accounting for a further 16% (Table VIII). Sr/Ca ratios vs salinity relations did not differ according to temperature (Figure 34). Individual variation in Sr/Ca was lower, with CI 95 ranging from 2.18 -2.26 to 2.25-2.42 mmol/mol, i.e. 4%-7% of the mean.
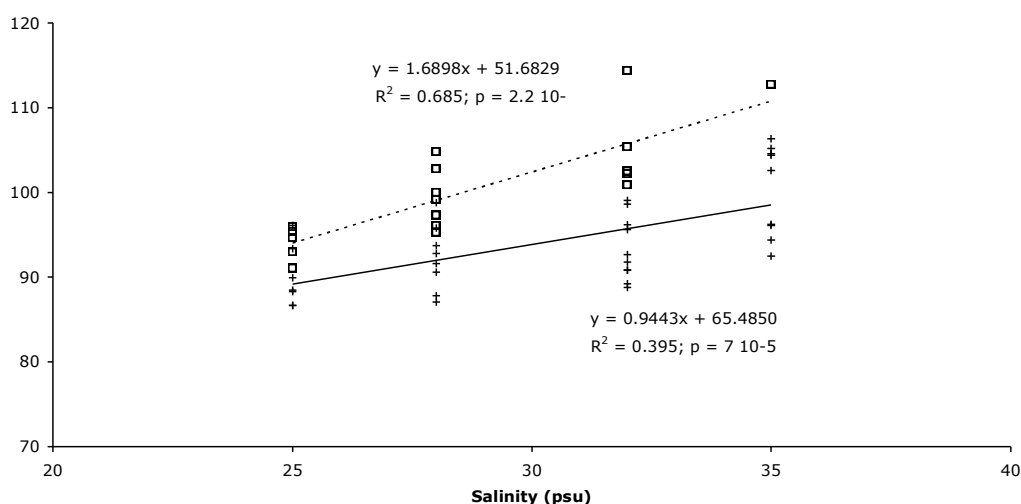

Figure 33. Mg/Ca ratio (mmol/mol) in the skeleton of *A. rubens* grown in aquarium according to salinity and temperature of growth (+ 11°C; □ 18°C); equations and parameters of the linear regressions at each temperature (— 11°C; ⋯⋯ 18°C).
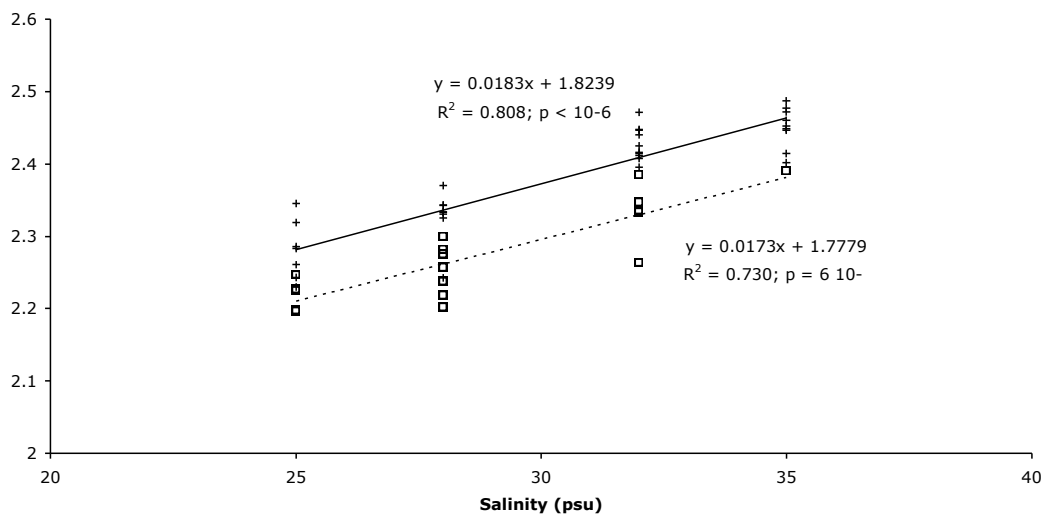
Figure 34. Sr/Ca ratio (mmol/mol) in the skeleton of *A. rubens* grown in aquarium according to salinity and temperature of growth (+ 11°C; □ 18°C); equations and parameters of the linear regressions at each temperature (— 11°C; ····· 18°C).

3.2.3 Oxygen isotope in cultured starfish

The $\delta^{18}O$ measurements performed on culture star fish reveal that the following temperature equation would apply for echinoderms (Figure 35):

$$T = 7.85 - 4.28 * (\delta^{18}O_c - \delta^{18}O_w)$$

This equation differs significantly from the one reported by (Epstein and Mayeda, 1953), with our results for $\delta^{18}O_c - \delta^{18}O_w$ being about 3 per mil lower. However, the slope value of the regression (-4.28) is similar and coherent with other published relationships.

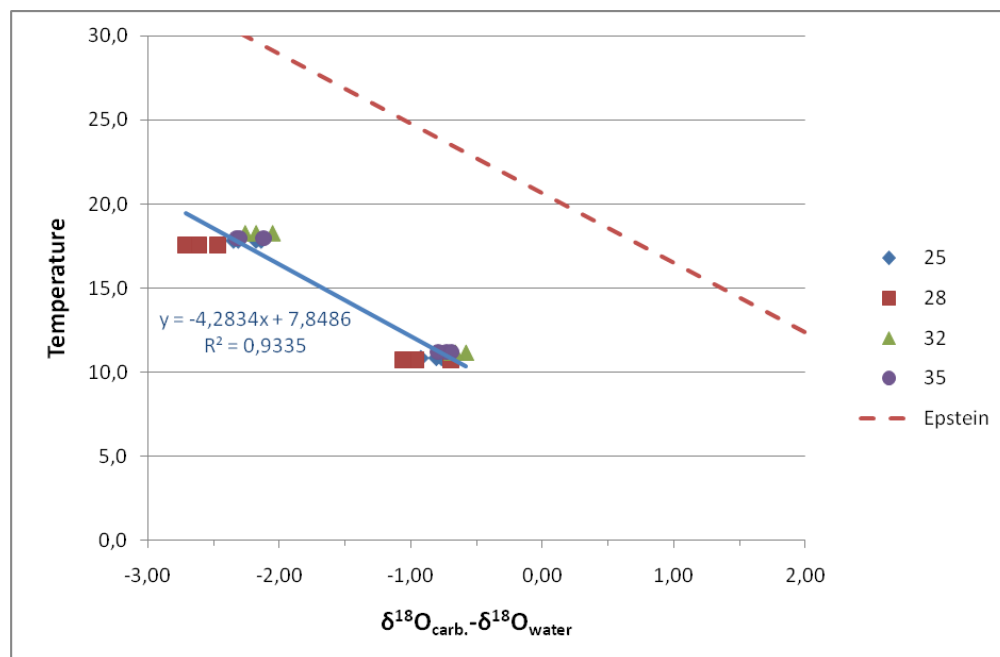**Figure 35. Paleotemperature equation for the starfishes grown under different salinity conditions (25, 28, 32 and 35‰); comparison with Epstein's equation (Epstein and Mayeda, 1953).**

3.2.4 Magnesium partition in the different body compartments of Asterias rubens

The Mg/Ca ratio was measured in the different types of ossicles forming the whole skeleton (adambulacral plates, adambulacral spines, ambulacral plates, aboral plates, upper marginal plates). Significant but weak differences were recorded between these different plates (p $_{\text{ANOVA repeated measures}}$ < 10^{-5}) (Table IX).

Type of calcified tissue	Mg/Ca (mmol/mol)
Skeleton bulk	112 ± 7^c
Adambulacral plates	113 ± 7^c
Adambulacral spines	106 ± 6^b
Ambulacral plates	96 ± 4^a
Aboral plates	96 ± 4^a
Upper marginal plates	97 ± 3^a

Table IX. Mg/Ca (mmol/mol) ratios in skeletal plates of *A. rubens* (mean ± standard deviation; n = 20). Values sharing the same superscript are not significantly different.

The skeletal Sr/Ca ratio was significantly dependent on the size of the starfish (Sr/Ca = −0.0028 * size + 2.6897; R^2 = 0.7812; $p_{regression}$ < 10^{-6}). On the contrary, the size had no significant effect on the skeletal Mg/Ca ratio ($p_{regression}$ = 0.061) (mean ± standard deviation = 104 ± 8; n = 92). Over this size range the CI 95 was 87–120 mmol/mol.

3.2.5 Temperature and salinity effects along environmental gradients

The skeletal Sr/Ca ratio was significantly dependent on the size of the starfish ($p_{regression}$ < 10^{-6}) (Figure 36). On the contrary, the size had no significant effect on the skeletal Mg/Ca ratio ($p_{regression}$ = 0.061) (m ± sd = 104 ± 8 ; n = 92). Over this size range the 95% confidence interval (CI 95) was 87 – 120 mmol/mol.

Adult *P. lividus* were collected in the field from Brittany (Atlantic Ocean) to Rhodes (Eastern Mediterranean Sea) following an increasing gradient of temperature and salinity. As these variables are highly correlated (r=0.95, p<10^{-8}) along this gradient, both variables were standardized and grouped. Mg/Ca ratio in the skeleton of field collected specimen was weakly linked to this grouped variable (R^2=0.175, p=0.004). On the contrary the Sr/Ca ratio variation along this gradient were almost totally explained by this grouped variable (R^2=0.92, p<10^{-8}) through a quadratic relation.
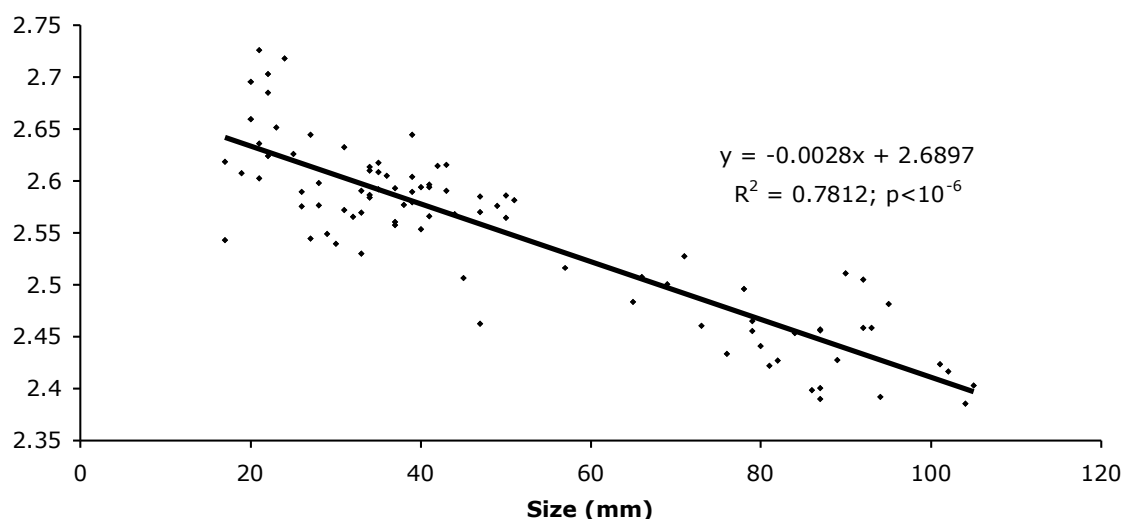

Figure 36. Sr/Ca (mmol/mol) in the skeleton of *A. rubens* according to size (mm) and regression line

3.2.6 Mg isotope in starfish skeleton

δ^{26}Mg of six different species of starfishes (Figure 37) exhibit relatively homogeneous signatures, ~-3.1‰ on average. As for sea urchin, these values appear to be different compared to the inorganic end-member of calcite precipitation -3.52 ± 0.2 ‰ (Galy et al., 2002). As for sea urchin but in a lower extent, starfish skeletal δ^{26}Mg values suggest the presence of vital effects favoring the heavy isotopic fraction. These vital effects do not display significant interspecies variability. This is also Mg/Ca ratio for which no phylogenetic difference in the skeleton was detected in these 6 sympatric species living in the same temperature and salinity conditions.
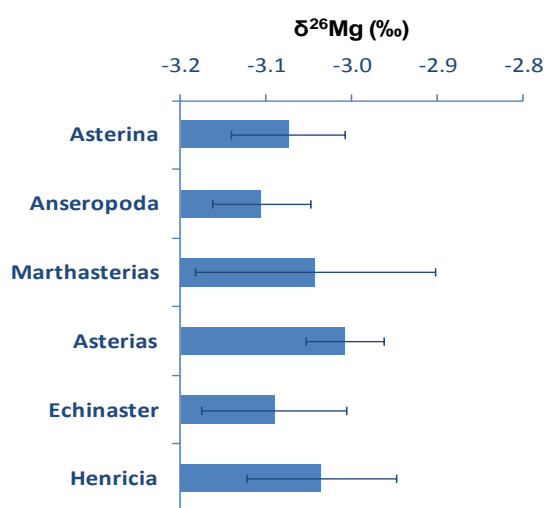
Figure 37. Mg isotopic ratios (δ^{26}Mg, in per mil) measured in six species of starfish *Asterias rubens*, *Marthasterias glacialis*, *Echinaster sepositus*, *Henricia sanguinolenta*, *Asterina gibbosa*, and *Anseropoda placenta* collected in Brittany (France).

3.2.7 Mg/Ca as a potential proxy in echinoderms

Skeletal elements of sea urchin present contrasted Mg contents. For example, the test of *Echinometra mathaei* contains 16.2% $MgCO_3$ (w/w) and its spines 7.5% $MgCO_3$ (w/w) (Weber, 1969). On the contrary, no strong differences of Mg/Ca ratio between ossicles were detected in the studied starfish. In *Asterias rubens*, the magnesium difference was between adambulacral plates, 9.3% $MgCO_3$ (w/w), and ambulacral plates, 8.0% $MgCO_3$ (w/w). Furthermore no difference between oral and aboral faces and between more or less external ossicle position were detected. This allows the use of the whole starfish skeleton for the Mg/Ca ratio analyses.

The Mg/Ca ratio in the skeleton of *Paracentrotus lividus* and *Asterias rubens* grown in experimental conditions is related to temperature. (Weber, 1969; Weber, 1973) suggested that the temperature effect observed on Mg/Ca was mainly driven by genetic factors and growth rate. However, our results showed that the skeletal Mg/Ca ratio is not linked to growth rate in aquarium grown sea urchins nor to size (age) in field collected starfishes. Because our experiment used specimens from a single population, genetic factors can also be ruled out.

In *P. lividus*, the relationship between the skeletal Mg/Ca ratio and temperature established in experimental conditions showed a saturation phase. This unusual saturation effect has not been observed in other calcitic groups, like foraminifera. In inorganic calcite, Van t'Hoff equation predicts an exponential rise of Mg/Ca with temperature. Such exponential increase has been observed in planktonic and benthic foraminifera (Lea, 2003). The observed Mg/Ca temperature relationship is better described by a non linear saturation model. The saturation observed in our experiment cannot be ascribed to calcite saturation. Indeed, echinoderm skeletal Mg/Ca ratios up to 0.341 mol/mol (to be compared to 0.118 mol/mol in the present study) have been reported in echinoids (Weber, 1969). It can be due to the saturation of either a magnesium transport system during skeletogenesis or a magnesium compartment. Magnesium transport mechanisms in echinoderms are currently unknown. A possibly saturated magnesium compartment is the organic matrix of mineralization. Acidic organic macromolecules are known to stabilize a transient amorphous phase during *in vitro* precipitation of calcium carbonate (Raz et al., 2000) and are suggested to play an important role in the hydration of this phase, allowing a higher incorporation of the magnesium ion which has a relatively large dehydration barrier (Cheng et al., 2007). As sea urchins are known to mineralize their skeleton through such amorphous calcium carbonate (ACC) phase, one may suggest that the organic matrix of mineralization of a given species is able to favour the hydration of the ACC phase with a maximum level, which would allow the incorporation of Mg to a given level. Genetical modulations of the synthesis of matrix proteins could account for the different Mg concentrations measured in different echinoderm species from the same location (Weber, 1969)(Weber 1969). Physiological modulation of matrix proteins is also possible and could also be involved in the level of Mg incorporation in the skeleton.

Minor change of salinity (3 psu) caused no significant variations of the skeletal Mg/Ca ratio of aquarium raised *P. lividus*. On the contrary, when a wide salinity range was used, a clear salinity effect on the Mg/Ca ratio was evidenced in *A. rubens*.

This difference is reminiscent of results obtained in Foraminifera (Nürnberg et al., 1996), where Mg/Ca ratios of aquarium grown individuals were only affected by drastic salinity changes (>10 psu). The salinity effect reported in *A. rubens* was not due to differences in growth rate depending on salinity. Differences in Mg and Ca transport or equilibrium according to salinity could be involved. *A. rubens* is an osmoconformer, its perivisceral and ambulacral fluids being isosmotic and isoionic with sea water except for Ca and K that are regulated (Binyon, 1962; Stickle and Diehl, 1987). If calcium uptake is at least partly controlled, magnesium concentration in inner fluids would vary more than calcium ones with seawater magnesium concentration and, thereby, with salinity. As a consequence, the Mg/Ca ratio of inner fluids would be lower at lower salinities. If removal of Mg before precipitation of the skeleton proceeds at similar rates whatever the salinity, the skeleton produced at lower salinity will have a lower Mg/Ca ratio. Alternatively, salinity could induce a modification in the composition or abundance of the intraskeletal organic matrix, which was suggested to control the Mg content of the echinoderm skeleton (Dubois and Chen, 1989). Such hypothesis was already proposed by (Vander Putten et al., 2000) to explain seasonal variations in the Mg content of *Mytilus edulis* calcite shell layer. We suggest this upregulation is too small to be detected when salinity changes are low, as in the sea urchin growth experiment (3 psu).

3.2.8 Sr/Ca as a potential proxy in echinoderms

In field collected *A. rubens*, the Sr/Ca ratio was negatively related to the starfish size, as already shown in planktonic foraminifera, other organisms with a high-magnesium calcite skeleton (Elderfield et al., 2002). On the contrary, no size effect was detected on the Sr/Ca ratio in the skeleton of the experimental starfishes probably because the size range (41-66 mm ray) was narrower than in the field study (17–105 mm ray) and thus impeded to detect an effect.

The skeletal Sr/Ca ratio of *P. lividus* juveniles grown in aquaria, increased with growth rate and temperature (until 19°C). Sr/Ca variations are correlated with growth rate variations and higher Sr/Ca observed here fits in the range of

optimal temperatures of somatic growth (18°C to 22°C) of *P. lividus* experimentally determined by (Le Gall et al., 1990). These relations between Sr/Ca, growth rate and temperature are usual in biogenic calcites (De Deckker et al., 1999; Lea et al., 1999; Lorrain et al., 2005; Stoll et al., 2002) and are attributed to a predominant positive temperature effect on crystal growth rate, which in turn controls strontium incorporation (Carré et al., 2006; Lorrain et al., 2005; Rickaby et al., 2002). The skeletal growth rate effect is usually attributed to a faster and less efficient discrimination of calcium ions against strontium ions.

In starfish skeleton, higher Sr/Ca ratios were recorded at lower temperature, a relation unusual for biogenic calcites in which Sr/Ca ratios are either unrelated or positively linked to temperature (De Deckker et al., 1999; Lea et al., 1999; Stoll et al., 2002). This unusual relation could be linked to supersaturation. (Wasylenki et al., 2005) showed that Sr incorporation into abiotic calcite increased with supersaturation. However, supersaturation in seawater increases with temperature (Morse and Mackenzie, 1990). Supersaturation level in the calcifying vacuole is unknown but metabolism increases with temperature and a higher ion transport is expected. A possible explanation could be provided by the surface enrichment model (Watson, 1996). According to this model, higher temperatures would increase the diffusivity of Sr ions in the near surface region of the crystal, decreasing their incorporation in the crystal lattice (Stoll et al., 2002).

Sr/Ca ratios in starfish skeleton increased with salinity. This relation cannot be explained by kinetic factors as growth rate had no influence on the skeletal Sr/Ca ratio. Furthermore as the seawater Sr/Ca ratio remains constant between 10 and 35 psu (Dodd and Crisp, 1982; Ingram et al., 1998; Shen et al., 1996), the variation of skeletal Sr/Ca ratio cannot be the result of variation in seawater Sr/Ca ratios. A metabolic effect due to salinity can be proposed. In *Mytilus trossulus*, salinity effects on skeletal calcite Sr/Ca ratio were detected in mussels showing high mantle metabolic efficiency (i.e. mussels showing low growth rate) (Klein et al., 1996a). In that case, intracellular transport of shell-forming inorganic components from the seawater to the site of mineralization dominated intercellular transport. As intracellular transport is more Ca-specific than intercellular transport, if salinity decreases, Ca concentration will be controlled and Sr concentration will decrease. The skeletal Sr/Ca ratio will then decrease with salinity. Interestingly, Ca, but not Sr,

has also been reported to be controlled in echinoderm inner fluids (Binyon, 1962; Stickle and Diehl, 1987).

The skeletal Sr/Ca ratio of aquarium grown *P. lividus* was negatively linked to salinity. This observation is antagonist to the very clear positive relation between Sr/Ca and salinity reported in aquarium grown *A. rubens*. However the effect observed in sea urchin is weak and encompasses a very restricted salinity range. Further research is clearly needed to determine the factors controlling the Sr/Ca ratio in the echinoderm skeleton. In particular, the involvement of the initial ACC in strontium incorporation deserves attention.

3.2.9 Implications for paleoreconstruction

Well-preserved fossils were used to reconstruct past Mg/Ca ratio in seawater up to the Phanerozoic (Dickson, 2002; Ries, 2004). (Ries, 2004) proposed algorithms which relate skeletal and seawater Mg/Ca ratios, taking into account the temperature effect, to reconstruct palaeoceanic Mg/Ca ratio. Using these algorithms we calculated the reconstructed seawater Mg/Ca ratio and the error induced by the salinity effect on the calcite Mg/Ca ratio. This induced an error in reconstructed seawater Mg/Ca ratio of between 2 and 5% at a difference of 1 psu and of between 16 to 46% for a difference of 10 psu (Figure 38) according to seawater Mg/Ca ratio. The highest error occurs for the lowest seaweater Mg/Ca ratio of 1.29, i.e. values inferred for a part of the Phanerozoic oceans (Dickson, 2002). This result emphasizes the need to consider the salinity effect, with the temperature effect, when reconstructing past seawater Mg/Ca ratio.
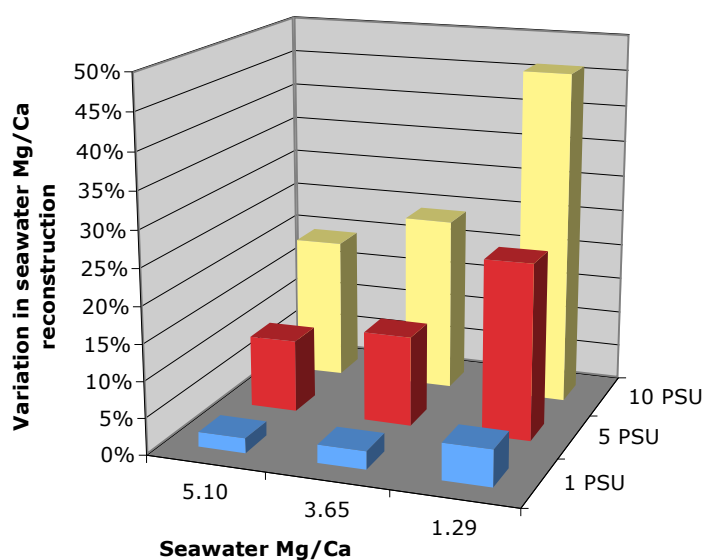
Figure 38. Impact of the salinity effect on the seawater Mg/Ca ratio reconstruction (%)

Temperature significantly controls the skeletal Mg/Ca ratio in P. lividus and this effect is not due to growth rate as previously suggested. At higher temperatures, a saturation process is observed, which limits the use of Mg/Ca ratio in P.lividus test as a temperature proxy to the lower temperatures. Because this saturation process is likely to occur at contrasted temperature thresholds according to species, any temperature correction to be applied to use the skeletal Mg/Ca ratio as a proxy of seawater Mg/Ca ratio (Ries, 2004) has to be specific.

3.3 Bivalves

3.3.1 Metal uptake kinetics studies

The results of these uptake and accumulation studies show that for alkaline-earth metals such as calcium and strontium uptake kinetics are fast and that equilibrium is reached within hours (Figure 39). However, in case of transition of post-transition elements the kinetics are considerably slower with no sign of equilibration within the experimental period.
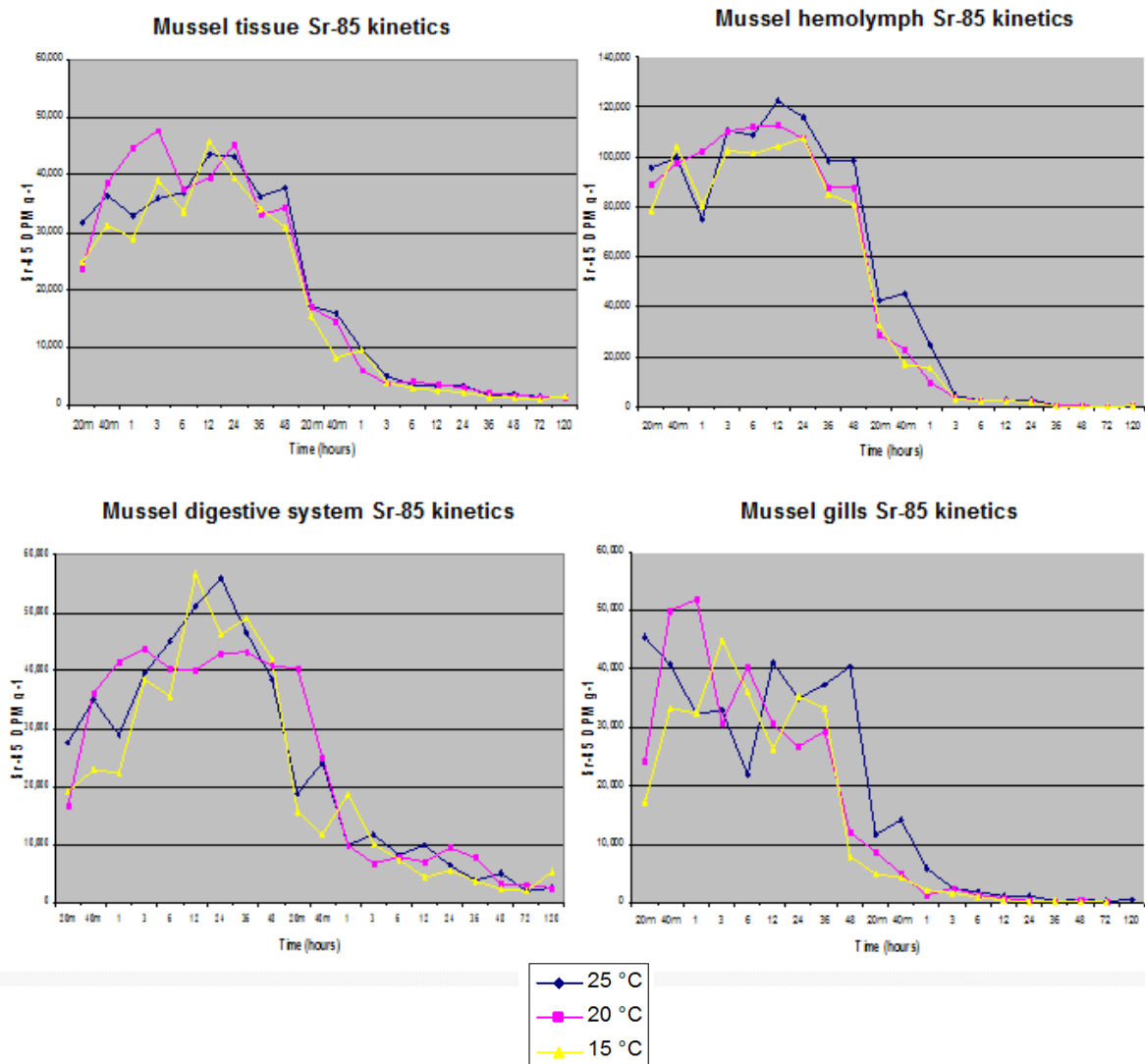
Figure 39. Uptake and elimination kinetics of strontium (measured as Sr85) in tissues of the common mussel, *Mytilus edulis*. Uptake and elimination kinetics are fast reaching equilibrium within 24 hours.

These results are in accordance with results from field monitoring in which the dynamics of metal accumulation has been followed across salinity and seasonal gradients. The elements showing fast exchange kinetics inside the mussels (i.e. the alkali and alkaline-earth metals) closely follow the external trends in relation to salinity gradients within hours or days. The transition and post-transition elements display considerably slower kinetics, which is largely attributed to the slow elimination of the elements from the tissues. In case of radioactive spiking the accumulation of metals on the shells during the whole animal exposures was measured by separately counting the shells after removal of the soft tissues at the end of an experiment.

These results show that direct accumulation of for example calcium on the shell is not a major route of calcium accumulation in or on the shells. Nonetheless, the accumulation of calcium and other elements with rapid biological exchange dynamics in the shell reflects the changes in the exposure environment due to the rapid equilibration of the elements between the exposure water and the soft tissues. These experimental observations are in good agreement with other studies relating environmental dynamics of elements used as proxies. They obtained results show how the dynamics of uptake, internal compartmentalization and elimination of the different elements provides an explanation for the close resemblance between changes in the environment, the soft tissues and the shell for a number of elements and the lack of such clear relationships in other cases. . We have not yet completed the analysis of the shells. These results will be used to incorporate the shell as a kinetic compartment in the whole mussel model.

3.3.2 Relative importance of water and particles (food) as sources of elements

For the major elements such as calcium or magnesium the direct exposure via seawater appears to be the dominant route due to the very high concentrations of the elements in the exposure water so that the contribution from food (or particulates) uptake is generally much less. For the elements which are present in lower concentrations in seawater the relative importance depends on the concentration of the elements in the water and food and the uptake rate constants from water and food. Short term exposure experiments with radiotracers have shown that uptake from water, at least for calcium and a number of transition metals, occurs via different interphases and is not limited to for instance the gills. In contrast uptake of particles occurs largely via the digestive system. In this case the uptake rate constants are function of the ingestion rate (or filtration rate) and the assimilation efficiency. The results in Figure 40 show the passage and elimination of several elements from the mussels after pulse exposure to labeled algae and subsequent follow up of the loss of the tracer. These kinetic results are used to estimate the assimilation efficiency and tissue elimination rates.

If the concentration in water, the concentration in food and the respective uptake rate constants from water and food (or ingestion rates and assimilation efficiency) are known than the relative importance of the two routes can be determined for different scenarios. We are currently performing a number of such simulations under different realistic scenarios and the results show that the model provides a good explanation for the observed dynamics of element incorporation in the soft tissues of mussels. Figure 41 shows a comparison of predicted and measured element concentrations in soft tissues of mussels under a number of water and food exposure scenarios. The predictions of element concentrations in shells will be added when the results of the shell analysis are incorporated. For example, it can be clearly shown how changes in food concentration and element concentrations in these (e.g. algal blooms) strongly alter the relative importance of water and food (e.g. in case of Ba as shown by other partners from field studies). We still have to incorporate the results of shell analysis in the model, but preliminary comparison with results from existing shell studies from field surveys indicates that our mussel soft body model is consistent with these independently obtained field based results.
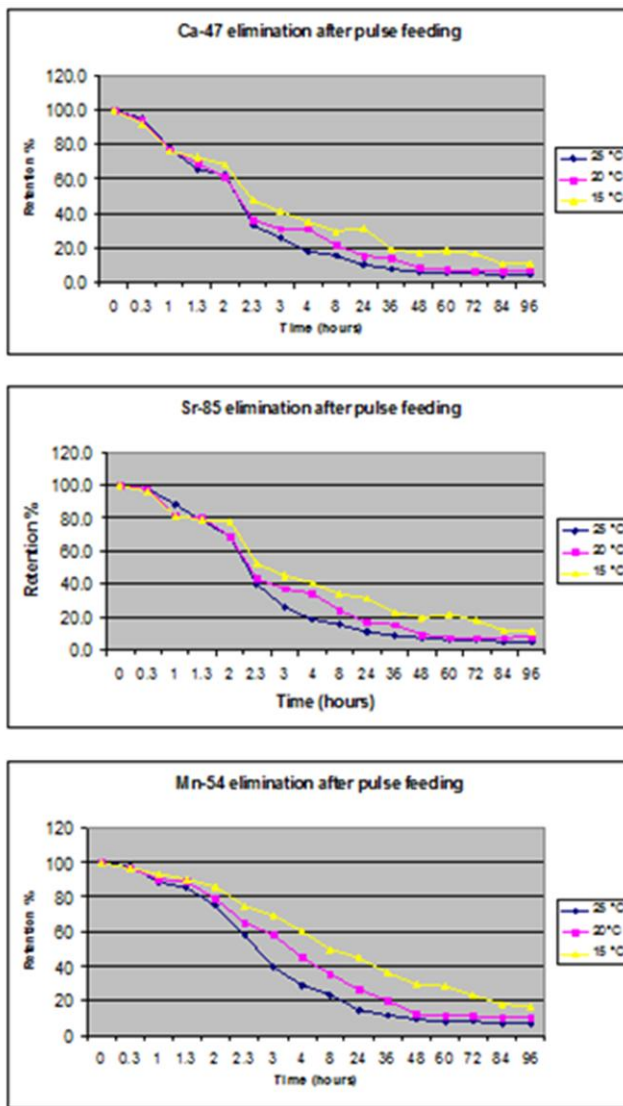
Figure 40. Elimination kinetics of calcium (measured as Ca47), strontium (measured as Sr85), manganese (measured as Mn54) in tissues of the common mussel, *Mytilus edulis* after pulse feeding with labelled food particles.Lower temperature results in increased assimilation efficiency probably due to longer gut passage time.
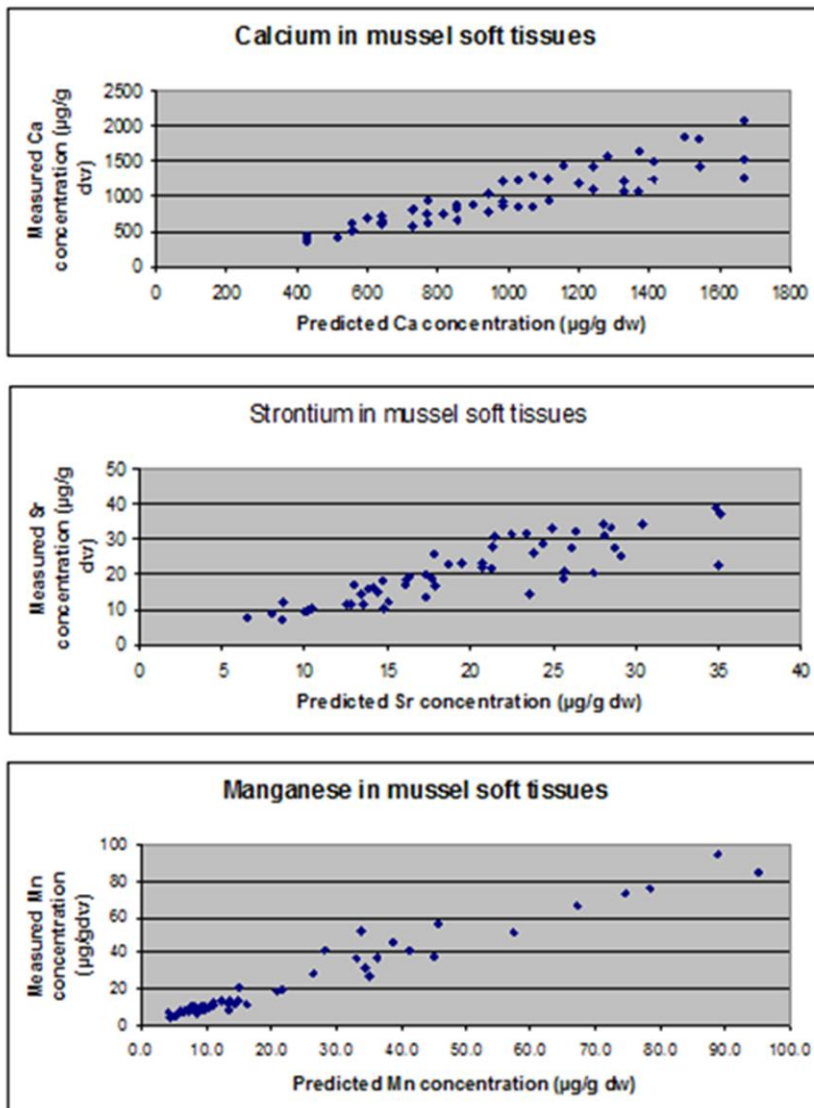
Figure 41. Comparison of predicted versus element concentrations in soft tissues of mussel, *Mytilus edulis* under various water and food exposure scenarios.

3.3.3 Mytilus edulis along the Scheldt estuary salinity gradient

3.3.3.1 Seasonal evolution of trace element in soft tissues

ICP-AES analysis revealed that lithogenic elements such as Fe (Figure 42), Al (Figure 43) and Mn (Figure 44) had similar temporal shifts in the mussel organs.

Figure 42. Temporal profile of Fe concentrations in different tissues of *Mytilus edulis*.
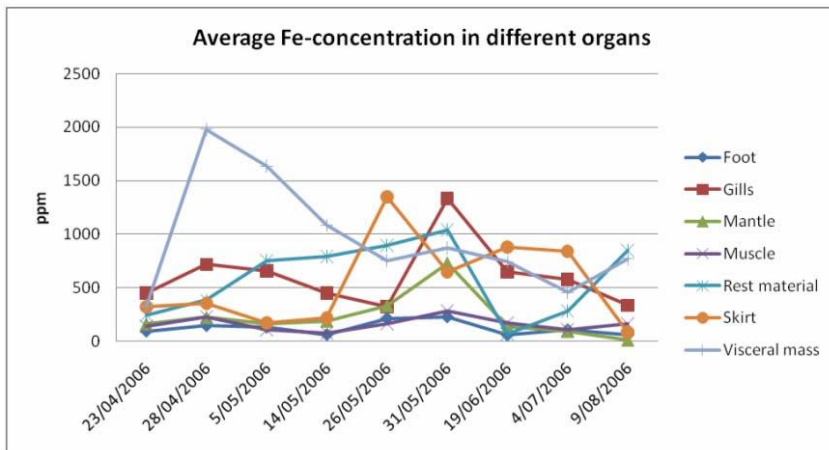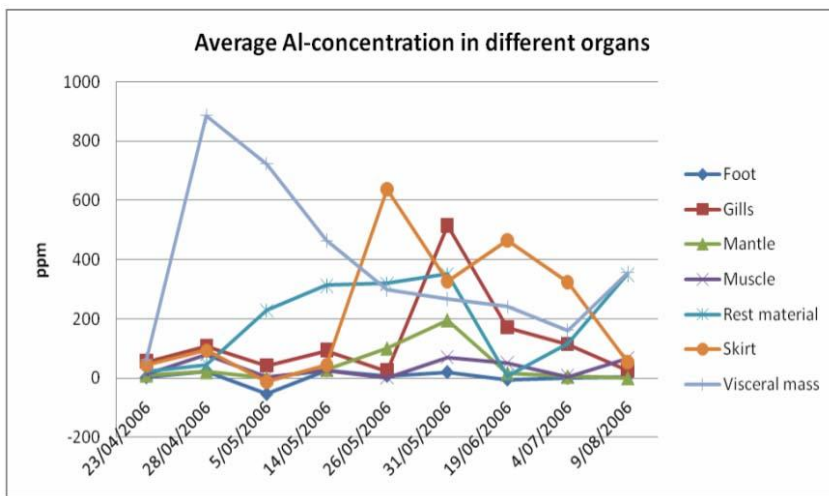

Figure 43. Temporal profile of Al concentrations in different tissues of Mytilus edulis.
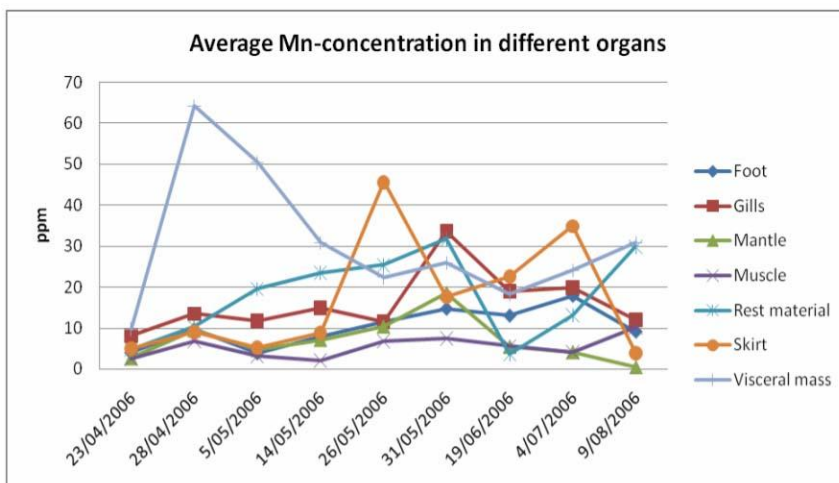

Figure 44. Temporal profile of Mn concentrations in different tissues of Mytilus edulis.

Peak concentrations occur in the visceral mass in early spring. Concentrations subsequently decrease to increase in rest material (consisting of the second part of the gut).

At the end of spring, about one month after concentrations peaked in the visceral mass, the skirt (attached to the shell) becomes enriched. The observed pattern is characteristic for all three elements. It possibly reflects slow sediment digestion/desorption with storage of elements in the visceral mass. Subsequently these elements are translocated to the skirt and periostracum (part of the latter is always dissected together with the skirt). Such results need to be compared with trace element temporal variation in shell new growth.

For Ba, All tissues show a similar temporal variation with a clear maximum at the end of spring. One remarkable fact is that the Ba-concentrations are higher in the foot and in the skirt than in the digestive organs. This could be due to a fast translocation of Ba from the digestive tract to muscles and shell. Another interesting observation is that Ba-concentrations in all organs are very low at the beginning of fall (Figure 45). This means that the hypothesis of Ba-stocks proposed by Gillikin *et al.* 2006 can now be rejected. Other elements (K, Mg, P, S and Sr except Ba) show a rather constant temporal concentration pattern in which there do not seem to be clear translocations from one compartment to another.

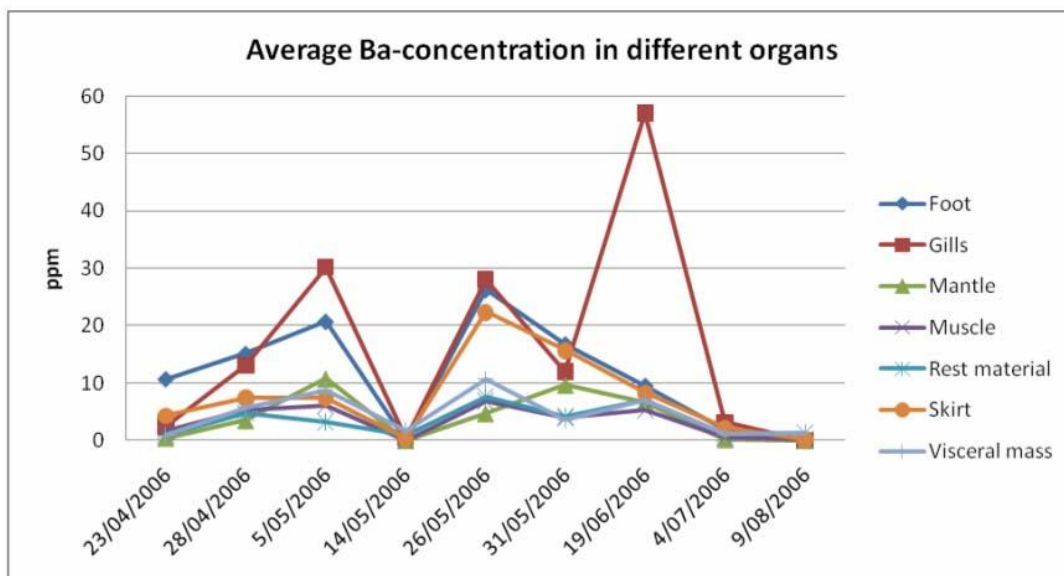**Figure 45. Ba concentration in different parts of *Mytilus edulis* soft tissues.**

3.3.3.2 δ¹³C of shell organic matrix with salinity

We measured the $\delta^{13}C$ composition of tissues (mantle and other), bulk shell organic matrix and specific compounds (palmitic acid, cholesterol) for *Mytilus edulis*.

All mussel compartments showed a clear decrease in $\delta^{13}C$ with decreasing salinity (Figure 46), the opposite trend is observed for $\delta^{15}N$ (Figure 47). The differences between the different compartments for a single site are larger than the variation within mussel compartments along the salinity gradient.

Figure 46. $\delta^{13}C$ in different compartments of mussel tissue, shell organic matter components and suspended organic matter sampled along a decreasing salinity gradient of the Scheldt estuary at Knokke, Hooftplaat, Griete and Ossenisse.

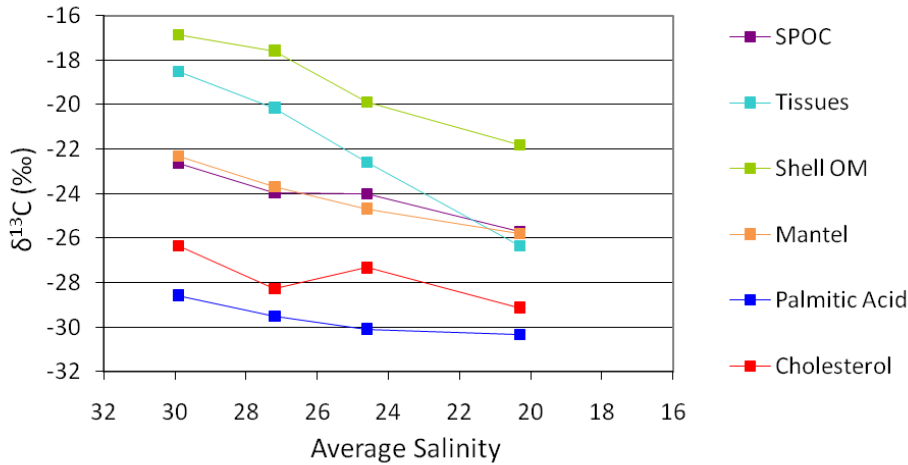**Figure 47. $\delta^{15}N$ in different compartments of mussel tissue, shell organic matter components and suspended organic matter sampled along a decreasing salinity gradient of the Scheldt estuary at Knokke, Hooftplaat, Griete and Ossenisse.**
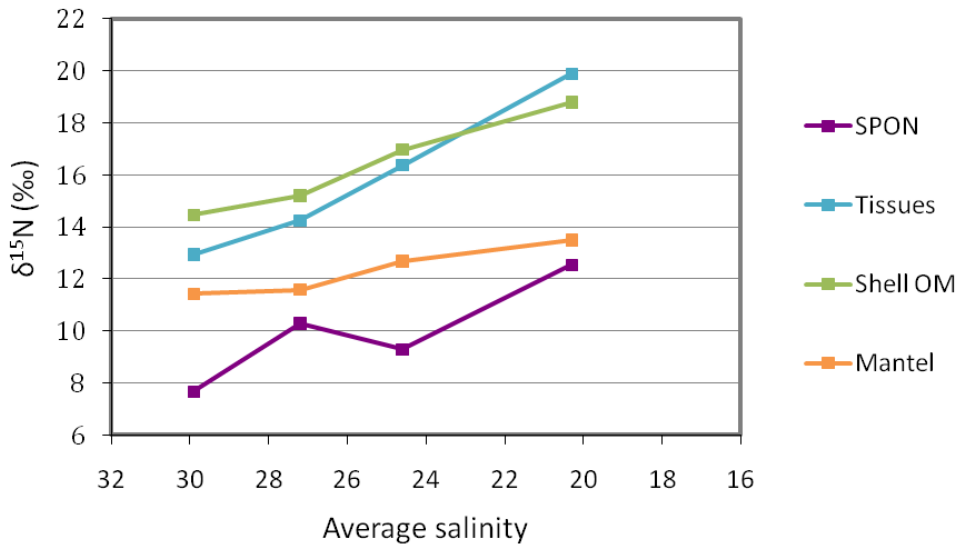
3.3.4 In vitro growth of M. edulis under controlled conditions

3.3.4.1 Shell $\delta^{18}O$ and $\delta^{13}C$

The $\delta^{18}O$ en $\delta^{13}C$ composition was measured along shell new growth for 3 replicate specimens (Figure 48).
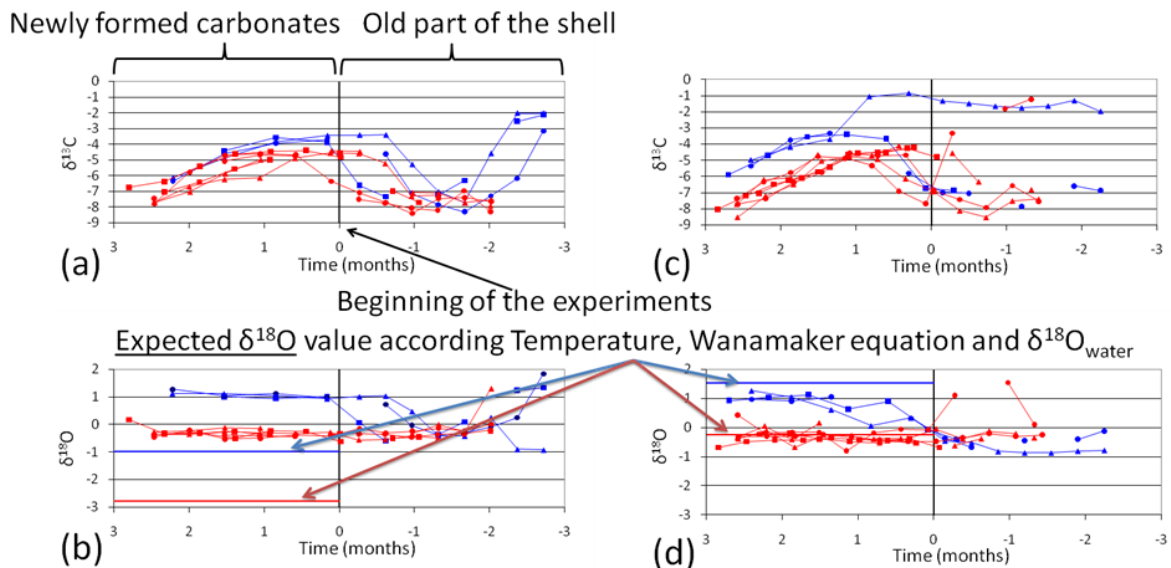
Figure 48. (a) $\delta^{13}C$ for low salinity (28) experiments, (b) $\delta^{18}O$ for low salinity experiments, (c) $\delta^{13}C$ for high salinity (18) experiments, (d) $\delta^{18}O$ for high salinity experiments, red lines correspond to high temperature (16°C) and blue lines to low temperature (8°C).

For mussels kept at salinity of 28 and two temperature conditions (8° and 16°C) the measured $\delta^{18}O$ agreed well with the values calculated using the following temperature reconstruction equation (Wanamaker et al., 2007):

$$T(°C)=16.28-4.57*(\delta18Os-\delta18Ow) +0.06*(\delta18Os-\delta18Ow)^2$$

For the mussels kept at lower salinity (18) shell $\delta^{18}O$ values were systematically higher (about 2‰) than calculated ones. These puzzling results are not explained yet, but it was suspected in first instance this had to do with changes in the alkalinity of the aquarium water (the latter consisted of Oosterschelde water (salinity 28; NIOO-CEME site) diluted to a salinity of 18 using Milli-Q grade water). However, after checking Zeebe and Wolf-Gladrow (2001), it appeared that this shift can neither be explained by a decrease in alkalinity nor a shift in pH. We plan to clarify this point by the comparison of mussels collected from two different estuaries characterized by very different alkalinities (The Scheldt in Netherlands and the gulf of Morbihan in France), the work is still in progress.

3.3.4.2 Trace elements

The trace elemental composition of all the shells grown under controlled laboratory conditions was analyzed by LA-ICP-MS (Figure 49).
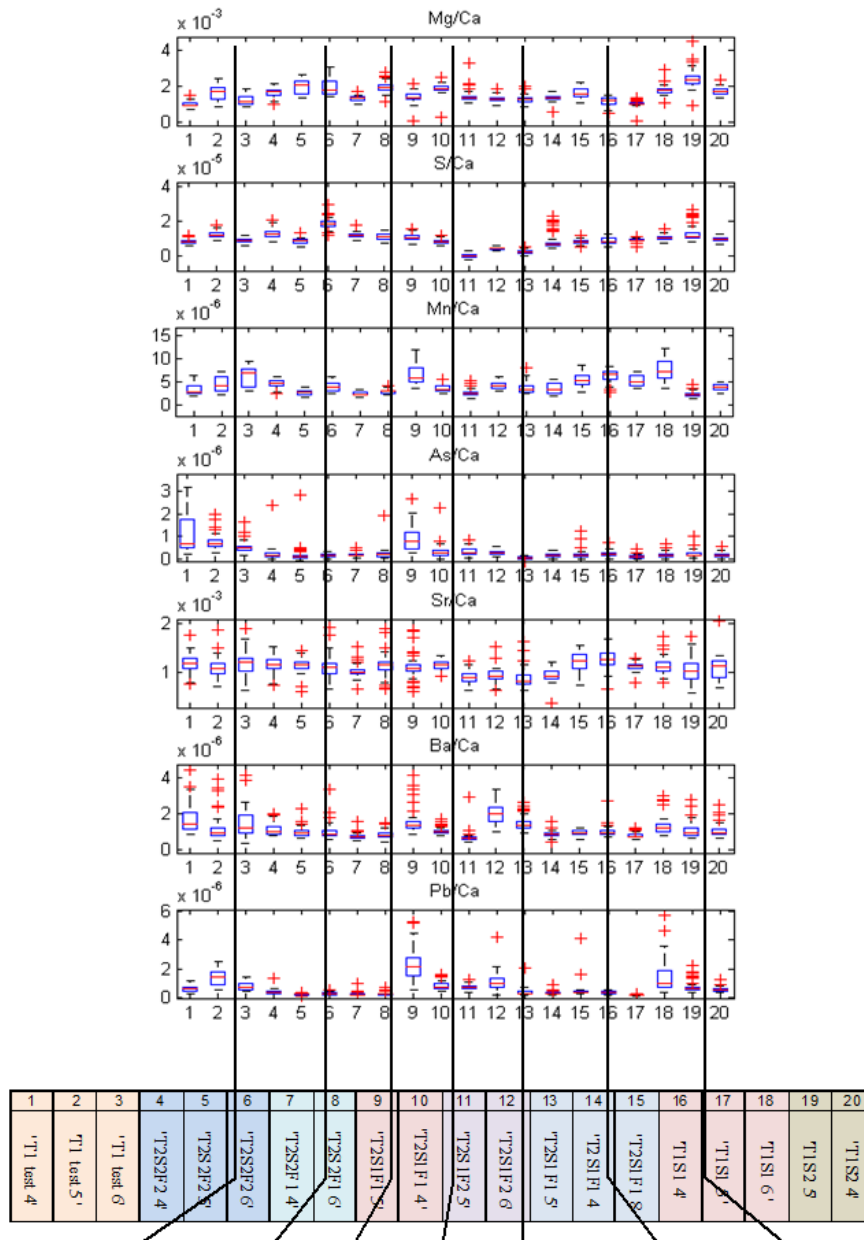
Figure 49. Growth experiment under controlled conditions. Box plots of the trace-element over Ca ratio in shell new growth. T1=18ºC, T2=8ºC, S1=18‰, S1=28‰, F1=8mg DW/week/org and F2=16mg DW/week/org.

It is clear that the different experimental conditions did not result in significant differences in trace-elemental concentrations. Such results contrast with previous studies (Wanamaker et al., 2008a) where clear temperature and salinity effects were observed for both Mg/Ca and Sr/Ca.

The lack of a salinity effect could be explained by the fact that the seawater in our experiment was diluted whit MQ-water so that the Element/Ca ratios in the ambient water are identical for the different salinities. This was not the case in Wanamaker's experiment since he diluted seawater with river water to attain desired salinities. The lack of temperature effect is less easy to explain. One explanation could be stress due to feeding situation (here: 2x/week; Wannamaker: 2x/day) but this conflicts whit the fact that mussels in our experiment grew 10 to 20 times faster. Another explanation can be that the effect is seen after a longer period (our total experimental time = 2 months; Wanamaker's total experiment time = 4 months). This suggests slow dynamical relationships between elements and environment parameters which have strong impacts on the interpretation of the relations.

3.3.5 Mg isotope in Ruditapes philippinarum

δ^{26}Mg and δ^{25}Mg signatures of various compartments involved in the calcification of the Manila clam (*Ruditapes philippinarum*) are presented in Table XTable X. Magnesium isotopic compositions and concentrations of Mg, Ca, Na and K in seawater, extrapaleal fluids, hemolymph, soft tissues (including mantle, muscle and remaining part) and shells (prismatic and nacreous layers) measured in the manila clams Ruditapes Philippinarum at two sampling sites (Locmariaquer and Le Bono) and in certified reference materials.. Strong δ^{26}Mg' versus δ^{25}Mg' correlation (r^2 = 0.999, Figure 50) demonstrates that Mg isotopes fractionate keeping a mass-dependent relationship (Young et al., 2002). The slope from the linear fit of the data (β = 0.520±0.002) is close to a value of 0.521 corresponding to an equilibrium isotope fractionation law (Young and Galy, 2004). Deviations from this law, expressed as Δ^{25}Mg' (Young et al., 2002) are reported in Table X. All analyzed samples show consistent equilibrium behavior at analytical uncertainties. Also in Table X, measured concentrations of major and minor elements (Mg, Ca, Na and K) and corresponding molar ratios (Mg/Ca and Mg/Na) are reported.

Location / Matrice	Sample Type		δ²⁶Mg ± Uc (‰)	δ²⁵Mg ± Uc (‰)	Δ²⁵Mg' (‰)	N(n)[d]	Mg µg/g	Ca µg/g	Na µg/g	K µg/g	Mg/Ca mol/mol	Mg/Na mol/mol
Locmariaquer												
Seawater[a]	1a		-0.82 ± 0.11	-0.42 ± 0.06	0.01	3(1)	1320	427	12155	-	5.1	0.10
	1b		-0.89 ± 0.17	-0.46 ± 0.08	0.01	1(1)	1198	391	10238	-	5.1	0.11
Internal fluids[a]	EPF	L1	-1.08 ± 0.11	-0.55 ± 0.06	0.01	3(2)	1165	499	10090	381	3.9	0.11
	Hemolymp	L1	-1.09 ± 0.15	-0.56 ± 0.07	0.01	3(2)	1154	476	9960	388	4.0	0.11
Soft tissues[b]	Mantle	L1	-0.35 ± 0.11	-0.19 ± 0.06	0.00	2(1)	4082	2132	24234	11417	3.2	0.16
	Muscle	L1	-0.33 ± 0.13	-0.18 ± 0.07	-0.01	2(1)	2358	1655	12143	7234	2.3	0.18
	Other	L1					3259	2338	17461	13396	2.3	0.18
Shell[c]	Prismatic layer	L1	-1.95 ± 0.12	-1.02 ± 0.07	0.00	4(2)	282	427273	4341	91	0.0011	0.06
	Prismatic layer	L1 bis	-1.93 ± 0.13	-1.01 ± 0.07	0.00	3(1)	293	362218	4503	77	0.0013	0.06
	Prismatic layer	L1-V2	-2.21 ± 0.11	-1.15 ± 0.06	0.01	2(1)	286	367171	4517	80	0.0013	0.06
	Nacreous layer	L1	-1.92 ± 0.12	-1.02 ± 0.06	-0.01	2(1)	302	386979	4363	35	0.0013	0.07
	Nacreous layer	L1-V2	-2.95 ± 0.18	-1.53 ± 0.10	0.00	2(1)	202	363308	4239	28	0.0009	0.05
Le Bono												
Seawater[a]	2a		-0.82 ± 0.11	-0.41 ± 0.06	0.01	2(1)	1115	368	9544	-	5.0	0.11
	2b		-0.81 ± 0.11	-0.42 ± 0.06	0.01	3(1)	1079	348	9335	-	5.1	0.11
Internal fluids[a]	EPF	B1	-0.87 ± 0.12	-0.45 ± 0.07	0.00	1(1)	971	383	8606	352	4.2	0.11
	EPF	B2	-1.23 ± 0.14	-0.64 ± 0.08	0.00	6(2)	978	394	8508	408	4.1	0.11
	EPF	B3	-1.15 ± 0.11	-0.59 ± 0.06	0.01	1(1)	942	386	8346	344	4.0	0.11
	EPF	B4	-0.95 ± 0.11	-0.49 ± 0.07	0.01	1(1)	953	404	8406	331	3.9	0.11
	Hemolymp	B1	-0.98 ± 0.12	-0.51 ± 0.07	-0.01	2(1)	940	368	8352	336	4.2	0.11
	Hemolymp	B2	-1.06 ± 0.14	-0.55 ± 0.10	0.00	3(1)	981	396	8512	333	4.1	0.11
	Hemolymp	B3	-1.26 ± 0.12	-0.66 ± 0.07	-0.01	1(1)	919	364	8176	349	4.2	0.11
	Hemolymp	B4	-0.96 ± 0.15	-0.50 ± 0.09	0.00	1(1)	987	399	8694	343	4.1	0.11
Soft tissues[b]	Mantle	B2	-0.33 ± 0.11	-0.18 ± 0.06	-0.01	3(1)	3052	1748	13233	12229	2.9	0.22
	Muscle	B2	-0.35 ± 0.14	-0.19 ± 0.07	-0.01	2(1)	1696	986	7206	9179	2.8	0.22
	Other	B2	-0.09 ± 0.11	-0.05 ± 0.06	0.00	2(1)	2163	1080	8756	14559	3.3	0.23
Shell[c]	Prismatic layer	B1	-2.61 ± 0.11	-1.36 ± 0.06	0.00	2(1)	291	393049	5061	87	0.0012	0.05
	Prismatic layer	B2	-4.06 ± 0.15	-2.12 ± 0.08	0.00	1(1)	156	320672	6711	151	0.0008	0.02
	Prismatic layer	B2 bis	-2.41 ± 0.14	-1.25 ± 0.10	0.01	3(1)	273	373013	4927	95	0.0012	0.05
	Prismatic layer	B3	-2.37 ± 0.09	-1.26 ± 0.07	-0.02	2(1)	270	386366	4852	87	0.0012	0.05
	Prismatic layer	B7	-4.35 ± 0.12	-2.26 ± 0.06	0.00	5(2)	246	337568	5176		0.0012	0.04
	Nacreous layer	B1	-3.18 ± 0.10	-1.63 ± 0.06	0.02	3(1)	151	399932	5040	37	0.0006	0.03
	Nacreous layer	B3	-3.22 ± 0.14	-1.67 ± 0.07	0.01	2(1)	101	421442	5412	61	0.0004	0.02
SRM												
Seawater[a]	CASS-4		-0.80 ± 0.08	-0.42 ± 0.05	0.00	11(3)	1144	352	10015	368	5.36	0.11
Oyster Tissue[b]	NIST SRM1566a		-0.23 ± 0.13	-0.14 ± 0.07	-0.02	3(1)	1150	1858	3950	7533	1.02	0.28
	Certified values						*1180*	*1960*	*4170*	*7900*	*0.99*	*0.27*
Aragonitic Coral[c]	JCp-1		-2.02 ± 0.12	-1.05 ± 0.06	0.00	15(4)	951	350800	4400	120	0.0045	0.20
	Certified values						*972*	*382000*	*4350*	*185*	*0.0042*	*0.21*
Giant Clams[c]	JCt-1		-2.80 ± 0.14	-1.45 ± 0.09	0.01	3(1)	260	343667	4167	67	0.0012	0.06
	Certified values						*295*	*390200*	*4440*	*89*	*0.0012*	*0.06*

[a] Concentrations expressed per unit mass of liquid
[b] Concentrations expressed per unit mass of dry tissue
[c] Concentrations expressed per unit mass of carbonate
[c] N refers to analyses replicates and n to chemistry replicates

Table X. Magnesium isotopic compositions and concentrations of Mg, Ca, Na and K in seawater, extrapaleal fluids, hemolymph, soft tissues (including mantle, muscle and remaining part) and shells (prismatic and nacreous layers) measured in the manila clams Ruditapes Philippinarum at two sampling sites (Locmariaquer and Le Bono) and in certified reference materials.
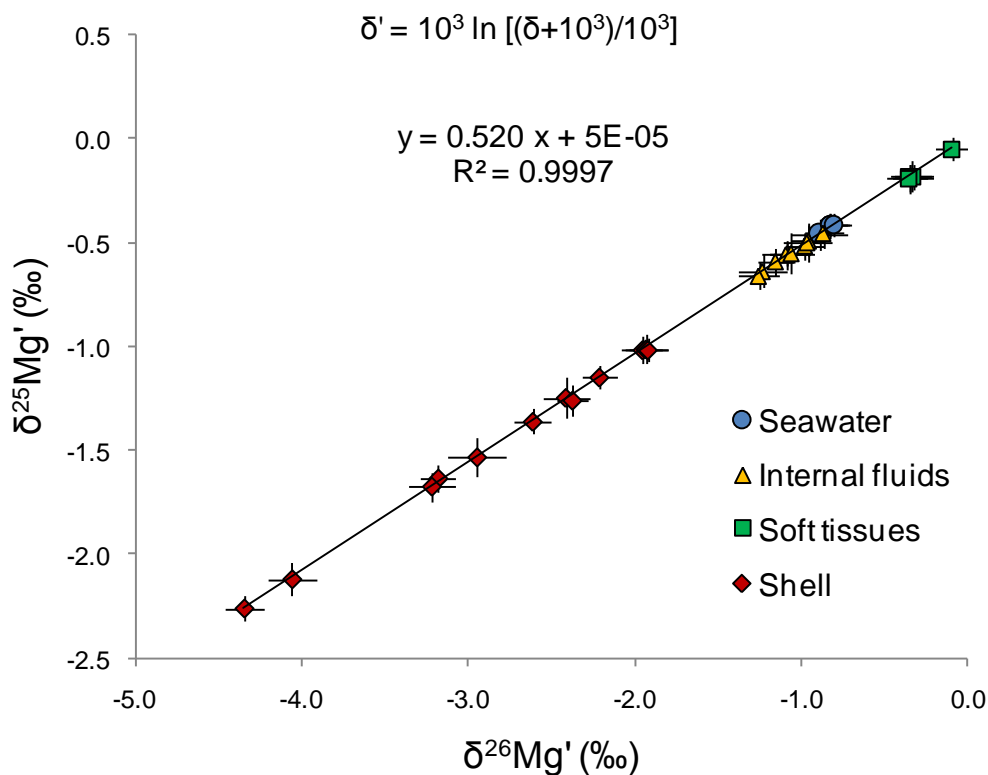
Figure 50. Magnesium three-isotope plot (δ²⁶Mg' versus δ²⁵Mg') of the different matrices of the Manila clam (*Ruditapes philippinarum*) originating from the two sampling sites (Locmariaquer and Le Bono). The solid line refers to the best fit of the data (N = 31) and highlights the mass-dependent relationship of Mg isotopes (β = 0.520) close to the equilibrium fractionation law (β = 0.521) evaluated from (Young et al., 2002).

3.3.5.1 Character of δ²⁶Mg data

Mg isotopic signatures vary in a large range from -0.09 ‰ in the soft tissues (remaining organs) to -4.35 ‰ in the prismatic layer of the aragonitic shell sampled at Le Bono site. This huge interval of fluctuations (~-4.2‰) represent approximatively two third of the terrestrial range so far identified (Black et al., 2008; Black et al., 2006; Buhl et al., 2007; Chang et al., 2004; Pogge Von Strandmann, 2008; Ra and Kitagawa, 2007; Tipper et al., 2008; Young and Galy, 2004).

Seawater samples, display homogeneous Mg isotopic compositions with average values for duplicates samples of -0.86±0.15‰ at Locmariaquer and -0.82±0.10‰ at Le Bono. These values are comparable with the seawater reference material CASS-4 (-0.80±0.08‰) considering the 2σ uncertainties, and also highly comparable with published values for open ocean Mg isotopic signature of -0.82±0.10‰ reported by several authors (Chang et al.,

2004; Pogge Von Strandmann, 2008; Ra and Kitagawa, 2007; Young and Galy, 2004). Internal fluids of the clam, hemolymph and extrapallial fluid (EPF), display comparable chemical composition (Table X) contrasting with their Mg isotopic signature which appears to be different from seawater as illustrated in Figure 51.
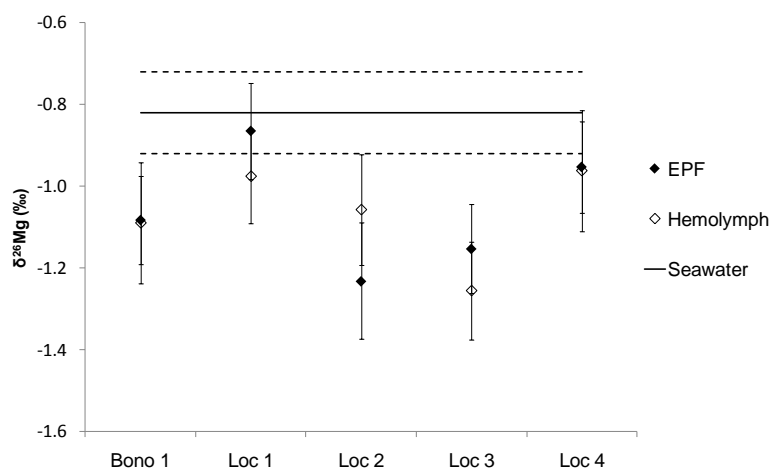

Figure 51. Comparison of EPF and hemolymph δ26Mg values obtained in different specimens with seawater. Uncertainties are at 95% confidence interval.

Soft tissues from different organs (mantle, muscle and remaining organs) show higher concentrations of major elements compared to seawater (expressed as dry weight of tissue, Table X). Their relative proportion also differs; Na being the most abundant cations followed by K and Mg, with mean molar ratios K/Na and K/Mg (0.56 and 2.7 mol/mol, respectively) consistently higher than in seawater (0.022 and 0.20 mol/mol, respectively). In these tissues, Mg isotopic ratios exhibit peculiar features with homogeneous values of -0.34±0.12‰ on average for the mantle and the muscle at both sites, whereas remaining organs display some heavier signature at -0.09±0.11‰. When compared to seawater (-0.86‰), δ26Mg for soft tissues indicate a preferential uptake of heavy isotopes during biological incorporation of Mg. Interestingly, similar trend is observed in the Oyster tissue (NIST SRM1566a) at -0.23±0.13‰ and in different chlorophyll forms of marine phytoplankton ranging from -0.56 to 0.09 ‰ (Ra and Kitagawa, 2007).

Clam shells show the lightest δ26Mg signatures from this study (see Table X), with a range from -1.93±0.13‰ to -4.35±0.12‰. At Locmariaquer the specimen collected reveal an in-between valves isotopic differentiation of ~1‰ which largely exceeds the external error (0.15‰).

One valve shows relatively homogeneous signatures with an average of -1.9±0.12‰ in both prismatic and nacreous parts, the prismatic signature being confirmed by a duplicate sample processed separately (specimen L1bis, Table X). The second valve shows lighter and more variable values, with -2.21±0.11‰ in the prism and -2.95±0.18‰ in the nacre. At le Bono site, large differences are also observed; first between specimens with a ~2‰ variability in the prismatic part, but also for a given specimen in the same valve (specimen B2, Table X). For this specimen, two distinct samples were collected consecutively with similar amounts (~15 mg of carbonate powder), but they differ by 1.6‰ in $\delta^{26}Mg$. Finally for Le Bono site, nacreous layers from two specimens show also light signatures (-3.2±0.1‰ on average) but with a lower inter specimen variability (0.5-0.8‰).

3.3.5.2 Isotopic fractionation along Mg incorporation pathway

Mg is a conservative element in seawater with a long residence time (~12My) (Berner and Berner, 1996) and its isotopic signature can be considered to be homogeneous in the ocean (Tipper et al., 2006) and in estuaries (Pogge Von Strandmann et al., 2008). Consequently, the Mg fractionation patterns observed in the clam compartments support a control by internal processes.

The slight isotopic changes observed in internal fluids, with $\Delta 26Mg_{EPF-seawater}$ of -0.26‰ at Locmariaquer and of -0.05‰ to -0.43‰ at Le bono can be related to the formation process of these fluids and especially the EPF. EPF represents a thin liquid pocket located between the inner epithelium and the inner shell surface where biomineralisation takes place (Wheeler, 1992; Wilbur and Saleuddin, 1983). During the secretion of EPF, shell forming cations cross through different biological barriers, including successively the mantle outer epithelium, the mantle itself and finally the inner epithelium (Crenshaw, 1980; Klein et al., 1996a).

EPF light signatures are accounted from the balance with soft tissues. Figure 52 illustrates that soft tissues accumulate significant amount of Mg, especially within the mantle which stores Mg at concentrations as large as 4080 to 3050 µg/g, in parallel with a strongly fractionated $\delta^{26}Mg$ signature ($\Delta^{26}Mg_{mantle-seawater}$: +0.48‰ on average). The heavier isotopic signatures of organic tissues, representative of the intracellular medium, show enrichments in heavy isotopes and indicate that Mg transport towards the cells is a selective process. As a consequence of this biological uptake which may occur from the hemolymph but also directly from the EPF, the isotopic composition of the

internal fluids is fractionated as a balance effect towards light isotopic signatures. Therefore the EPF enrichments in lighter Mg ($\Delta^{26}Mg_{EPF-seawater}$ of -0.26‰ at Locmariaquer and of -0.04‰ to -0.43‰ at Le bono) potentially trace a biological demand of Mg in order to sustain the metabolic activity of the clam.
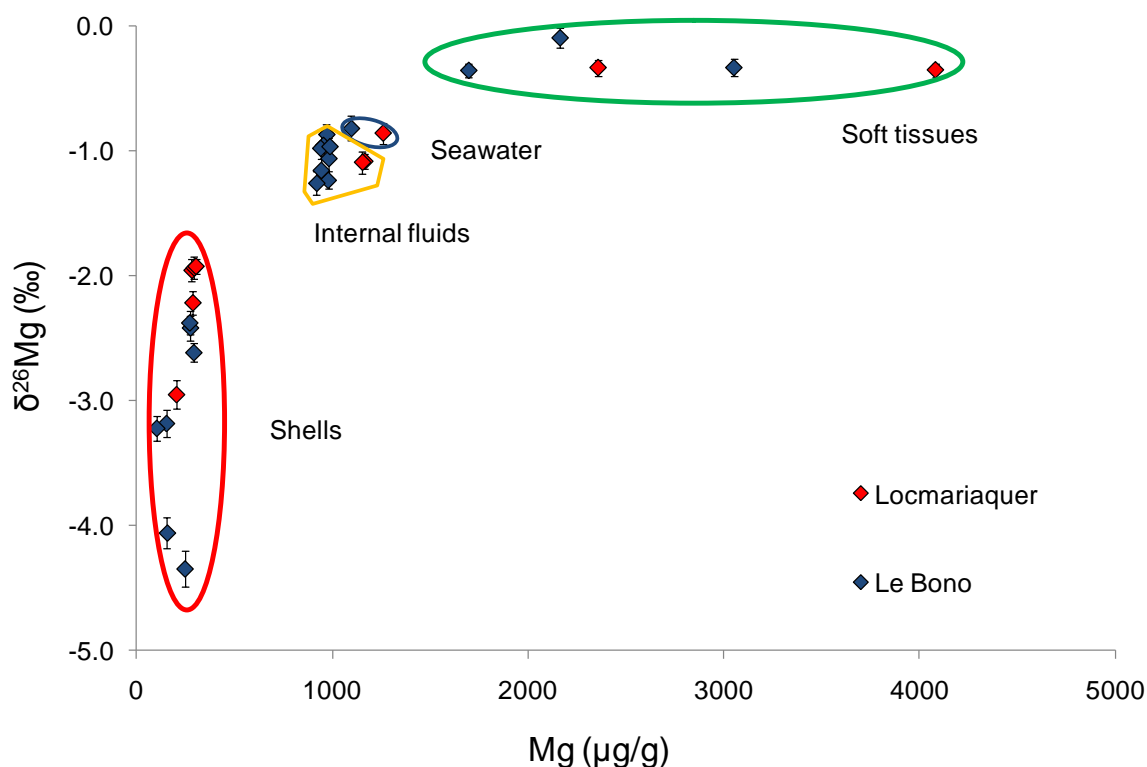

Figure 52. Comparative plot of δ²⁶Mg (in per mil) versus Mg concentrations (in μg/g) determined in the different matrices involved in the calcification process of the Manila clam (*Ruditapes Philippinarum*) and in the seawater from the two sampling sites (Locmariaquer and Le Bono). The Mg concentrations reported for the seawater and the internal fluids (EPF and hemolymph) are expressed in μg per gram of liquid, for the soft tissues (mantle, muscle and remaining parts) in μg per gram of dry tissue and for the shells (inner nacreous part and outer prismatic part) in μg per gram of carbonate. Uncertainties associated with δ²⁶Mg represent 2σ error (95% confidence interval).

$\Delta^{26}Mg_{shell-seawater}$ obtained for the aragonitic bivalve show a marked difference compared to corals and sclerosponges, ranging from -1.1‰ to -3.5‰ for the manila clam and at -2.0±0.2‰ for the Giant clam (Figure 53). For *Ruditapes philippinarum*, the higher end of the range (-1.1±0.2‰) found at the oceanic site (Locmariaquer) is comparable to coral values which likely represent the inorganic end-member of aragonite precipitation with $\Delta^{26}Mg_{aragonite-seawater}$ of -1.0±0.2‰ (Chang et al., 2004). By contrast most other data are scattered towards lower values showing that some important

additional mechanisms fractionate towards lighter signatures. These variations which appear to be larger at estuarine site (Le Bono) compared to oceanic site (Locmariaquer) have been registered in both nacreous and prismatic layers. This strong variability may be attributed to some strong changes in the isotopic composition of the EPFs.
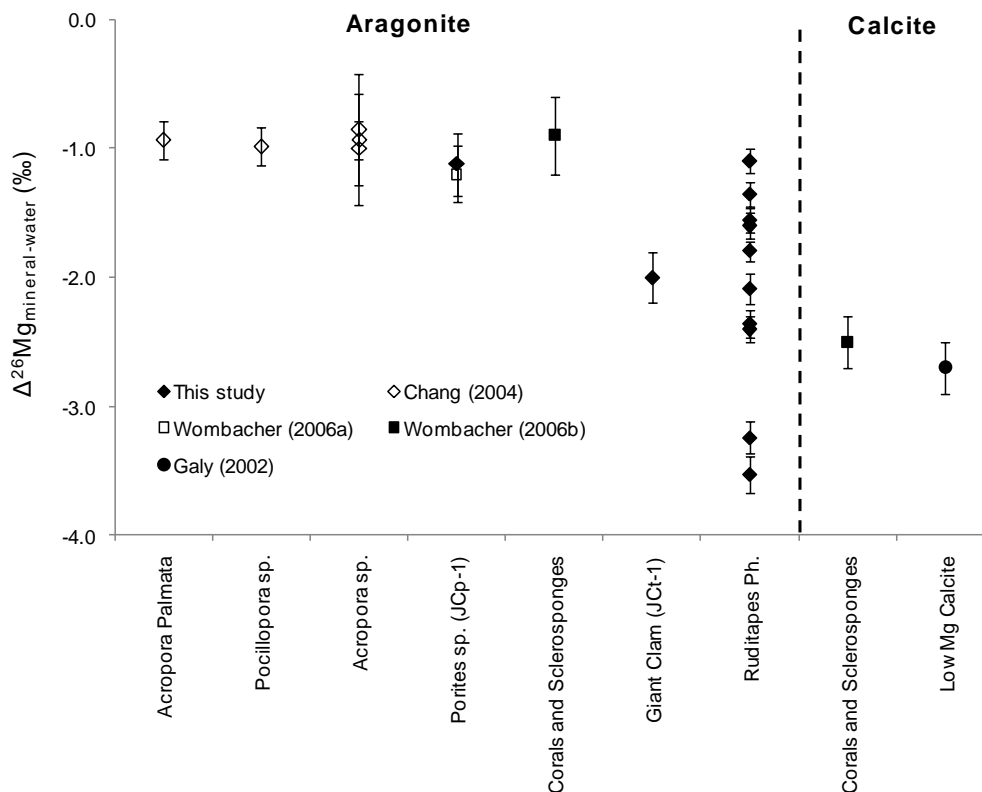

Figure 53. Comparison of the fractionation factors ($\Delta^{26}Mg$ mineral-seawater, in per mil) determined in the shell of aragonitic clams *Ruditapes philippinarum* and Giant Clam (JCt-1) to those encountered in three distinct species of corals (*Acropora palmata*, *Pocillopora sp.*, and *Acropora sp.*) from (Chang et al., 2004), in corals and sclerosponges (species not specified) by (Wombacher et al., 2006) and in the coral standard reference material JCp-1 (*Porites sp.*) analyzed in this study and by (Wombacher et al., 2009). For comparison, the $\Delta^{26}Mg_{calcite-water}$ observed in calcitic corals and sclerosponges (species not specified) from (Wombacher et al., 2006) and in the inorganic low-Mg calcite precipitated in speleothems (Galy et al., 2002) are also reported. Corresponding uncertainties are at 95% confidence interval (2σ).

If we consider $\delta^{26}Mg$ of the shells and precipitation factor ($\Delta^{26}Mg_{aragonite-seawater}$ of -1.0±0.2‰), potential values of EPF are ranging from -0.93‰ to -1.95‰ at Locmariaquer and from -1.37‰ to -3.35‰ at Le Bono. If we further compared to the seawater signature (-0.82‰), these ranges suggest that EPF has been potentially enriched in light isotopes to various degrees; $\Delta^{26}Mg_{EPF-seawater}$ from -0.10‰ to -1.12‰ at Locmariaquer and from -0.55 to -2.52‰ at Le

Bono. As identified earlier, these EPF enrichments might be linked to the interaction with organic tissues and the related Mg uptake from the internal fluids.

3.3.5.3 Changes in δ^{26}Mg of the shell with salinity

The strong differences observed in δ^{26}Mg of the shells collected at the two sampling sites give support for a major impact of salinity on the Mg isotopic fractionation. At the oceanic site (Locmariaquer) δ^{26}Mg values from the prismatic layer range between -1.93±0.2‰ to -2.21±0.2‰. Taking into account the offset induced by the aragonite precipitation, shell data for this specimen give a potential value for the EPF comprise between -1.11 to -1.39‰ and appear to be highly comparable with the EPF analyzed at -1.09‰. These data support a shell formation close to inorganic precipitation of aragonite, similar to what is observed in aragonitic corals and sclerosponges. This situation claims for a visible but limited impact of the metabolic activity (range -0.11 to -0.39‰) at this oceanic site. By contrast, the specimens from Le Bono which show consistently lighter δ^{26}Mg values in the prismatic layer, from -2.37±0.09‰ to -4.35±0.14‰, are no more comparable with the inorganic end-member. At this site, salinity fluctuates with the tidal cycle. Large enrichments observed in δ^{26}Mg of the shell suggest that EPF of these specimens have been strongly fractionated towards light isotope. This situation can result from two combined factors. The first one is the acceleration of metabolic activity responding to the salinity stress already observed for *Ruditapes ph.* (Kim et al., 2001; Robert et al., 1993); it may indeed provoke some larger Mg retention within the intracellular medium to maintain some osmotic equilibrium. The second can be linked to lowering of Mg content in the parent seawater (up to 60% with a salinity of 14%), with a Mg uptake that remains unchanged. In both case, the balance effect on isotopic composition of the fluid would be also larger. Both factors can converge to significantly lower δ^{26}Mg and they cannot be easily deciphered from our data. However comparatively to Mg/Ca ratios which remain relatively constant in the shells at both sites (from 0.8 to 1.3 mmol/mol), the salinity impact on δ^{26}Mg values provides a potential tool to record salinity changes from the bivalve shell.

3.3.6 δD in the lipid fraction of M. edulis shells, soft tissues and sediments

Preliminary results are shown in Figure 54. The isotopic values of bulk sediment organic matter and shell both show only a weak trend with salinity. The δD of total lipid extracts from shell and sediment present a clearer trend, with values decreasing with decreasing salinities. The expected δD variation between the 2 end-member sites (i.e., Knokke and Ossenisse) is around 20‰, as estimated from the variation of the $\delta 18OH2O$ with salinity (Figure 55).
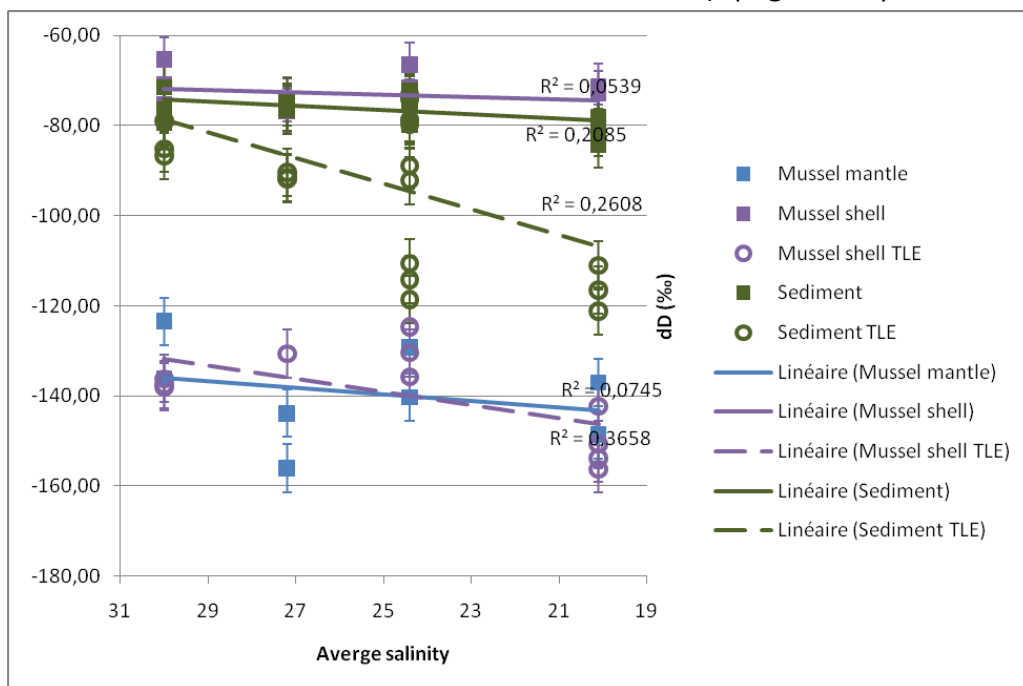

Figure 54. δD in bulk sediment organic matter, soft tissues and bulk shell organic matter in the Scheldt estuary. Decreasing trends are observed in all lipid fractions, from sediments to mussel tissue (mantle) and shells.
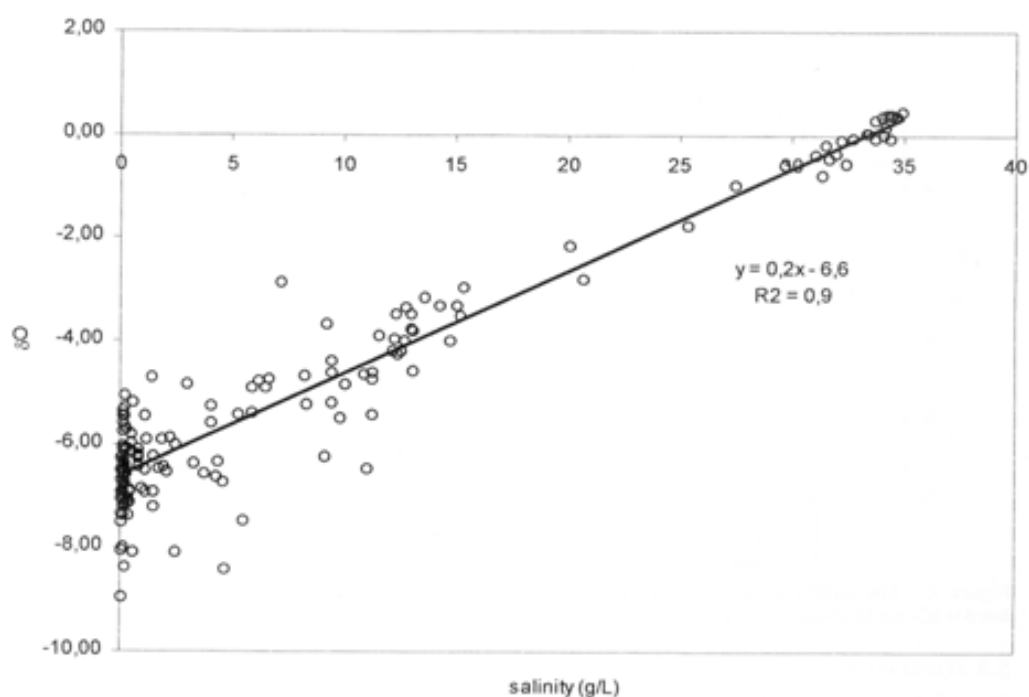
Figure 55. δD and δ^{18}O isotopic composition of Scheldt water, data from (Van Den Driessche, 2001).

The deuterium isotopic composition of specific compounds extracted from bivalves shells are scheduled for analysis at the end of September 2009 (at Royal NIOZ).

3.3.7 Archaeological M. edulis as indicators of past anthropogenic eutrophication in the Scheldt estuary

δ^{18}O and δ^{13}C observed In archaeological *M. edulis* (Figure 56), a clear shift towards lower δ^{18}O and δ^{13}C values can be observed (indicating lower salinities) at the end of 17th century.

Figure 56. δ18O (red, left axis) and δ13C (blue, right axis) of *M. edulis* from ~1300 yr BP to actual period. In both isotope systems there is a clear shift towards lower values at the end of the 17th century

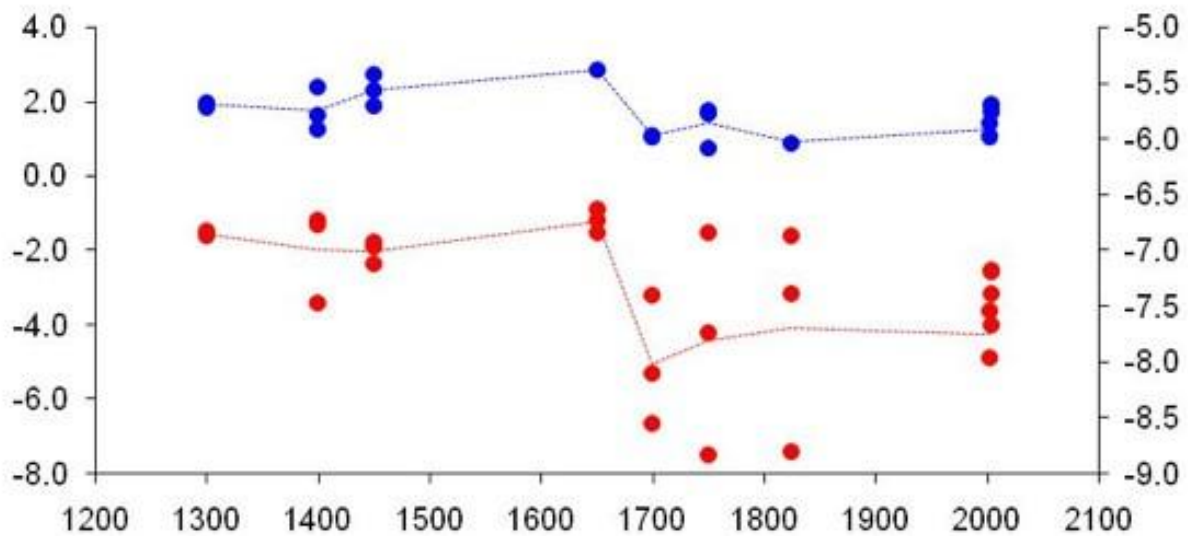This important isotopic shift can be potentially attributed to increased amounts of wastewater from the fast-growing cities of Antwerp and Brussels, or by the gradual shift of the main Scheldt drainage from the Oosterschelde to the Westerschelde.

Nitrogen stable isotope ratios ($\delta^{15}N$) have the potential of discriminating between these two hypotheses. It has been demonstrated that $\delta^{15}N$ values of dissolved inorganic nitrogen (DIN) become elevated under the influence of anthropogenic eutrophication, like septic wastewater. These elevated $\delta^{15}N$ values of DIN are faithfully recorded in the soft tissues and in the shell organic matter of bivalves. $\delta^{15}N$ analyses are ongoing on the archaeological *M. edulis* shells. As a reference collection we also analyse a collection of modern specimens from different time intervals in the 20th and 21st century, representing different levels of wastewater treatment.

3.3.8 Is Greenland ice cap meltwater runoff recorded in growth increment chemistry of the bay mussel (Mytilus trossulus)?

Laser ablation ICP-MS determination has started only recently (2009) and revealed annual and sub-annual cyclicity in several trace elements in the *M. trossulus* shells. Example of one shell profile for Mg/Ca and Ba/Ca are presented in Figure 57. Mg/Ca appears to be a suitable proxy for temperature, enabling us to apply δ18O values for reconstruction of salinity

and hence meltwater fluxes from the Greenland ice cap. Analyses on these shells are still in progress.
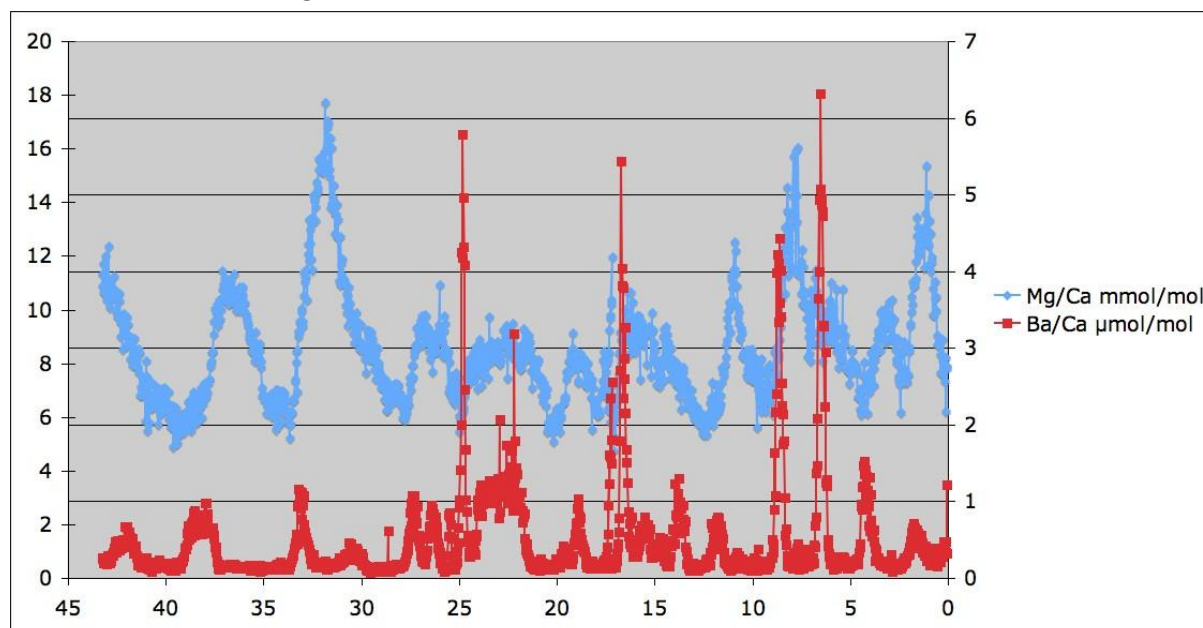
Figure 57. Mg/Ca (blue, left axis) and Ba/Ca record (red, right axis) from a *M. trossulus* shell from Disko Bay (West Greenland). On the horizontal axis is the distance from the growth margin (mm). Mg/Ca is probably a proxy for temperature (each cycle is one year), whereas Ba/Ca may give insight into salinity and/or phytoplankton blooms.

Mytilus shells are readily found in Greenland archaeological finds from different settlement periods. The developed proxy can give insight in the climatic circumstances accompanying the rise and demise of Greenland cultures, such as the Norse settlement period during the Medieval Warm Period.

3.3.9 Anadaria senilis in the West African blood cockle: Archives of current and past climate shifts?

Anadara senilis from Banc d'Arguin also exhibits annual and sub-annual patterns in several trace elements. Figure 58 gives an example of Ba/Ca shell profile.

Figure 58. Ba/Ca of *A. senilis*. Barium is one of many elements exhibiting seasonal cycles. It is probably connected to primary productivity. Comparison of these records with δ¹⁸O values will give insight in the timing of barium peaks within a year.
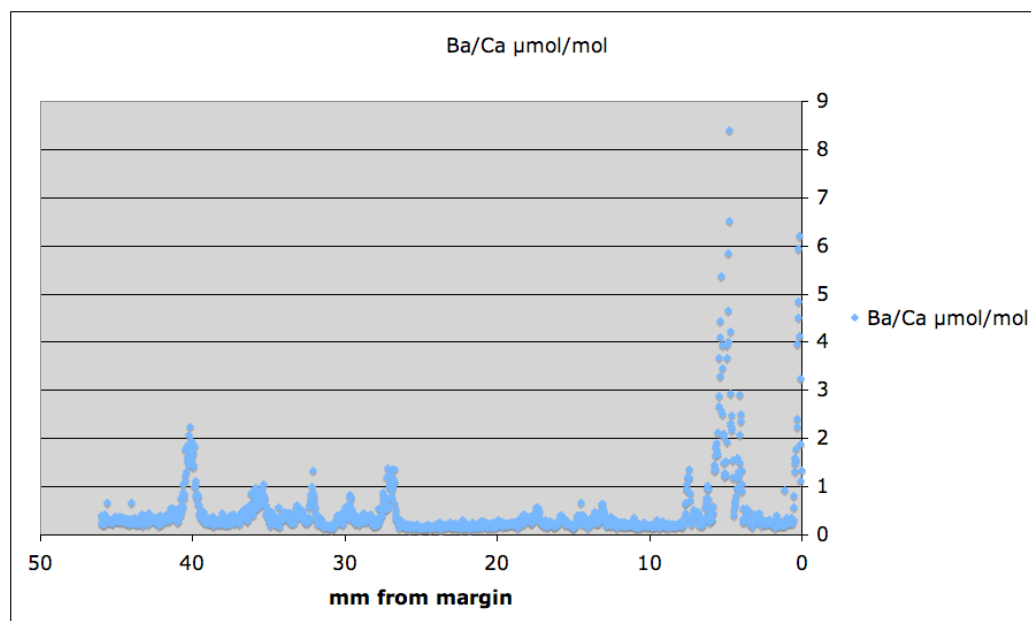
Both LA-ICP-MS and stable isotope measurements are still ongoing. We expect to be able to determine in which seasons the shells were collected. Furthermore, we expect to reconstruct temperatures and precipitation amounts during the early-to-middle Holocene in West Africa, which was then still a savannah. In addition we hope to gain insight in the timing of, and the climatic circumstances under which human settlements were abandoned when Saharan climate changed to the current conditions about 2700 years BP.

3.4 Modeling and data processing

3.4.1 applications of the bias elimination method to proxy records

Both the non-parametric method and the parametric method were applied to a number of environmental archives which are all potential paleo-reconstructers. First of all the method was validated with real mangrove data set. Mangroves were chosen instead of bivalves for the validation of both methods, because the sampling procedures are non-destructive and, as a consequence, identical sections can be measured with different sample sizes, enabling to check the methods.

The non-parametric method was then applied to the bivalve Chione cortezi, a short living bivalve species, which grows relatively fast. Finally, the non-

parametric method was tested on otolith of a *Paraconger papointi* data which grows very slow.

3.4.1.1 Mangrove trees

Mangrove trees were chosen as validation data because the sampling procedures are non-destructive and, as a consequence, identical sections can be measured with different sample sizes, enabling to check the algorithm. A stem disc of a mangrove tree R. mucronata was collected in November 1999 from Makongeni, Kenya (39.46°E, 5.7°S), located 50 km South of Mombasa.

The bimodal distribution of the Kenyan climate is locally expressed by a long rainy season from April to July and a short one from October to November, with a mean annual precipitation of 1144 mm (1980-1985) (Leith et al. 1999). The temperatures range from 23.3 to 29.9 °C, with a mean annual temperature of 26.1°C (1931-1990) (Leith et al. 1999). The vessel density in R. mucronata is a proxy for the rainfall in the tropics: during the rainy season earlywood with a low vessel density is produced and during the dry season latewood with a high vessel density is produced. The bimodal climate distribution is reflected in this vessel density by more than one frequency peak.

The stem discs were air dried and their transversal sections were polished (sand grain 100-1200 grit). In Figure 59a an example of such a disc is shown. The vessel density was measured in adjacent windows along a radial transect on the sanded stem discs, from bark to pith. Two window widths were used (300 μm and 1200 μm, the height was constant at 2092.9 μm) to measure the exact, same section. The vessels were counted at a magnification of 12 x using image analysis software (AnalySIS 3.0) and recalculated to find the vessel density per square millimeter. Figure 59 shows an example of such an image. Since identical sections are measured with both windows, the results are expected to be identical, though this is not the case. When sampling procedures are at the base of diverse results, a calibration is needed; this is the role of the methods presented here.
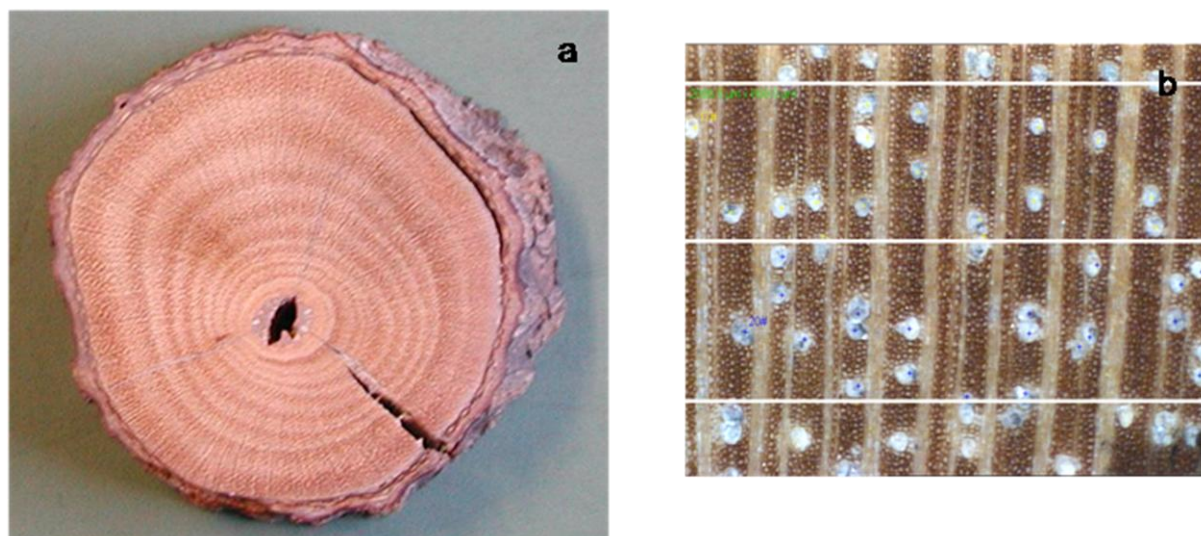
Figure 59. (a) A stem disc of *R. mucronata*. The dark rings correspond to low vessel densities and the light rings to high vessel densities. (b) Image with a microscope. White dots: vessels; horizontal lines: delimitation of the windows.

The reason for the results being non-identical is: the larger the sample width, the larger the averaging effect. As a consequence, an underestimation of the variability of the data measured with 1200 μm window is expected in comparison with the data measured with the 300 μm window. Furthermore, the 300 μm window was much smaller than the variation of interest, resulting in no correction. This dataset is then the 'true' dataset, i.e. as it was recorded by the mangrove tree. As a consequence, it is expected that after correction, the 1200 μm window data would be similar to this 'true' dataset. The vessel density measured with the 300 μm window was compared with that measured with the 1200 μm window and the expected underestimation of the variability was observed.

Both datasets were subjected to the non-parametric correction for averaging. For the vessel density measured with a window of 300 μm, the results showed no significant change, so it was concluded that this is the 'true' dataset. The results for the vessel density measured with a window of 1200 μm showed a significant improvement towards the 'ideal' dataset; this can be seen in Figure 60.
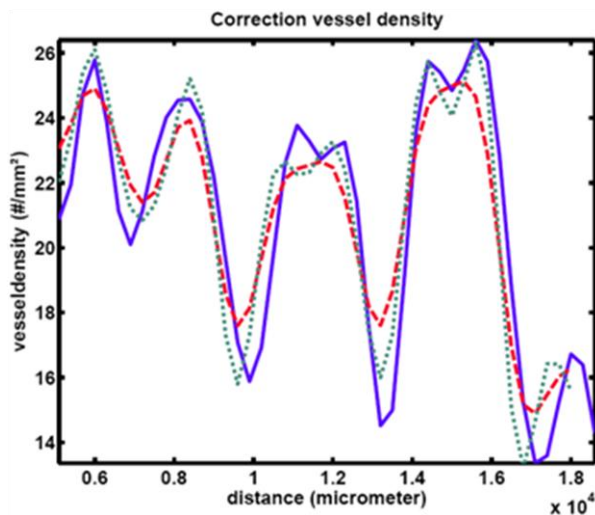
Figure 60. Correction for vessel density. Dashed: vessel density 1200 μm, full: vessel density 300 μm and dotted: corrected vessel density 1200 μm.

The results were then transformed to a time scale using the Time Base Distortion Method (TBD) (De Ridder et al., 2005) this is shown in Figure 61a. It is clear that the corrected data reflect the bimodal climate in Kenya, whereas the measured data do not. This becomes even clearer in the frequency domain Figure 61b. The measured dataset shows one strong frequency component and a very weak frequency component, while the corrected dataset shows two clear frequency components. The higher the frequency, the more the peaks are corrected. The improvement in the second peak accounts for the sudden appearance of the bimodal climate structure.

Figure 61. Correction for vessel density in time domain. (a) On a time scale. (b) In the frequency domain. Dashed: measured data, dotted: corrected data.

Parametric correction. The 1200 μm data was subjected to the parametric correction method. Note the non-equidistant spacing of the growth rings, indicating a non-constant growth speed and, hence, a non-linear distance-

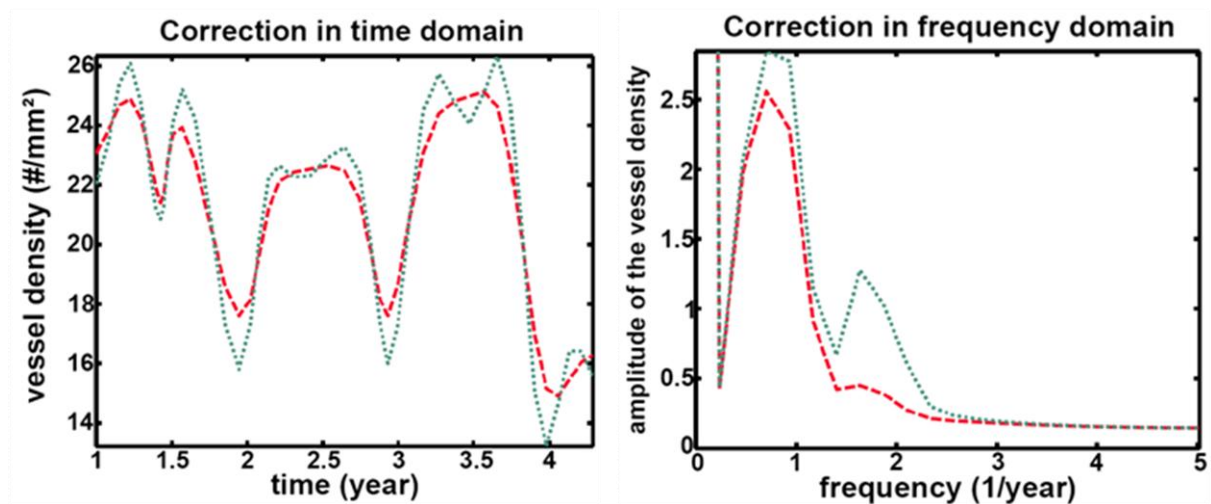time relationship. The data record is 37 samples long and covers 3 years. In Figure 62a the vessel density data on a distance scale is shown. The optimal model complexity was chosen, based on the cost function and knowing that the Kenyan climate has a bimodal distribution. This resulted in a signal model (Equation (3) and (6)) consisting of H = 5 harmonics, A, and a distortion model (5) with b = 4 parameters, B, giving a total of 15 signal parameters. After estimating these parameters, the nonlinear distortion (Equation (4)), the signal model for the measured averaged vessel density (Equation (6)), and the signal model for the continuous, true vessel density (Equation (6) can be calculated. A time base can be calculated using Equation (7) and (8), with $t_{end} - t_1 = 3$ year. In Figure 62b the vessel density data as well as the signal model for the measured averaged vessel density is shown on the newly calculated time axis.
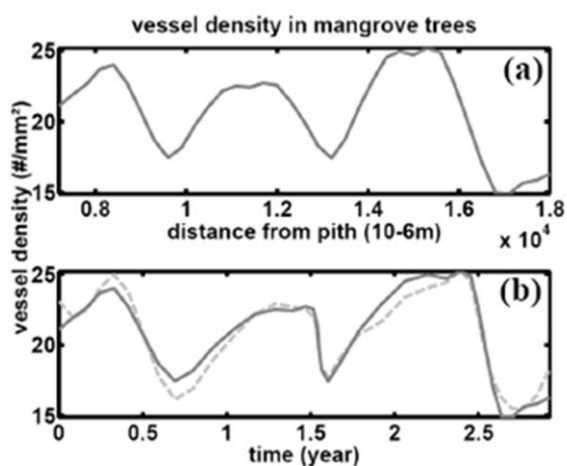
Figure 62. Vessel density in mangrove trees measured with δ = 1200 μm: a: measured data on a distance scale; b: measured data on the constructed time scale (full line) and the averaged signal model $\overline{y}(x_n, \theta)$ **(Equation (6)) (dashed line).**

Figure 63a shows the signal model for the measured averaged vessel density and the signal model for the continuous vessel density (i.e. corrected for the averaging effect) on the newly calculated time axis. In Figure 63b, the Fourier spectra of both of these models are shown. Peaks can be observed at a frequency of 1 and 2 year-1 for both models, which was expected. The non-averaged signal model shows an increase of its amplitudes and reveals some new harmonics.
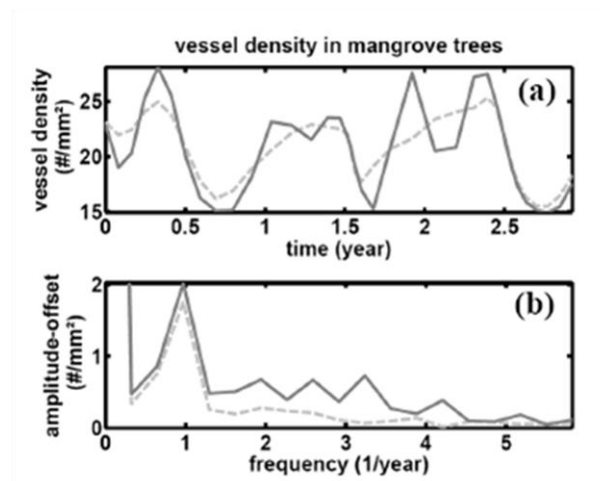
Figure 63. The averaged signal model $\overline{y}(x_n,\theta)$ **of the measured vessel density versus the signal model corrected for averaging** $y(x_n,\theta)$ **(Equation (18)) dashed line: signal model for the measured vessel density; full line: signal model for the vessel density corrected for averaging. a: signal models in the time domain; b: signal models in the frequency domain.**

In order to test whether this increase of the amplitudes is significant, the estimated amplitudes are compared with the standard deviation. From Table XI it can be seen that all the estimated magnitudes of the amplitudes are significant. The differences between the magnitudes of the amplitudes are not always significant. For the first two harmonics, the difference is insignificant, for the third harmonic the difference is significant, and the fourth and fifth harmonic the amplitudes of the measured averaged vessel density cannot be estimated. This is what we expect, the higher the frequency at which these amplitudes occur, the more the averaging effect is present. At high frequencies the averaging pushes the amplitudes near the noise level. This means that, overall, the correction is significant. Note also that the ratio standard deviation/amplitude of the continuous vessel density (Table XI, left column) increases with the harmonic number. This is consistent with the observation that the spatial averaging decreases the harmonic amplitudes as one over the spatial frequency (see the 1st approach).

$\sqrt{A_k^2 + A_{k+H}^2} \pm std$ *	$\sqrt{A_k^2 + A_{k+H}^2} \pm std$ **
1.84 ± 0.27	1.71 ± 0.22
3.25 ± 0.34	3.24 ± 0.22
1.89 ± 0.50	0.79 ± 0.21
2.78 ± 0.50	-
2.18 ± 0.77	-

Table XI. Significance of the amplitude difference between the amplitudes for the continuous vessel density* and the amplitudes of the measured averaged vessel density**.

Comparison of the different methods

The non-parametric method and the parametric method were compared with the 300 µm data. A signal model (19) with the same number of harmonics and the same number of distortion parameters as in the parametric method was fitted onto the 300 µm data record and the corrected data from the non-parameteric method. The results can be seen in Figure 64.
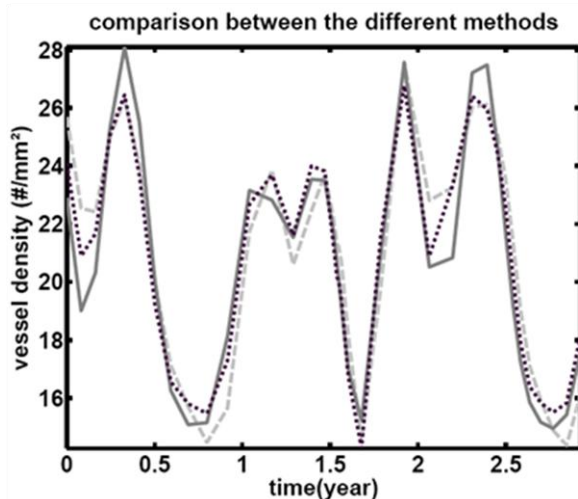
Figure 64. Comparison of the current method to the harmonic signal model of the non-parametric correction of the data [4] and the harmonic signal model of the measurements with window height of 300 µm. Full dark grey line: signal model for the vessel density measured with a window height of 1200 µm, dashed light grey line: signal model for the measurements with a 300 µm window, dotted black line: signal model for the non-parametrically corrected 1200 µm data.

In order to see whether the difference between these 3 estimates is significant, the difference between the signal model for the parametric correction (current method) and the signal model for the measurements with a 300 µm window (small samples), and the difference between the signal model for the parametrically correction (current method) and the signal model for the nonparametric correction (1st approach) is plotted with the 95% confidence interval (based on the standard deviation on the parameters

of the current method) in Figure 65. It is clear from this figure, that the nonparametric method falls better in the 95% confidence interval than the method measured with a 300 µm window. For the non-parametric method 13 of the 37 points fall out of the confidence interval, while for the 300 µm window only 21 of the 37 points fall out of the 95% confidence interval. This can be explained by residual signal modeling errors. Overall the results are quite good.
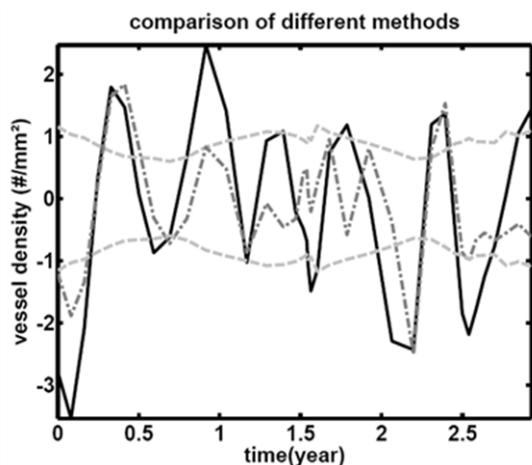
Figure 65. Comparison of the three estimated signal models. Black full line: the signal model $y(x_n, \theta)$ **for the vessel density measured with a window height of 1200 µm, parametrically corrected (current method) minus the signal model** $y(x_n, \theta)$ **for the measurements with a 300 µm window (small samples). Dark grey dashed-dotted line: the signal model** $y(x_n, \theta)$ **for the vessel density measured with a window height of 1200 µm minus the signal model** $y(x_n, \theta)$ **for the non-parametrically corrected (1st approach). Light grey dashed line: 95% confidence interval, based on the standard deviation of the current method.**

3.4.1.2 Non-parametric correction of Bivalves shell record

The data used in this section are those reported by (Goodwin et al., 2003) and are of the bivalve *Chione cortezi*. In this paper specimen IP1-A1R was sampled with a 300 µm drill bit, this resulted in a $\delta^{18}O$ record of sixty-four samples. Samples were taken from the outer shell layer along the axis of growth between the umbo and the comissure. For more details see (Goodwin et al., 2003). In Figure 66 the full black line represents the measured $\delta^{18}O$ profile. Signal amplitude decreases going from the umbo to the comissure, possibly reflecting the effect of time-base averaging. The non parametric method was applied to this data set and the results are shown in Figure 66.

Figure 66. Correction for averaging on *Chione cortezi*. Full line: measured data set. Dashed line: corrected data set with correction method [2]

It appears that this record is approximately 6 years of length and that growth rate declined with age. One would thus expect that the averaging effect will be larger near the comissure (to the right). This is true, though not visible, as the correction for averaging is not significant.

Chione cortezi are fast growers, thus a small enough drill bit was available to measure this record. These results also imply that the decrease in amplitude with age is due to physiological effects and not to averaging, as is assumed in (Goodwin et al., 2003).

In order to verify this result a reverse simulation was done. Instead of correcting an averaged signal, a simulated signal was averaged. For this a sine wave was constructed with a period of 4,2 mm, a amplitude of 0,90 and an offset of 1.5, this are more or less the settings of the last period of the *Chione cortezi* record. The averaged record was calculated by using a sample width of 300 μm (drill bit of 300 μm diameter). The result is shown in Figure 67 It is clear from this figure that the simulated record to be measured and simulated measured record (averaged record) overlap completely under these conditions. This confirms the conclusion that the averaging effect is not significant and that the decline of the $\delta^{18}O$ record is probably due to physiological factors.
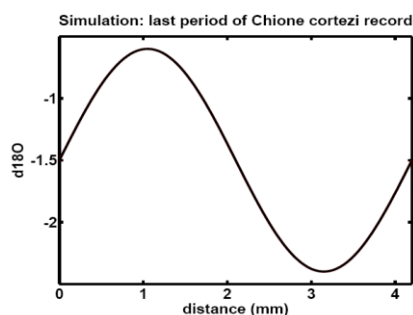
Figure 67. Inverse simulation. Full black line: simulated measured δ18O record. Dashed grey line: simulated to be measured signal δ18O record, this line is not visible because the full black line and the dashed grey line are overlapping.

The next step is to test the method on *Artica islandica* which has a much longer life span and slows down growth significantly with age. It is expected that sampling *Artica islandica* shells which are older than 20 year will induce large averaging effects, which could then be corrected with both methods.

3.4.1.3 Non-parametric correction applied to otoliths.

This data set was chosen as a case study, because the sample shape was by approximation rectangular. Fish otoliths are calcareous secretions in the inner ear of the fish. δ18O is typically a proxy for temperature. The data used in this section was provided by Daan Vanhove, the fish species was *Paraconger papointi*. An average sample width was chosen, i.e. 126 μm. The resulting δ18O record was 14 samples long.

The non-parametric method was applied to this data set and results are shown in Figure 68. High δ18O values are characteristic for winter, low values for summer, so it is easy to see that this record spans 2.5 years. Moreover, we can see that the otholith grew slower during the first year than during the second year. Expected is thus that the averaging effect will be bigger for the measurements of the first year. The correction (the grey, dashed line) shows us exactly that.
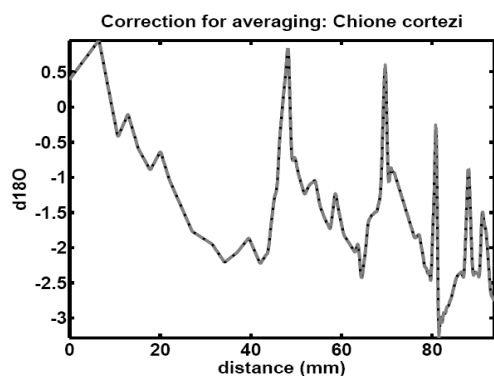
Figure 68. Correction for averaging on *Paraconger papointe*. Full line: measured data set. Dashed line: corrected data set with correction method [2].

3.4.2 Application of the non-linear multi-proxy approach
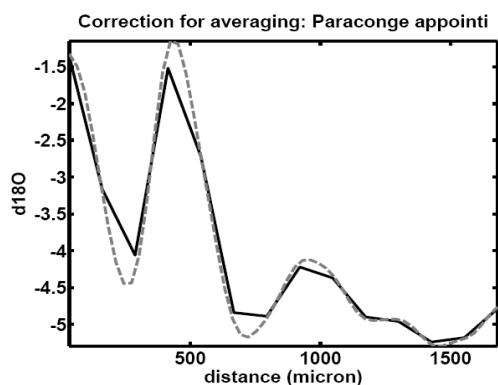
The non-linear multi-proxy approach is presently tested using two different datasets:

(1) Measurements of Mg, Sr, Mn Ba and Pb in *Mytilus edulis* shells collected during spring and summer in Terneuzen, Breskens and Hoofdplaat (Vander Putten et al., 2000): the results of this first dataset are promising because it was already possible to reconstruct temperature with a precision up to ±0.33°C.

(2) Measurements of Sr, Mg, Ba, $\delta^{18}O$ and $\delta^{13}C$ of 4 shells of *Ruditapes philippinarum* from 2 sites in the Gulf of Morbihan. Since the variation on these measurements was high, the precision on the reconstructed temperature was only ±0.6°C. We believe that the prediction capacity can be ameliorated if some systematical errors are corrected.

(3) We tested the effect of site and time specificity using the 'intuitive' method. Proxy results (Mg/Ca, Ba/Ca, Sr,Ca, Pb/Ca) for a Terneuzen *Mytilus edulis* shell were used to train the model, which was subsequently used to reconstruct temperature from proxy data for shells from other sites (Breskens, Ossenisse, Knokke). Reconstructed temperatures were compared with instrumental temperature records. For the Knokke shell (different site, different year) proxy record, our 'intuitive' model achieves a precision of 1.5°C.

3.4.2.1 Comparison of the Intuitive approach with two other methods

We compared the outcome of our 'intuitive approach' (IA) non-linear model with two more complex, non-linear, multi-dimensional methods used in engineering science: these are the Support Vector Regression (SVR) and the Weight Determination by Manifold Regularization (WDMR) methods (Ohlsson

et al. 2008). Our own original intuitive method performs rather well in comparison with these two other methods, but clearly, the Weight Determination by Manifold Regularization method is less sensitive to site specificity and the model is able to reconstruct SST whit a Mean Absolute Error (MAE) of less than 1°C for shells coming from study sites whit a salinity range from 32‰ to 15‰. Compared with other paleo-thermometry methods this performance appears very robust to changes in salinity. The advantage of our method is two-fold: First, the combination of several proxies implies that proxy variation induced by non-temperature environmental parameters can be compensated by information about these parameters in other proxies. Second, the use of non-linear models can disclose less obvious proxy-environment relationships. The comparison of the results obtained by the three methods is shown in Figure 69.

3.4.2.2 Weight Determination by Manifold Regularization applied to other datasets

The Weight Determination Manifold Regularization method was successfully used to construct a non-linear multi proxy model based on $\delta^{18}O$, $\delta^{13}C$, Mg, Sr, and Ba for *Ruditapes philippinarum*. Unfortunately, reconstruction performance was poor when the same method was applied to freshwater mussels (Unionidae) from Rhine and Meuse. Probably the model was stuck in a local minimum and further investigation is needed to resolve this.
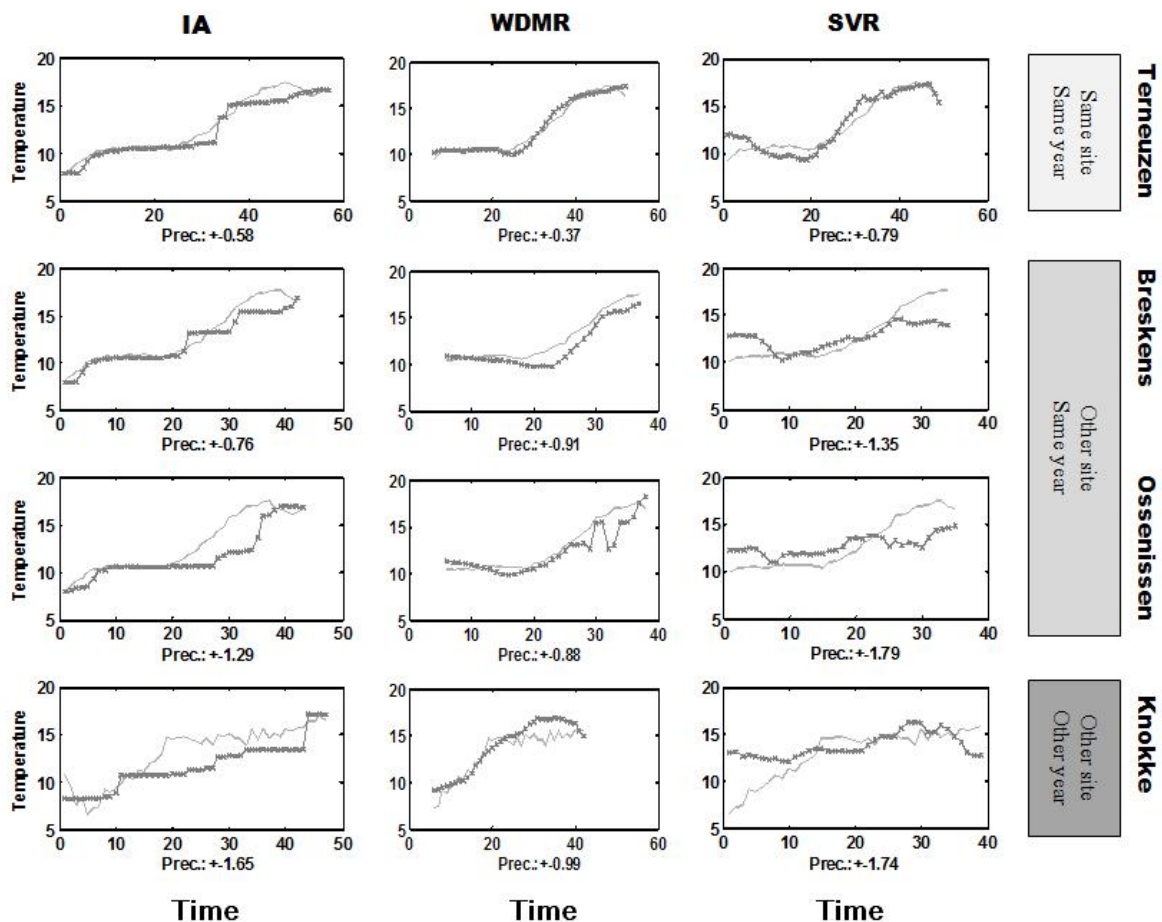
Figure 69. Comparison of the reconstructed temperatures (dark line) and the measured temperatures (light line) as a function of age (i.e., along the shell growth axis) for the different study sites, using an intuitive approach, support vector regression and weight determination by manifold regularization. The precisions given are mean absolute errors in °C.

3.4.2.3 Proxy evaluation using Weight Determination by Manifold Regularization

To investigate whether all proxies contributed to the final result (i.e., temperature reconstruction) and to quantify this contribution, a new model was constructed based on limited datasets in which a limited amount of proxies was used. This was done for the 4 study sites, thus allowing verification whether the contribution of the proxies is site-specific.

The proxy evaluation (Figure 70) demonstrates that the combination of Mg, Sr, Ba and Pb into one model limits the effects of site specificity on the model outcome. In comparison with models based on limited proxy combinations the four-proxy (Mg, Sr, Ba, Pb) model is least sensitive to site-specific variations. Even though models based on Mg, Mg-Sr or Mg-Pb perform better for the shells from Terneuzen and Ossenisse, these one or 2-proxy models are less reliable when they are applied for shells from higher salinity ranges.

The robustness of this model results from the fact that variations in one proxy, due e.g. to salinity, may be canceled out by variations in other proxies. But it is obvious that not all proxies contribute in the same way to the final temperature reconstruction. Though our results confirm that Mg contains significant temperature-related information, the latter, however, appears influenced by site-specific factors (e.g. salinity). Mg alone can thus not be used to reconstruct temperature of shells that lived in another environment.
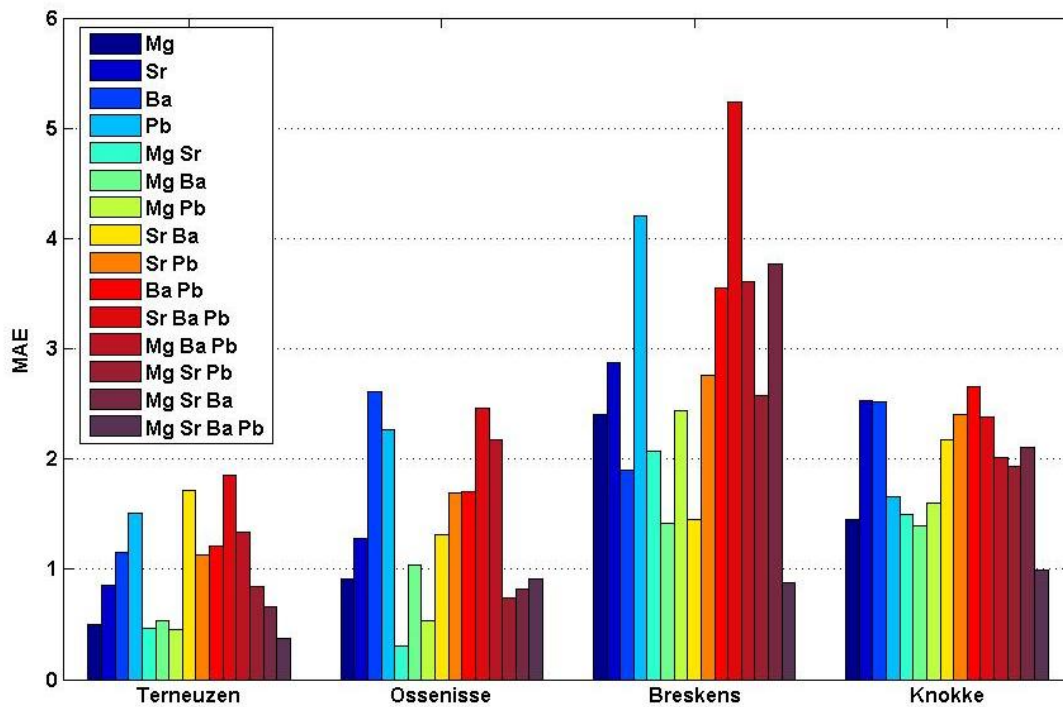
Figure 70. Reconstruction performance (in Mean Absolute Error) of models trained on datasets whit a limited number of proxies.

4. POLICY SUPPORT

In addition to the above statements directly drawn from CALMARSII scientific results, there are other activities which are relevant to policy support in the framework of the expertise developed by CALMARS. In Belgium, we have been involved in the following actions:

- CALMARSII scientists have been consulted regularly in 2008-2009 by BELSPO during the feasibility study of the R/V *New Belgica*, a project that would shape marine Belgian research on a long-term perspective. We have provided inputs regarding which infrastructure and technical specifications would be required for such new research vessel, taking into account international research prospective for the next two decades in oceanography. Some CALMARSII scientists have also been consulted by BELSPO in 2009 to provide their opinion on the *European Strategy Forum on Research Infrastructures* (roadmap 2008), which includes the European icebreaker project, R/V *Aurora Borealis*.
- Experts from CALMARSII have been involved in the evaluation of the proposals for the *Antarctic InBev-Baillet Latour Fellowship Award*. The award of €150,000 is designed to promote research activities in, or in the vicinity of, the Princess Elisabeth Antarctica research station.
- A CALMARSII promotor (PhD) was member of the bureau of BENCORE the Belgian implementation of ENCORA (http://www.bencore.be/).

CALMARS partners were frequently addressed to advice on international research policies. As an Example, CALMARSII partner Vrije Universiteit Brussel is a participant in the extension (beyond 2009) of the Antarctic Climate and Ecosystem CRC program.

5. DISSEMINATION AND VALORISATION

Since 2005 CALMARSII has produced 24 peer-reviewed publications and one is currently under revision or accepted for publication. For the research community, scientific publications represent the best means to ensure dissemination, valorization and long-term availability of data produced. CALMARS partners gave several tens of communications at international symposia since 2005.

A CALMARS logo has been created and the website has been updated regularly (**http://www.vub.ac.be/calmar/**).

In 2009, The CALMARSII network has organized an international workshop in Brussels at the Flemish Academy of Sciences. The Workshop focussed on the "Bivalve shell proxy incorporation" and was advertised via (among others): Sclerochronology list server, The Palaeobiological Society of the Netherlands/Flanders, PAGES online calendar, Netherlands Research School of Sedimentary Geology (NSG), Centre for Geo-ecological Research (ICG).

The workshop has brought together more than 35 participants with scientists involved in the broad field of biomineralisation. Further details on the workshop (program, list of participants, etc…) can be found on the CALMARSII website:

http://www.vub.ac.be/calmar/WorkshopBivalves/index.html/

6. PUBLICATIONS

6.1 Peer-review

Submitted and in press:

Bauwens Maite, Ohlsson Henrik, Beelaerts Veerle, Barbé Kurt, Schoukens Johan and Dehairs Frank, (2011) On Climate Reconstruction using Bivalve Shells: Three Methods to Interpret the Chemical Signature of a Shell, Computer Methods and Programs in Biomedicine, (in press)

GILIS, M., GOSSELIN, P., DUBOIS, Ph & WILLENZ, Ph. 2011. Seasonal Modifications and Morphogenesis of the Mediterranean Hypercalcified Sponge Petrobiona massiliana Vacelet and Lévi 1958 (Porifera, Calcarea, Calcaronea). Invertebrate Biology (In Press).

F. Planchon, C. Poulain, D. Langlet, Y.-M. Paulet and L. André. Mg stable isotopic fractionation in the manila clam (*Ruditapes Philippinarum*): New insights into the calcification process of Bivalves. *Geochimica et Cosmochimica Acta* (Submitted).

2011

Beelaerts Veerle, Bauwens Maite, Versteegh Emma, Dehairs Frank, Pintelon Rik (2011) Periodic time series modeling of environmental proxy records with guaranteed positive growth rate estimation. *Mathematical Geosciences* (accepted)

Hermans J, André L, Navez J, Pernet Ph, Dubois Ph (2011). Relative influences of solution composition and presence of intracrystalline proteins on magnesium incorporation in calcium carbonate minerals: insight into the vital effects. J. Geophys Res. 116, G01001, doi:10.1029/2010JG001487.

2010

Bauwens Maite, Ohlsson Henrik, Beelaerts Veerle, Barbé Kurt, Schoukens Johan and Dehairs Frank (2010), A nonlinear multi-proxy model based on manifold learning to reconstruct water temperature from high resolution trace element profiles in biogenic carbonates, *Geoscientific Model Development* 3, 653-6670.

Hermans J, Dubois Ph, André L, Vacelet J, Willenz Ph. 2010. Growth rate and chemical features of the massive calcium carbonate skeleton of Petrobiona massiliana (Baeriida, Calcaronea, Calcispongiae). Journal of the Marine Biological Association of United Kingdom 90: 749-754.

Hermans J, Borremans C, Willenz Ph, André L, Dubois Ph. 2010.Temperature, salinity and growth rate dependences of Mg/Ca and Sr/Ca ratios of the skeleton of the sea urchin Paracentrotus lividus (Lamarck): an experimental approach. Marine Biol. 157: 1293-1300.

Versteegh Emma A. A., David P. Gillikin and Frank Dehairs (2010). Analysis of $\delta^{15}N$ values in mollusk shell organic matrix by EA-IRMS without acidification: an evaluation and effects of long-term preservation, *Rapid Communication in Mass Spectrometry*, 25, 675-680.

2009

Beelaerts Veerle, Fjo De Ridder, Nele Schmitz, Maite Bauwens, Frank Dehairs, Johan Schoukens and Rik Pintelon (2009). On the Elimination of Bias Averaging-Errors in Proxy Records, *Mathematical Geosciences*, 41:128-144.

Borremans, C., Hermans, J., Baillon, B., André, L. and Dubois, Ph. 2009 Salinity effects on the Mg/Ca and Sr/Ca in starfish skeletons and the echinoderm relevance for paleoenvironmental reconstructions . *Geology*, 37(4):351-354.

de Brauwere A., F. De Ridder, R. Pintelon, J. Schoukens and F. Dehairs, 2009. A Comparative study of methods to reconstruct a periodic time series from an environmental proxy record, *Earth Science Reviews*, 95, 97-118.

Rosenheim, B.E., Swart, P.K., Willenz, Ph. 2009. Calibration of Sclerosponge Oxygen Isotope Records to Temperature Using High-Resolution δ18O data, *Geochimica et Cosmochimica Acta*, **73**(18): 5308-5319 and doi: 10.1016/ j.gca.2009.05.047

Versteegh, E.A.A., Troelstra, S.R., Vonhof, H.B., Kroon, D., 2009. Oxygen isotope composition of bivalve seasonal growth increments and ambient water in the rivers Rhine and Meuse, *Palaios* 24(8): 497-504.

2008

Beelaerts V., De Ridder F., Schmitz N., Bauwens M., Dehairs, F., Schoukens J. and Pintelon R., 2008. On the elimination of bias averaging-errors in proxy records, *Mathematical Geosciences*, 42 (4): 129-144.

de Brauwere A., F. De Ridder, R. Pintelon, J. Meersmans, J. Schoukens and F. Dehairs, 2008. Identification of a periodic time series from an environmental proxy record, Computer Geosciences, 34, 12, 1781-1790.

Gillikin, D. P., A. Lorrain, Y.-M. Paulet, L. André and F. Dehairs, 2008. Synchronous barium peaks in high-resolution profiles of calcite and aragonite marine bivalve shells, *Geo-Marine Letters*, DOI 10.1007/s00367-008-0111-9.

2007

Gillikin D., A. Lorrain, M. Li and F. Dehairs, 2007. A large metabolic carbon contribution to the δ13C record of marine aragonitic bivalve shells, *Geochimica et Cosmochimica Acta*, 71, 2936–2946.

De Ridder, F., A de Brauwere, R. Pintelon, J. Schoukens, F. Dehairs, W. Baeyens, & B.H. Wilkinson, 2007. Comment on: Paleoclimatic inference from stable isotope profiles of accretionary biogenic hardparts—a quantitative approach to the evaluation of incomplete data, by Wilkinson, B.H., Ivany, L.C., 2002. *Palaios,* 185, 95–114. *Palaios,* 248: 473-476.

2006

Gillikin, D. P., A. Lorrain, S. Bouillon, Ph. Willenz & F. Dehairs. 2006. Stable carbon isotopic composition of *Mytilus edulis* shells: relation to metabolism, salinity δ13C_{DIC} and phytoplankton. *Organic Geochemistry* 37: 1371-1382.

Gillikin, D.P., F. Dehairs, A. Lorrain, D. Steenmans, W. Baeyens, & L. André. 2006. Barium uptake into the shells of the common mussel (Mytilus edulis) and the potential for estuarine paleo-chemistry reconstruction. Geochimica et Cosmochimica Acta 70: 395-407.

De Ridder, F., A. de Brauwere, R. Pintelon, J. Schoukens, & F. Dehairs, 2006. Identification of the accretion rate for annually resolved archives. *Biogeosciences Discussions* 3: 321-344.

2005

Gillikin D.P., F. De Ridder, H. Ulens, M. Elskens, E. Keppens, W. Baeyens and F. Dehairs, 2005. Assessing the reproducibility and reliability of estuarine bivalve shells (Saxidomus giganteus) for sea surface temperature reconstruction: Implications for paleoclimate studies, *Palaios*, 228, 70-85.

Gillikin D.P, F. Dehairs, W. Baeyens, J. Navez and L. André, 2005. Inter- and intra-annual variations of Pb/Ca ratios in clam shells (*Mercenaria mercenaria*): a record of anthropogenic lead pollution? *Marine Pollution Bulletin*, 50, 1530-1540.

6.2 Conference proceedings

Beelaerts, V., De Ridder, F., Schmidtz, N., Bauwens, M., and Pintelon, R. " Identification of a harmonic signal in the presence of additive noise, an unknown time base distortion, and an averaging effect," I2MTC 2008– IEEE International Instrumentation and Measurement Technology Conference, Victoria, Vancouver Island, Canada, May 12–15, 2008, Conference Proceedings, p533-535.

Bauwens Maite, Ohlsson Henrik, Beelaerts Veerle, Barbé Kurt, Schoukens Johan and Dehairs Frank, On Climate Reconstruction using Bivalve Shells: Three Methods to Interpret the Chemical Signature of a Shell, 7th IFAC Symposium on Modeling and Control in Biomedical Systems (including Biological Systems), Aalborg, Denmark, 12-14 August, 2009

Bauwens Maite, Ohlsson Henrik, Beelaerts Veerle, Barbé Kurt, Schoukens Johan and Dehairs Frank, Non linear multi proxy methods for temperature reconstruction, Non linear multi proxy methods for temperature reconstruction, Workshop on Bivalves biomineralisation: Archival potential and proxy incorporation, Brussels, Belgium, 4-5 May 2009
Henrik Ohlsson, Maite Bauwens, Lennart Ljung, On Manifolds, Climate Reconstruction and Bivalve Shells, 48th IEEE Conference on Decision and Control, Shanghai, China, 16 – 18 December 2009

Bauwens Maite, Ohlsson Henrik, Beelaerts Veerle, Barbé Kurt, Schoukens Johan and Dehairs Frank, On Climate Reconstruction using Bivalve Shells: Three Methods to Interpret the Chemical Signature of a Shell, 7th IFAC Symposium on Modeling and Control in Biomedical Systems (including Biological Systems), Aalborg, Denmark, 12-14 August, 2009 (Poster Presentation)

Henrik Ohlsson, Maite Bauwens, Lennart Ljung, On Manifolds, Climate Reconstruction and Bivalve Shells, 48th IEEE Conference on Decision and Control, Shanghai,China,, 16 – 18 December 2009.

Bauwens Maite, Ohlsson Henrik, Beelaerts Veerle, Barbé Kurt, Schoukens Johan and Dehairs Frank, Non linear multi proxy methods for temperature reconstruction, Non linear multi proxy methods for temperature reconstruction, Workshop on Bivalves biomineralisation: Archival potential and proxy incorporation, Brussels, Belgium, 4-5 May 2009 (Oral communication)

F. Planchon, D. Cardinal, C. Borremans, J. Hermans, P. Dubois and L. André. Mg isotopes fractionation processes in marine calcareous skeletons: methodology developments and preliminary results on echinoderms (sea urchin and starfish). Geophysical Research Abstracts, Vol. 9, 03804, 2007.

F. Planchon, J. Hermans, C. Borremans, Ph. Dubois, C. Poulain, Y.-M. Paulet, and L. André. Mg isotopes in biocarbonates: new insight into vital effects associated to echinoderms and bivalves calcification Eos Trans. AGU, 88(52), Fall Meet. Suppl., Abstract B44C-07.

6.3 Posters and presentations

Beelaerts Veerle De Ridder Fjo, Schmitz Nele, Bauwens, Maite, Pintelon Rik, & Ieee (2008). Identification of a harmonic signal in the presence of additive noise, an unknown time base distortion, and an averaging effect. In 2008 Ieee Instrumentation and Measurement Technology Conference, Vols 1-5, pp. 533-535. Ieee, 12-15 May 2008, Victoria, BC.

Beelaerts V., De Ridder F., Pintelon R., Schoukens J. and Dehairs F., 'Time averaging in solid substrates', BENELUX-meeting on systems and control, Lommel, Belgium, March 2007, Conference proceedings, p 109.

Beelaerts V., De Ridder F., Bauwens M., Pintelon R., 'Identification of a harmonic signal in the presence of additive noise, an unknown time base distortion, and an averaging effect', BENELUX-meeting on systems and control, Heeze, the Netherlands, March 2008, Conference proceedings, p122.

Beelaerts V., De Ridder F., Schmitz N., Bauwens M., and Pintelon R. 'On the construction of a time base and the elimination of averaging errors in proxy records' 1blz, EGU general assembly, Vienna, Austria, April 2009, Conference proceedings, EGU2009-2019-2.

Beelaerts V., Bauwens M., De Ridder F., Dehairs F. And the CALMARs group. Environmental records from calcareous marine skeletons. VLIZ Young Scientists' Day, Brugge, Belgium, March 31, 2006, Book of abstracts, p22.

Beelaerts V. Averaging in solid substrates. Interuniversity Attraction pole IAP VI/4, "Dynamical systems, control, and optimization", Study day, Court St Etienne, Belgium, April 16, 2007, Book of abstracts, p 20.

Bauwens Maite, Beelaerts Veerle, Schoukens Johan and Dehairs Frank, Wich proxies shoul be integrated in a multi-proxy model? 2nd Internationsl Sclerocronology conference, 24-28 July 2010, Mainz, Germany (Oral Presentation)

Bauwens M., Beelaerts V., De Ridder F., Dehairs F. and CALMARs group. 2006. 'Calcereous marine skeletons as recorders of global climate changes'. EGU General Assembly 2006, Vienna, Austria. Geophysical Research Abstracts, Vol 8, EGU06-A-06290. (Poser Presentation)

Bauwens Maite, Beelaerts Veerle, Barbe Kurt, Schoukens Johan, Dehairs Frank, Climate reconstruction based on archaeological shells: a non-linear multi-proxy approach, 27th Benelux Meeting on Systems and Control, Heeze, The Netherlands, March 18-20, 2008 (oral communication)

Bauwens Maite, Poulain Celine, Beelaerts Veerle, Servaes Fabrice, Schoukens Johan, Dehairs Frank, A non-linear multi-proxy approach for climate reconstruction based on archeaological shells, EGU general assembly, Vienna, Austria, Geophysical Research Abstracts, Vol. 10, EGU2008-A-02636, 13-18 April 2008, (Poster Presentation)

Bauwens Maite, Servaes Fabrice, Beelaerts Veerle, Poulain Celine, Dubois Philippe, Schoukens Johan, Dehairs Frank, Climate reconstruction based on archaeological bivalve shells, VLIZ jongerencontactdag, 2008, (Poster Presentation)

Bauwens Maite, Ohlsson Henrik, Beelaerts Veerle, Barbé Kurt, Schoukens Johan and Dehairs Frank, Three ways to do temperature reconstruction based on Bivalve-proxy information, 28th Benelux Meeting on Systems and Control, Spa, Belgium, March 16-18, 2009 (Oral communication)

Bauwens Maite, Ohlsson Henrik, Beelaerts Veerle, Barbé Kurt, Schoukens Johan and Dehairs Frank, Non-linearity's in proxy space: Three methods to deal with the non-linear behavior of proxies in calcareous marine skeletons. EGU, Vienna, Austria, April 19-24, 2009, Geophysical Research Abstracts, Vol. 11, EGU2009-0 (Poster Presentation).

Borremans C, Ranner H, André L, Dubois Ph. 2006. Mg/Ca and S/Ca ratios in the skeleton of the starfish Asterias rubens. Gordon Research Conference on Biomineralization 2006", New London NH, USA, 30 juillet – 4 août 2006 (Poster presentation)

Dubois Ph, Moureaux C, Borremans C, Hermans J, Mannaert G, André L. 2008. Plasticity of the echinoderm skeleton. Gordon Research Conference on Biomineralization 2008", New London NH, USA, 10-15 août. (Poster presentation)

Dubois Ph, Moureaux C, Borremans C, Hermans J, Mannaert G, André L. 2009. Plasticity of the echinoderm skeleton. 13th International Echinoderm Conference. Hobart, Tasmania, Australie, 5-9 janvier. (Poster presentation)

Hermans J, Gosselin P, Dubois Ph, Willenz Ph. 2006. Study of the massive skeleton of the calcareous sponge Petrobiona massiliana. Gordon Research Conference on Biomineralization 2006", New London NH, USA, 30 juillet – 4 août 2006 (Poster presentation)

Hermans J, Willenz Ph, Monin L, Navez J, André L, Dubois Ph. 2007 Skeletal chemistry of the sea urchin Paracentrotus lividus as a new environmental proxy. Biodiversity and Climate Change Conference, Brussels (Belgium), May 21-22 (Poster presentation)

Mas, R., van der Meer, MTJ, Keppens, E, Claeys, P, Dehairs, F, and Schouten, S (2009) Lipid hydrogen isotope ratios from mussel shells and salinity in the Scheldt estuary; Geological Society of America 2009 Annual Meeting - October 18-21, Portland, Oregon, USA. (oral)

Mas, R.; Bauwens, M.; Navez J.; Keppens E. and Dehairs F. (2009) Carbonate stable isotopes of Mytilus edulis shell grown in aquarium; Bivalves Workshop, 4-5 May 2009, Bruxelles, Belgium (oral)

Mas, R. Servaes F. Bauwens, M. Poulain, P. Keppens, E. Claeys, P. & Dehairs F. (2008) VUB bivalve group contribution to PaleoSalt program, June 16-17, 2008, Angers, France (oral)

Mas, R. (2007) Stable isotopes in bivalves shell organic matrix; Workshop on Bivalves in PaleoSalt framework, October 4-5, 2007, Brest, France (oral)

Mas, R. (2007) Sclerosponges and $\delta^{13}C$ - Suess effect; PaleoSalt Workshop, October 4-5, 2007, Brest, France (oral).

Mas R., P. Claeys, E. Keppens and F. Dehairs (2009) Stable isotopic composition of bivalve shells : Mytilus edulis; Bivalve Workshop, 4-5 May 2009, Brussels, Belgium (poster) .

Mas R., C. Borremans, P. Dubois, F. Dehairs, P. Claeys, and E. Keppens (2009) Stable oxygen isotopic composition of starfish skeletons grown under controlled temperature and salinity conditions; Bivalve Workshop, 4-5 May 2009, Brussels, Belgium (poster).

Mas, R. (2009) CALMARS II network Instrumental facilities; Bivalves Workshop, 4-5 May 2009, Brussels, Belgium (poster)

Mas R., P. Claeys, E. Keppens, and F. Dehairs (2009) Stable isotopic composition of bivalve shell organic matrix: Mytilus edulis collected along the Scheldt estuary; EGU General Assembly 2009, 19-24 April 2009, Vienna, Austria (poster)

Mas R., C. Borremans, P. Dubois, F. Dehairs, P. Claeys, and E. Keppens (2009) Stable oxygen isotopic composition of starfish skeletons grown under controlled temperature and salinity conditions ; EGU General Assembly 2009, 19-24 April 2009, Vienna, Austria (poster)

R. Mas, V. Beelaerts, M. Bauwens, F. Servaes, F. Planchon, L. André, J. Schoukens, E. Keppens , P. Claeys, F. Dehairs (2008) Bivalves for salinity reconstruction: the case of Mytilus edulis ; EuroCLIMATE final conference, 29-30 September 2008, Presqu'île de Giens, France (poster).

Mas R., C. Poulain, P. Claeys, F. Dehairs, and E. Keppens (2008) Stable isotope (C,N) composition of bivalve shell organic mater and salinity. Geophysical Research Abstracts, Vol. 10, EGU General Assembly 2008, Vienna, Austria (poster).

Mas R., C. Poulain, P. Claeys, F. Dehairs, and E. Keppens (2008) Stable isotope (C,N) composition of bivalve shell organic mater and salinity. VLIZ Special Publication, 40, VLIZ Young Scientists Day 2008, Brugge, Belgium (poster).

Mas R. (2007) Perspectives on deuterium analysis of bivalves shells; First annual meeting of PaleoSalt, June 4-5, 2007, Barcelona, Spain (poster).

Poulain C., Y.M. Paulet, L. Chauvaud, M. Benoît, R. Mas, F. Dehairs, E. Keppens and P. Claeys (2007) Salinity effect on strontium and magnesium incorporation in clam, Ruditapes philippinarum, shells ; First annual meeting of PaleoSalt, June 4-5, 2007, Barcelona, Spain (oral)

Servaes F., F. Dehairs, R. Mas, M. Bauwens and V. Beelaerts (2007) General presentation of WP5 : Salinity effects on proxy incorporation in bivalves ; First annual meeting of PaleoSalt, June 4-5, 2007, Barcelona, Spain (oral)

Versteegh, E. A. A., Troelstra S. R., Dehairs, F., 2009. Is Greenland ice cap meltwater runoff recorded in growth increment chemistry of the bay mussel (*Mytilus trossulus*)? Geological Society of America 2009 Annual Meeting - From Volcanoes to Vineyards: Living with Dynamic Landscapes, October 18-21, Portland, Oregon, USA.

6.4 PhD Theses

Bauwens, M., 2011. Nonlinear and dynamical multi-proxy models for climate reconstructions on bivalve shells, Doctoral thesis, Vrije Universiteit Brussel, 208 pp.

Beelaerts, V., 2010. Time series reconstruction of environmental proxy records, Doctoral Thesis, Vrije Universiteit Brussel, 175 pp.

Hermans, J., 2010. Incorporation du magnesium dans les squelettes calcitiques des échnodermes et des éponges hypercalcifiés, Thèse de Doctorat, Université Libre de Bruxelles, 139pp.

7. ACKNOWLEDGMENTS

8. REFERENCES

Barusseau, J.-P., Descamps, B. M., Diop, E. H. S., Giresse, P., and Saos, J.-L., 1995. Coastal evolution in Senegal and Mauritania at 103, 102 and 101-year scales: Natural and human records. *Quatern. Int.* **29-30**, 61-73.

Barusseau, J.-P., Vernet, R., J.-F., S., and Descamps, C., 2007. Late Holocene sedimentary forcing and human settlements in the Jerf el Oustani - Ras el Sass region (Banc d'Arguin, Mauritania). *Géomorphologie: relief, processus, environnement* **1**.

Bentov, S. and Erez, J., 2006. The impact of biomineralization processes on the Mg content of foraminiferal shells: A biological perspective. *Geochem. Geophy. Geosy.* **7**, 10.1029/2005GC001015.

Berner, E. K. and Berner, R. A., 1996. Global environment: Water, air, and geochemical cycles. Prentice Hall, Upper Saddle River, N.J.

Binyon, J., 1962. Ionic regulation and mode of adjustment to reduced salinity of the starfish Asterias rubens. *L. J. mar. biol. Ass. U.K.* **42**, 49-64.

Black, J. R., Epstein, E., Rains, W. D., Yin, Q.-z., and Casey, W. H., 2008. Magnesium-Isotope Fractionation During Plant Growth. *Environmental Science & Technology* **42**, 7831-7836.

Black, J. R., Yin, Q.-z., and Casey, W. H., 2006. An experimental study of magnesium-isotope fractionation in chlorophyll-a photosynthesis. *Geochim. Cosmochim. Acta* **70**, 4072-4079.

Blust, R., 2001. Radionuclide accumulation in freshwater organisms: concepts and models. In: *Radioecology Radioactivity & Ecosystem. International Union of Radioecology*, Van der Stricht, E. and Kirchmann, R. (Eds), 57-89.

Böhm, F., Gussone, N., Eisenhauer, A., Dullo, W.-C., Reynaud, S., and Paytan, A., 2006. Calcium isotope fractionation in modern scleractinian corals. *Geochim. Cosmochim. Acta* **70**, 4452-4462.

Buhl, D., Immenhauser, A., Smeulders, G., Kabiri, L., and Richter, D. K., 2007. Time series [delta]26Mg analysis in speleothem calcite: Kinetic versus equilibrium fractionation, comparison with other proxies and implications for palaeoclimate research. *Chem. Geol.* **244**, 715-729.

Carré, M., Bentaleb, I., Bruguier, O., Ordinola, E., Barrett, N. T., and Fontugne, M., 2006. Calcification rate influence on trace element concentrations in aragonitic bivalve shells: Evidences and mechanisms. *Geochim. Cosmochim. Acta* **70**, 4906-4920.

Carroll, M., Romanek, C., and L., P., 2006. The relationship between the hydrogen and oxygen isotopes of freshwater bivalve shells and their home streams. *Chem. Geol.* **234**, 211-222.

Chang, V. T. C., Makishima, A., Belshaw, N. S., and O'Nions, R. K., 2003. Purification of Mg from low-Mg biogenic carbonates for isotope ratio determination using multiple collector ICP-MS. *J. Anal. Atom. Spectrom.* **18**, 296-301.

Chang, V. T. C., Williams, R. J. P., Makishima, A., Belshawl, N. S., and O'Nions, R. K., 2004. Mg and Ca isotope fractionation during CaCO3 biomineralisation. *Biochem. Bioph. Res. Co.* **323**, 79-85.

Chave, K. E., 1954. Aspects of the biogeochemistry of magnesium 1. Calcareous marine organisms. . *Journal of Geology* **62**, 266-283.

Cheng, X., Varona, P. L., Olszta, M. J., and Gower, L. B., 2007. Biomimetic synthesis of calcite films by a polymer-induced liquid-precursor (PILP) process-1. Influence and incorporation of magnesium. *J Cryst Growth* **307**, 395-404, 10.1016/j.jcrysgro.2007.07.006.

Clarke, F. W. and Wheeler, W. C., 1922. The inorganic constituents of marine invertebrates. *Prof Pap US geol Surv* **124**, 56

CoBabe, E. A. and Pratt, L. M., 1995. Molecular and isotopic compositions of lipids in bivalve shells - a new prospect for molecular paleontology. *Geochimica Cosmochimica Acta* **59**, 87-95.

CoBabe, E. A. and Ptak, A. J., 1999. Comparison of in situ mineral-associated lipid compositions in modern invertebrate skeletons: preliminary evidence of dietary and environmental in uence. *Paleobiology* **25**, 201-211.

Crenshaw, M., 1980. Mechanisms of shell formation and dissolution. In: *Skeletal growth of aquatic organisms*, Rhoads, D. and Lutz, R. (Eds), 115-132.

De Deckker, P., Chivas, A. R., and Shelley, J. M. G., 1999. Uptake of Mg and Sr in the euryhaline ostracod Cyprideis determined from in vitro experiments. *Palaeogeography Palaeoclimatology Palaeoecology* **148**, 105-116, 10.1016/S0031-0182(98)00178-3.

De Ridder, F., Pintelon, R., and Schoukens, J., 2005. Reduction of the Gibbs phenomenon applied on non-harmonic time base distortions. *IEEE Trans. Instrum. Meas.* **54**, 1118-1125.

de Villiers, S., Dickson, J. A. D., and Ellam, R. M., 2005. The composition of the continental river weathering flux deduced from seawater Mg isotopes. *Chem. Geol.* **216**, 133-142.

Dickson, J. A. D., 2002. Fossil echinoderms as monitor of the Mg/Ca ratio of Phanerozoic oceans. *Science* **298**, 1222-1224.

Dodd, J. R. and Crisp, E. L., 1982. Non-linear variation with salinity of Sr/Ca and Mg/Ca ratios in water and aragonitic bivalve shells and implications for paleosalinity studies. *Palaeogeogr. Palaeoclim.* **38**, 45-56.

Dubois, P. and Chen, C. P., 1989. Calcification in echinoderms. In: *Echinoderm Studies*, Jangoux, M. and Lawrence, J. M. (Eds), **3**, 109-178.

Eisenman, E. A. and Alfert, M., 1981. A new fixation procedure for. preserving the ultrastructure of marine invertebrate tissues. *Journal of Microscopy* **125**, 117-120.

Elderfield, H., Vautravers, M., and Cooper, M., 2002. The relationship between shell size and Mg/Ca, Sr/Ca, delta O-18, and delta C-13 of species of planktonic foraminifera. *Geochem. Geophy. Geosy.* **3**, U1-U13.

EPICA Community members, 2007. Eight glacial cycles from an Antartic ice core. *Nature* **429**, 623-628.

Epstein, S. and Mayeda, T., 1953. Variation of 18O content of waters from natural sources. *Geochim. Cosmochim. Acta* **4**, 213-224.

Farre, B. and Dauphin, Y., 2009. Lipids from the nacreous and prismatic layers of two Pteriomorpha Mollusc shells. *Comparative Biochemistry and Physiology A-Molecular & Integrative Physiology: Part B* **152** 103-109.

Fietzke, J. and Eisenhauer, A., 2006. Determination of temperature-dependent stable strontium isotope (88Sr/86Sr) fractionation via bracketing standard MC-ICP-MS. *Geochem. Geophy. Geosy.* **7**, 10.1029/2006gc001243.

Freitas, P. S., Clarke, L. J., Kennedy, H. A., and Richardson, C. A., 2008. Inter- and intra-specimen variability masks reliable temperature control on shell Mg/Ca ratios in laboratory- and field-cultured Mytilus edulis and Pecten maximus (bivalvia). *Biogeosciences* **5**, 1245-1258.

Galy, A., Bar-Matthews, M., Halicz, L., and O'Nions, R. K., 2002. Mg isotopic composition of carbonate: insight from speleothem formation. *Earth Planet. Sci. Lett.* **201**, 105-115.

Galy, A., Belshaw, N. S., Halicz, L., and O'Nions, R. K., 2001. High-precision measurement of magnesium isotopes by multiple-collector inductively coupled plasma mass spectrometry. *Int. J. Mass Spectrom.* **208**, 89-98.

Galy, A., Yoffe, O., Janney, P. E., Williams, R. W., Cloquet, C., Alard, O., Halicz, L., Wadhwa, M., Hutcheon, I. D., Ramon, E., and Carignan, J., 2003. Magnesium isotope heterogeneity of the isotopic standard SRM980 and new reference materials for magnesium-isotope-ratio measurements. *J. Anal. Atom. Spectrom.* **18**, 1352-1356, DOI: 10.1039/b309273a.

Gillikin, D., Lorrain, A., Paulet, Y.-M., André, L., and Dehairs, F., 2008. Synchronous barium peaks in high-resolution profiles of calcite and aragonite marine bivalve shells. *Geo-Mar Lett* **28**, 351-358.

Gillikin, D. P. and Bouillon, S., 2007. Determination of δ18O of water and δ13C of dissolved inorganic carbon using a simple modification of an elemental analyzer - isotope ratio mass spectrometer (EA-IRMS): an evaluation. *Rapid Communications in Mass Spectrometry* **21**, 1475-1478.

Gillikin, D. P., De Ridder, F., Ulens, H., Elskens, M., Keppens, E., Baeyens, W., and Dehairs, F., 2005. Assessing the reproducibility and reliability of estuarine bivalve shells (Saxidomus giganteus) for sea surface temperature reconstruction: Implications for paleoclimate studies. *Palaeogeogr. Palaeoclim.* **228**, 70-85.

Gillikin, D. P., Dehairs, F., Lorrain, A., Steenmans, D., Baeyens, W., and Andre, L., 2006a. Barium uptake into the shells of the common mussel (Mytilus edulis) and the potential for estuarine paleo-chemistry reconstruction. *Geochim. Cosmochim. Acta* **70**, 395-407.

Gillikin, D. P., Lorrain, A., Bouillon, S., Willenz, P., and Dehairs, F., 2006b. Stable carbon isotopic composition of Mytilus edulis shells: relation to metabolism, salinity, delta C-13(DIC) and phytoplankton. *Org. Geochem.* **37**, 1371-1382.

Goodwin, D. H., Schöne, B. R., and L., D. D., 2003. Resolution and fidelity of oxygen isotopes as paleotemperature proxies in bivalve mollusk shells: models and observations. *PALAIOS* **18**, 110-125.

Hanssen, H., Blust, R., and de Boeck, G., 2008. Climate change induced temperature effects: A physiological kinetic model for the incorporation of calcium and strontium in the bivalve Mytilus edulis. *Comparative Biochemistry and Physiology A-Molecular & Integrative Physiology* **150**, S169-S169.

Henderson, G. M., 2002. New oceanic proxies for paleoclimate. *Earth Planet. Sci. Lett.* **203**, 1-13.

Ingram, B. L., De Deckker, P., Chivas, A. R., Conrad, M. E., and Byrne, A. R., 1998. Stable isotopes, Sr/Ca, and Mg/Ca in biogenic carbonates from Petaluma Marsh, northern California, USA. *Geochim. Cosmochim. Acta* **62**, 3229-3237.

Joiris, C. R. and Azokwu, M. I., 1999. Heavy Metals in the Bivalve Anadara (Senilia) senilis from Nigeria. *Mar Pollut Bull* **38**, 618-622.

Joiris, C. R., Azokwu, M. I., Otchere, F. A., and I.B., A., 1998. Mercury in the bivalve Anadara (Senilia) senilis from Ghana and Nigeria. *The Science of The Total Environment* **224**, 181-188.

Jones, W. C. and Jenkins, D. A., 1970. Calcareous sponges spicules: a study of magnesian calcites. *Calcified Tissue International* **4**, 314-329.

Kim, W. S., Huh, H. T., Huh, S. H., and Lee, T. W., 2001. Effects of salinity on endogeneous rhythm of the Manila clam, *Ruditapes philippinarum* (Bivalvia: Veneridae). *Mar. Biol.* **2001**, 157-162.

Klein, R. T., Lohmann, K. C., and Thayer, C. W., 1996a. Bivalve skeletons record of seas-surface temperature and δ18O via Mg/Ca and 18O/16O ratios. *Geology* **24**, 415-418.

Klein, R. T., Lohmann, K. C., and Thayer, C. W., 1996b. Sr/Ca and 13C/12C ratios in skeletal calcite of *Mytilus trossulus*: Covariation with metabolic rate, salinity, and carbon isotopic composition of seawater. *Geochim. Cosmochim. Acta* **60**, 4207-4221.

Komjarova, I. and Blust, R., 2008. Multi-metal interactions between Cd, Cu, Ni, Pb and Zn in water flea Daphnia magna, a stable isotope experiment. *Aquatic Toxicology* **90**, 138-144.

Lazareth, C. E., Willenz, P., Navez, J., Keppens, E., Dehairs, F., and André, L., 2001. Sclerosponges as a new potential recorder of environmental changes: Lead in Ceratoporella nicholsoni. *Geology* **28**, 515-518.

Le Gall, P., Bucaille, D., and Grassin, J. B., 1990. Influence de la température sur la croissance de deux oursins comestibles Paracentrotus lividus et Psammechinus miliaris. In: *Echinoderm Research*, De Ridder C, D. P., Lahaye MC, Jangoux M (Ed.), 183-188.

Lea, D. W., 2003. Elemental and Isotopic Proxies of Past Ocean Temperatures. In: *The Oceans and Marine Geochemistry*, Elderfield, H. (Ed.), **6**, 365-390.

Lea, D. W., Mashiota, T. A., and Spero, H. J., 1999. Controls on magnesium and strontium uptake in planktonic foraminifera determined by live culturing. *Geochim. Cosmochim. Acta* **63**, 2369-2379.

Lorrain, A., Gillikin, D. P., Paulet, Y.-M., Chauvaud, L., Le Mercier, A., Navez, J., and André, L., 2005. Strong kinetic effects on Sr/Ca ratios in the calcitic bivalve Pecten maximus. *Geology* **33**, 965-968.

Marriott, C. S., Henderson, G. M., Crompton, R., Staubwasser, M., and Shaw, S., 2004. Effect of mineralogy, salinity, and temperature on Li/Ca and Li isotope composition of calcium carbonate. *Chem. Geol.* **212**, 5-15.

Miyajima, T., Yamada, Y., and Hanba, Y. T., 1995. Determining the stable isotope ratio of total dissolved inorganic carbon in lake water by GC/C/IRMS. *Limnol. Oceanogr.* **40**, 994-1000.

Morse, J. W. and Mackenzie, F. T., 1990. The oceanic carbonate system and calcium carbonate accumulation in deep sea sediments. In: *Geochemistry of sedimentary carbonates: Developments in Sedimentology*, Morse, J. W. and Mackenzie, F. T. (Eds), **48**, 133-177.

Neufeld, D. S. and Wright, S. H., 1996. Response of cell volume in Mytilus gill to acute salinity change. *Journal of Experimental Biology* **199**, 473-484.

Nürnberg, D., Bijma, J., and Hemleben, C., 1996. Assessing the reliability of magnesium in foraminiferal calcite as a proxy for water mass temperatures. *Geochim. Cosmochim. Acta* **60**, 803-814.

O'Donnell, T. H., Macko, S. A., Chou, J., Davis-Hartten, K. L., and Wehmiller, J. F., 2003. Analysis of δ13C, δ15N, and δ34S in organic matter from the biominerals of modern and fossil Mercenaria spp. *Org. Geochem.* **34**, 165-183.

Otchere, F. A., 2003. Heavy metals concentrations and burden in the bivalves (Anadara (Senilia) senilis, Crassostrea tulipa and Perna perna) from lagoons in Ghana: Model to describe mechanism of accumulation/excretion. *African Journal of Biotechnology* **2**, 280-287.

Pogge von Strandmann, P. A. E., 2008. Precise magnesium isotope measurements in core top planktic and benthic foraminifera. *Geochem. Geophy. Geosy.* **9**, 10.1029/2008gc002209.

Pogge von Strandmann, P. A. E., James, R. H., van Calsteren, P., Gíslason, S. R., and Burton, K. W., 2008. Lithium, magnesium and uranium isotope behaviour in the estuarine environment of basaltic islands. *Earth Planet. Sci. Lett.* **274**, 462-471.

Prosser, S. J., Brookes, S. T., Linton, A., and Preston, T., 1991. Rapid, automated-analysis of 13C and 18O of CO2 in gas samples by continuous-flow, isotope ratio mass-spectrometry. *Biological Mass Spectrometry* **20**, 724-730.

Ra, K. and Kitagawa, H., 2007. Magnesium isotope analysis of different chlorophyll forms in marine phytoplankton using multi-collector ICP-MS. *J. Anal. Atom. Spectrom.* **22**, 817-821.

Rainbow, P. S., Wolowicz, M., Fialkowski, W., Smith, B. D., and Sokolowski, A., 2000a. Biomonitoring of trace metals in the Gulf of Gdansk, using mussels (Mytilus trossulus) and barnacles (Balanus improvisus). *Water Res* **34**, 1823-1829.

Rainbow, P. S., Wolowicz, M., Fialkowski, W., Smith, B. D., and Sokolowski, A., 2000b. Biomonitoring of trace metals in the Gulf of Gdansk, using mussels (*Mytilus trossulus*) and barnacles (*Balanus improvisus*). *Water Res.* **34**, 1823-1829.

Raz, S., Hamilton, P. C., Wilt, F. H., Weiner, S., and Addadi, L., 2003. The transient phase of amorphous calcium carbonate in sea urchin larval spicules: the involvement of proteins and magnesium ions in its formation and stabilization. *Advanced Functional Materials* **13**.

Raz, S., Weiner, S., and Addadi, L., 2000. Formation of high-magnesian calcites via an amorphous precursor phase: possible biological implications. *Adv Mater* **12**, 38-42.

Rickaby, R. E. M., Schrag, D. P., Zondervan, I., and Riebesell, U., 2002. Growth rate dependence of Sr incorporation during calcification of Emiliania huxleyi. *Global Biogeochemical Cycles* **16**, 1-8.

Ries, J. B., 2004. Effect of ambient Mg/Ca ratio on Mg fractionation in calcareous marine invertebrates: A record of the oceanic Mg/Ca ratio over the Phanerozoic. *Geology* **32**, 981-984, 10.1130/g20851.1.

Robert, R., Trut, G., and Laborde, J. L., 1993. Growth, reproduction and gross biochemical composition of the Manila clam Ruditapes philippinarum in the Bay of Arcachon, France. *Mar. Biol.* **116**, 291-299.

Rosenheim, B. E., Swart, P. K., and Thorrold, S. R., 2005a. Minor and trace elements in sclerosponge Ceratoporella nicholsoni: Biogenic aragonite near the inorganic endmember? *Palaeogeogr. Palaeoclim.* **228**, 109-129.

Rosenheim, B. E., Swart, P. K., Thorrold, S. R., Eisenhauer, A., and Willenz, P., 2005b. Salinity change in the subtropical Atlantic: Secular increase and teleconnections to the North Atlantic Oscillation. *Geophys. Res. Lett.* **32**, 10.1029/2004GL021499.

Rosenheim, B. E., Swart, P. K., Thorrold, S. R., Willenz, P., Berry, L., and Latkoczy, C., 2004. High-resolution Sr/Ca records in sclerosponges calibrated to temperature in situ. *Geology* **32**, 145-148.

Salata, G. G., Roelke, L. A., and Cifuentes, L. A., 2000. A rapid and precise method for measuring stable carbon isotope ratios of dissolved inorganic carbon. *Marine Chemistry* **69**, 153-161.

Sarà, M., 1963. Una nuova specie di Feretronidi (Petrobiona incrustans) dal Mediterraneo e considerazioni sulla sistematica delle Calcispongie. *Monitore Zoologico Italiano* **70-71**, 229-237.

Sauer, P. E., Eglinton, T. I., Hayes, J. M., Schimmelmann, A., and Sessions, A. L., 2001. Compound-specifc d/h ratios of lipid biomarkers from sediments as a proxy for environmental and climatic conditions. *Geochimica Cosmochimica Acta* **65**, 213-222.

Schmitt, A.-D., Chabaux, F., and Stille, P., 2003. The calcium riverine and hydrothermal isotopic fluxes and the oceanic calcium mass balance. *Earth Planet. Sci. Lett.* **213**, 503-518.

Schöne, B. R., Fiebig, J., Pfeiffer, M., Gle, R., Hickson, J., Johnson, A. L. A., Dreyer, W., and Oschmann, W., 2005. Climate records from a bivalved Methuselah (Arctica islandica, Mollusca; Iceland). *Palaeogeogr. Palaeoclim.* **228**, 130-148.

Schöne, B. R., Freyre Castro, A. D., Fiebig, J., Houk, S. D., Oschmann, W., and Kröncke, I., 2004. Sea surface water temperatures over the period 1884-1983 reconstructed from oxygen

isotope ratios of a bivalve mollusk shell (Arctica islandica, southern North Sea). *Palaeogeogr. Palaeoclim.* **212**, 215-232.

Schoukens, J., Pintelon, R., and Vandersteen, G., 1997. A sine-wave fitting procedure for characterizing data acquisition channels in the presence of time base distortion and time jitter. *IEEE Trans. Instrum. Meas.* **46(),** , 1005-1010.

Schouten, S., Ossebaar, J., Schreiber, K., Kienhuis, M. V. M., Langer, G., Benthien, A., and Bijma, J., 2006. The effect of temperature, salinity and growth rate on the stable hydrogen isotopic composition of long chain alkenones produced by Emiliania huxleyi and Gephyrocapsa oceanica. *Biogeosciences* **3** 113-119.

Serban, A., Engel, M. H., and Macko, S. A., 1988. The distribution, stereochemistry and stable isotopic composition of amino acid constituents of fossil and modern mollusk shells. *Org. Geochem.* **13:**, 1123-1129.

Shen, C.-C., Lee, T., Chen, C.-Y., Wang, C.-H., Dai, C.-F., and Li, L.-A., 1996. The calibration of D[Sr/Ca] versus sea surface temperature relationship for Porites corals. *Geochim. Cosmochim. Acta* **60**, 3849-3858.

Spurr, A. R., 1969. A low-viscosity epoxy resin embedding medium for electron microscopy. *J. Ultrastr. Res.* **26**, 31-43.

Stickle, W. B. and Diehl, W. J., 1987. Effects of salinity on echinoderms. In: *Echinoderm studies*, M. Jangoux, J. M. L. (Ed.), **2**, 235-285.

Stoll, H. M., Rosenthal, Y., and Falkowski, P., 2002. Climate proxies from Sr/Ca of coccolith calcite: calibrations from continuous culture of Emiliania huxleyi. *Geochim. Cosmochim. Acta* **66**, 927-936.

Tipper, E. T., Galy, A., and Bickle, M. J., 2008. Calcium and magnesium isotope systematics in rivers draining the Himalaya-Tibetan-Plateau region: Lithological or fractionation control? *Geochim. Cosmochim. Acta* **72**, 1057-1075.

Tipper, E. T., Galy, A., Gaillardet, J., Bickle, M. J., Elderfield, H., and Carder, E. A., 2006. The magnesium isotope budget of the modern ocean: Constraints from riverine magnesium isotope ratios. *Earth Planet. Sci. Lett.* **250**, 241-253.

Vacelet, J., 1964. Etude monographique de l'éponge calcaire pharétronide de Méditerranee Petrobiona massiliana In: *Les Pharétronides actuelles et fossiles*, Vacelet, J. and Lévi (Eds), **34**, 1-125.

Vacelet, J., 1991. Recent Calcarea with a reinforced skeleton ("Pharetronids"). In: *Fossil and Recent Sponges*, Reitner, J. and Keupp, H. (Eds), 252-265.

Van Campenhout, K., Bervoets, L., Redeker, E. S., and Blust, R., 2009. A kinetic model for the relative contribution of waterborne and dietarycadmium and zinc in the common carp (Cyprinus carpio). *Environmental Toxicology & Chemistry* **28**, 209-219.

Van Den Driessche, K., 2001. Potentials of stable water isotopes as a natural tracer in the Schelde basin, Vrije Universiteit Brussel.

Van der Meer, M. T. J., Baas, M., Rijpstra, W. I. C., Marino, G., Rohling, E. J., Sinninghe Damsté, J. S., and Schouten, S., 2007. Hydrogen isotopic compositions of long-chain alkenones record freshwater flooding of the Eastern Mediterranean at the onset of sapropel deposition. *Earth Planet. Sci. Lett.* **262**, 594-600.

Van der Meer, M. T. J., Sangiorgi, F., Baas, M., Brinkhuis, H., Sinninghe Damsté, J. S., and Schouten, S., 2008. Molecular isotopic and dinoflagellate evidence for Late Holocene freshening of the Black Sea. *Earth Planet. Sci. Lett.* **267**, 426-434.

Vander Putten, E., Dehairs, F., Keppens, E., and Baeyens, W., 2000. High resolution distribution of trace elements in the calcite shell layer of modern Mytilus edulis: Environmental and biological controls. *Geochim. Cosmochim. Acta* **64**, 997-1011.

Vandersteen, G., Rolain, Y., and Schoukens, J., 2001. An identification technique for data acquisition characterization in the persence of nonlinear distortions and time base distortions. *IEEE Trans. Instrum. Meas.* **50**, 1355-1363.

Verheyden, A., De Ridder, R., Schmitz, N., Beeckman, H., and Koedam, N., 2005. High-resolution time series of vessel density in Kenian mangrove trees reveal a link with climate. *New Physiologist* **167**, 425-435.

Verspecht, J., 1994. Accurate spectral estimation based on measurements with a distorted-time base digitizer. *IEEE Trans. Instrum. Meas.* **43**, 210-215.

Wanamaker, J. A., Kreutz, K., Wilson, T., Borns, J. H., Introne, D., and Feindel, S., 2008a. Experimentally determined Mg/Ca and Sr/Ca ratios in juvenile bivalve calcite for Mytilus edulis : implications for paleotemperature reconstructions. *Geo-Marine Letters* **28**, 359-368.

Wanamaker, J. A., Kreutz, K. J., Borns, J. H. W., Introne, D. S., Feindel, S., Funder, S., Rawson, P. D., and Barber, B. J., 2007. Experimental determination of salinity, temperature, growth, and metabolic effects on shell isotope chemistry of Mytilus edulis collected from Maine and Greenland. *Paleoceanography* **22**, 12.

Wanamaker, J. A. D., Kreutz, K. J., Schöne, B. R., Pettigrew, N., Borns, H. W., Introne, D. S., Belknap, D., Maasch, K. A., and Feindel, S., 2008b. Coupled North Atlantic slope water forcing on Gulf of Maine temperatures over the past millennium. *Climate Dynamics* **31**, 183-194.

Wassenaar, L. I. and Hobson, K. A., 2000. Improved method for determining the stable-hydrogen isotopic composition (delta D) of complex organic materials of environmental interest. *Environmental Science and Technology* **34**, 2354-2360.

Wassenaar, L. I. and Hobson, K. A., 2003. Comparative equilibration and online technique for determination of non-exchangeable hydrogen of keratins for use in animal migration studies. *Isotopes in Environmental and Health Studies* **39**, 211-217.

Wasylenki, L. E., Dove, P. M., Wilson, D. S., and De Yoreo, J. J., 2005. Nanoscale effects of strontium on calcite growth: An in situ AFM study in the absence of vital effects. *Geochimica Cosmochimica Acta* **69**, 3017-3027.

Watson, E. B., 1996. Surface enrichment and trace-element uptake during crystal growth. *Geochim. Cosmochim. Acta* **60**, 5013-5020.

Weber, J. B. and Raup, D. M., 1966. Fractionation of the stable isotopes of carbon and oxygen in marine calcareous organisms: the echinoidea. Part I. Variation of 13C and 18O content within individuals. *Geochim. Cosmochim. Acta* **30**, 681-703.

Weber, J. N., 1968. Fractionation of the stable isotopes of carbon and oxygen in calcareous marine invertebrates--the Asteroidea, Ophiuroidea and Crinoidea. *Geochim. Cosmochim. Acta* **32**, 33-70.

Weber, J. N., 1969. The incorporation of magnesium into the skeletal calcites of echinoderms. *American Journal of Science* **267**, 537-566.

Weber, J. N., 1973. Temperature dependence of magnesium in echinoid and asteroid skeletal calcite: a reinterpretation of its significance. *Journal of Geology* **81**, 543-556.

Weber, J. N. and Woodhead, P. M. J., 1972. Temperature Dependence of Oxygen-18 Concentration in Reef Coral Carbonates. *J. Geophys. Res.* **77**, 463-473, 10.1029/JC077i003p00463.

Weiner, S. and Dove, P. M., 2003. An overview of biomineralization processes and the problem of the vital effect. In: *Biomineralization*, Dove, P. M., De Yoreo, J. J., and Weiner, S. (Eds), Reviews in Mineralogy & Geochemistry, **54**, 1-29.

Wheeler, A. P., 1992. Mechanisms of molluscan shell formation. In: *Calcification in biological systems*, Bonucci, E. (Ed.), 179-216.

Wilbur, K. M. and Saleuddin, A. S. M., 1983. Shell formation. In: *The Mollusca*, Saleuddin, A. S. M. and Wilbur, K. M. (Eds), 236-279.

Willenz, P. and Hartman, W. D., 1989. Micromorphology and ultrastructure of Caribbean scerosponges. 1. Ceratoporella nicholsoni and Stromatospongia norae (Ceratoporellidae, Porifera). *Mar. Biol.* **103**, 387-401.

Wombacher, F., Eisenhauer, A., Böhm, F., Gussone, N., Kinkel, H., Lezius, J., Noé, S., Regenberg, M., and Rüggeberg, A., 2006. Magnesium Stable Isotope Compositions in biogenic CaCO3. *Geophys. Res. Abst.* **8**, 06353.

Wombacher, F., Eisenhauer, A., Heuser, A., and Weyer, S., 2009. Separation of Mg, Ca and Fe from geological reference materials for stable isotope ratio analyses by MC-ICP-MS and double-spike TIMS. *J. Anal. Atom. Spectrom.* **24**, 627 - 636, DOI: 10.1039/b820154d.

Young, E. D. and Galy, A., 2004. The isotope geochemistry and cosmochemistry of magnesium. In: *Geochemistry of Non-Traditional Stable Isotopes*, Johnson, C. M., Beard, B. L., and Albarede, F. (Eds), Review in Mineralogy and Geochemistry, **55**, 197-230.

Young, E. D., Galy, A., and Nagahara, H., 2002. Kinetic and equilibrium mass-dependent isotope fractionation laws in nature and their geochemical and cosmochemical significance. *Geochim. Cosmochim. Acta* **66**, 1095-1104.

Zühlsdorff, C., Wien, K., Stuut, J. B. W., and Henrich, R., 2007. Late Quaternary sedimentation within a submarine channel-levee system offshore Cap Timiris, Mauritania. *Mar. Geol.* **240**, 217-234.